Agrociencia

eISSN: 2521-9766

VOLUME 58, NUMBER 4 | MAY 16 - JUNE 30, 2024 | MEXICO

AGRICULTURA
SECRETARÍA DE AGRICULTURA

All correspondence (subscription information, sales, advertising, author contributions, etc.) should be addressed to:

Central Office:

Agrociencia
Guerrero #9, Esquina Avenida Hidalgo.
56220. San Luis Huexotla. Texcoco,
State of Mexico

Phone: 595 92 84427

https://agrociencia-colpos.org/index.php/agrociencia

Cover: *Calendula officinalis* L.
Photography and credits: Luis Francisco Salomé-Abarca

AGRICULTURA
SECRETARÍA DE AGRICULTURA Y DESARROLLO RURAL

Contents

Volume 58, Number 4 | May 16 - June 30, 2024

Crop Science

Food Science

Agrociencia

PHENOTYPIC DIVERSITY IN *Calendula officinalis* L. REGARDING PLANT GROWTH, PHOTOSYNTHETIC TRAITS, FLOWER YIELD, AND OIL CONTENT

Luis Francisco **Salomé-Abarca**[1], Víctor Arturo **González-Hernández**[2*], Ramón Marcos **Soto-Hernández**[3], Iván **Ramírez-Ramírez**[2], Nicacio **Cruz-Huerta**[4]

[1]Colegio de Postgraduados. Posgrado de Recursos Genéticos y Productividad-Fruticultura. Carretera México-Texcoco Km. 36.5. Montecillo, Texcoco de Mora, México. Z. C. 56264.
[2]Colegio de Postgraduados. Posgrado de Recursos Genéticos y Productividad-Genética. Carretera México-Texcoco Km. 36.5. Montecillo, Texcoco de Mora, México. Z. C. 56264.
[3]Colegio de Postgraduados. Posgrado en Botánica. Carretera México-Texcoco Km. 36.5. Montecillo, Texcoco de Mora, México. Z. C. 56264.
[4]Colegio de Postgraduados. Posgrado de Recursos Genéticos y Productividad-Fisiología Vegetal. Carretera México-Texcoco Km. 36.5. Montecillo, Texcoco de Mora, México. Z. C. 56264.
* Author for correspondence: vagh@colpos.mx

Citation: Salomé-Abarca, LF, González-Hernández VA, Soto-Hernández RM, Ramírez-Ramírez I, Cruz-Huerta N. 2024. Phenotypic diversity in *Calendula officinalis* L. regarding plant growth, photosynthetic traits, flower yield, and oil content. **Agrociencia.** https://doi.org/ 10.47163/agrociencia.v58i4.2922
Agrociencia 58(4): 405-426.
Editor in Chief: Dr. Fernando C. Gómez Merino

Received: December 11, 2022.
Approved: June 06, 2024.
Published in Agrociencia: June 24, 2024.

ABSTRACT

Pot marigold (*Calendula officinalis* L.) is an annual herb-shrub distributed worldwide. It possesses multiple therapeutic applications as an antimicrobial, antioxidant, antiviral, anti-inflammatory, anti-cancer, and cosmetic agent. Despite its importance, its physiological traits, including photosynthetic parameters, plant growth kinetics, and oil content variation among phenotypes, remain unknown. Five contrasting phenotypes (S1 to S5), derived from a single variety, were characterized. Physiological variables evaluated included plant growth kinetics, growth rate indexes, A-C_i response curves, flower and oil yield, and oil chemical composition across eight harvesting dates. Phenotype S1 yielded the highest biomass because of its extended acceleration and deceleration growth stages during a longer period. Phenotype S1 also produced higher yields of harvested flowers and essential oil. Phenotype S2 also showed a high content of essential oils. This phenotypic diversity found in a single variety of pot marigold could be used for breeding this crop; for example, the crossing of S1 x S2 may produce F1 progenies with improved growth rates, flower yields, photosynthetic rates, and essential oil yield. Besides, phenotype S1 could be used directly for commercial planting.

Keywords growth rate, growth stages, leaf area, essential oil, δ-cadinene.

INTRODUCTION

Pot marigold (*Calendula officinalis* L.) is an annual herb-shrub distributed and cultivated worldwide that stands out because of its beautiful yellow-orange colors (Givol *et al.*, 2019). This species is widely recognized for its multiple medicinal properties, which include antibacterial, antifungal, antioxidant, antiviral, anti-inflammatory, and anti-cancer effects, as well as cosmetic applications (Muley *et al.*, 2009; Jan *et al.*, 2018; Silva

et al., 2021; Jabborova *et al*., 2019; Cruceriu *et al*., 2018; Mur *et al*., 2021). These multiple benefits are linked to specialized metabolites such as essential oils, carotenoids, and flavonoids (Salomé-Abarca *et al*., 2015; Ashwlayan *et al*., 2018). Pot marigold breeding has been focused on improving four traits: ornamental value, flower yield and oil volume per hectare, medicinal-derived product quality, and plant resistance to diseases and pests. Thus, new pot marigold cultivars should grow efficiently, allocate more biomass to flowers, and produce a higher flower yield (Zitterl-Eglseer *et al*., 2001; Baciu *et al*., 2013; Samatadze *et al*., 2019). In addition, the physiological and chemical characterization of the phenotypic variation in traits like photosynthesis, growth, and metabolite content should help identify outstanding individuals.

In this context, in the Central High Valleys of Mexico, morphological and pigment variation among individual plants of a common and heterogeneous variety was reported (Soto-Hernández *et al*., 2013). Such variation also included differences in flower yields. From these variants, five phenotypes were selected based on their persistent and stable flower traits (Figure 1). This study focused on the physiological characterization of these five selected phenotypes regarding plant growth efficiency, photosynthetic parameters in response to leaf internal CO_2 concentrations, flower/oil yield, and oil chemical composition. The study determined what growth characteristics are determinants of higher total biomass accumulation and flower/oil yield and proposed the best phenotypes for pot marigold breeding and commercial production.

Figure 1. Flower heads of five selected phenotypes of pot marigold (*Calendula officinalis* L.) named from S1 to S5.

MATERIALS AND METHODS

Greenhouse and field management

Seeds from each phenotype were germinated under greenhouse conditions in trays with 200 cavities filled with a 1:1 forest soil:peat moss mixture, and each cavity received one seed. The 90-day-old seedlings were then transplanted to a field experimental station at 19° 19′ N, 98° 53′ W, at an altitude of 2250 m (29.8 °C maximum, 10.4 °C minimum, 39.6 mm of rain). Plants were distributed into 95 cm-wide rows, with 60 cm between plants along the row, achieving a planting density of 22 600 plants ha^{-1}. The

experimental unit was three rows of 5 m long. The five phenotypes were randomly assigned in a completely randomized design with three replicates. The field-grown plants were fertilized three times: twice with Bayfolan Forte™ (11.5N-8P-6K, Bayer) sprayed at 20 and 40 days after transplant (DAT), and one third time with Yaramila™ Complex (12N-11P-18K) applied at 90 DAT. Plants were irrigated every 2 weeks, except during the rainy season.

Plant growth analysis

For this analysis, one plant per phenotype and per replicate was sampled every 2 weeks for 16 weeks. Each sampled plant was dissected into leaves, stems, roots, and mature and immature flower heads (when present). All plant organs were oven-dried at 70 °C (Riosa™ Inc., Mexico) for 72 h. The dry weight of each organ, representing the accumulated biomass at each sampling date, was measured with an analytical scale (Explorer™, Ohaus, USA). The averages of organ weight (n = 3) for each phenotype and sampling date were plotted against plant age, and then several growth models were tested for each curve. The best-fit equations per organ and phenotype were chosen according to the highest coefficient of determination (R^2) provided by the software Curve Expert Professional V. 2.0™, as reported by the logistic model (Equation 1). To visually appreciate the fitness of predicted data against recorded data, both were plotted on the same graph. The growth phases for each phenotype were determined by the changes in their growth rates across the season, according to the predicted data:

$$Y = \frac{a}{(1 + be^{-cx})} \quad (1)$$

where a = asymptotic weight; b = initial weight; e = Euler's number (2.7182); c = growth rate; and x = days after transplant.

Growth rate analysis

Growth rates (GR) and relative growth rates (RGR) were calculated using the formulas quoted by Kumar *et al.* (2018) from data predicted by the best-fit models (Equations 2 and 3). Biomass allocation was assessed for two organ groups: vegetative and reproductive organs. GR (in g d^{-1}) was calculated as follows:

$$GR = (P2 - P1) / (t2 - t1) \quad (2)$$

where $P1$ and $P2$ = dry weights at two successive samplings; and $t1$ and $t2$ = days after transplant at sampling dates 1 and 2.

RGR (in g g^{-1} d^{-1}) was calculated as follows:

$$RGR = ln\ (P2 - P1) / ln\ (t2 - t1) \quad (3)$$

where *ln* = natural logarithm (based on Euler's number, 2.71828); *P*1 and *P*2 = predicted dry weights at two successive sampling dates; and *t*1 and *t*2 = days after transplant at dates 1 and 2.

The sink strength (SSt) per organ was estimated by the product of the sink size (SSz, in grams of biomass) multiplied by the sink activity (SA, estimated by the relative growth rate RGR, in g g^{-1} d^{-1}), as previously reported by Aguilar-León *et al*. (2006).

Leaf area (LA)

The leaf area per plant was measured on each fresh individual leaf separated from every-plant in each phenotype (three plants per phenotype). LA measurements were done with a leaf area meter LI-3100® (LICOR, Inc.; Lincoln, NE, USA), and means were expressed in cm^2 per plant ± standard deviation.

Flower yield

Four plants per phenotype were sampled to determine flower yield per plant at eight harvesting dates (n = 160). The initial flower sampling was done when 30 % of the plants had started to bloom; thereafter, only fully open, mature flowers were harvested every week. Flowers were harvested manually by cutting right under their bases and oven-dried at 40 °C for 48 h. The flower dry weight was measured with an analytical scale (Explorer™, Ohaus, USA), and the total flower dry weight per plant (sum of the 8 harvest dates) was reported as floral yield (g $plant^{-1}$) and as floral biomass per hectare (kg ha^{-1}) ± standard deviation (n = 4).

Photosynthetic kinetics (*A*-C_i curves)

A photosynthetic curve for each marigold phenotype was constructed with the following traits: instantaneous photosynthetic rate (*A*) at the youngest-mature leaf per plant, in response to increasing concentrations of atmospheric CO_2 (*Co*) and intracellular CO_2 (*Ci*), in four different plants per phenotype (n = 20). A portable infrared gas analyzer (LI-COR model LI-6400™, USA) was used for these measurements. This equipment was coupled to a LICOR CO_2 dispenser (LI-COR 6400-01™) to provide the following series of CO_2 concentrations for each curve: 400, 300, 200, 100, 0, 400, 600, 800, 1200, and 1600 μmol CO_2 mol^{-1}. In each replicate, the environmental conditions were kept at 21 °C for leaf temperature and 45 % relative humidity. All measurements were done under field conditions between 11:00 and 14:00 h, under completely clear skies, on randomly selected plants for each phenotype.

The LI-6400 analyzer calculated the C_i for each measured leaf based on the *Co*. The *A*-*Ci* curves for each phenotype were constructed with the averages (n = 4) of *A* and *Ci* for each CO_2-imposed concentration. A trend line was then adjusted by linear and non-linear regressions to each graph, and the compensation and saturation points (CP and SP) were estimated from the adjusted curves. The rubisco efficiency was calculated by fitting a linear regression in the transition zone between respiration

and photosynthesis. The maximum carboxylation velocity (V_{cmax}), ribulose phosphate regeneration (J_{max}), and the use of triose phosphates (TPU_{max}) were calculated with the program developed by Sharkey *et al.* (2007).

Enfleurage

Essential oils were extracted by the enfleurage technique applied to the dried inflorescences harvested from each marigold phenotype at four harvesting dates. Briefly, 100 g of vitellaria vegetable fat (*Vitellaria paradoxa*) were heated at 40 °C until a liquid state was reached, without boiling. Immediately, 3 g of dry inflorescences were added for oil extraction at 40 °C for 20 min. The vitellaria liquid fat containing the flowers was poured on top of a glass plate placed over ice for rapid solidification. Subsequently, 5 g of flowers were spread over the solidified fat layer. After 4 d of extraction, the fat was heated again and extracted with 50 mL of cold ethanol 95 %. The aromatic extracts were centrifuged at 4499.95 X*g* for 5 min and then vacuum filtered. Ethanol was then evaporated in a rotary evaporator at 30 °C, and the extracted oils were transferred to 1.5 mL glass vials under a fume hood, to allow the remaining solvent to evaporate at room temperature. The oil yield was then calculated by multiplying the oil weight by 100 and dividing the product by the inflorescence dry weight used for extraction (8 g).

Gas chromatography coupled to mass spectrometry (GC-MS)

The chemical composition of the essential oils extracted from the five phenotypes at different harvesting dates was determined by GC-MS. A Hewlett Packard HP 6890 Series® chromatograph coupled to a single quadrupole mass detector (HP 5973) was employed to perform these analyses. The GC was equipped with an HP5-MS column (30 m x 0.250 µm and 0.25 µm stationary phase thickness). Helium (99.9 % purity) was used as carrier gas at a flow rate of 1 mL min^{-1}. The oven temperature started at 40 °C and then increased at a rate of 5 °C min^{-1} until reaching 220 °C.

Compound identification was made by comparing the obtained mass spectra with those available in the NIST library V. 2014. Additionally, *n*-alkane co-injections were done to calculate the modified Kovat indexes (KI) with the van de Dool and Kratz equation (Equation 4):

$$KI = 100 * C + 100 \frac{(t'_R) \times - (t'_R)\, c}{(t'_R)\, c + 1 - (t'_R)\, c} \quad (4)$$

where C = number of carbons in the compound; $(t'_R) \times$ = corrected retention time of the compound calculated with the toluene retention time; $(t'_R)\, c + 1$ = corrected retention time of the alkane detected after the peak of the target compound; and $(t'_R)\, c$ = retention time of the alkane detected before the target compound.

Statistical analysis

For the biomass allocation analysis, we used averaged data from the sixth (87 DAT) and seventh (102 DAT) sampling dates, which corresponded to the dates with the highest biomass accumulation in all phenotypes. These data were statistically analyzed using the Tukey test for mean comparisons ($p \leq 0.05$). Flower yields were analyzed, considering phenotype and harvest date as the sources of variation in a completely randomized experimental design under a factorial arrangement of treatments (phenotype x harvest date). All tests ($p \leq 0.05$) were done with the statistical software SAS V. 8.1 (SAS Institute).

RESULTS AND DISCUSSION

Plant growth analyses

The five marigold phenotypes showed sigmoidal growth kinetics with four or five stages (La, lag; A, acceleration; Li, linear; D, deceleration; and S, stationary); only S1 did not show the linear stage (Figure 2). At 87 DAT, phenotype S1 reached its highest biomass accumulation with 228 g of dry biomass per plant, a dry weight at least 20 % heavier than the other phenotypes, which accumulated less than 200 g of biomass per plant. Phenotypic contrasts were also detected on growth parameters for the logistic model: S1 had the highest values in the initial (a) and maximum (b) weight parameters, while S2 stood out by having the highest growth rate (c) (Table 1). All chosen models showed statistically high fitness values ($R^2 > 0.98$), so they are reliable models for predicting marigold growth kinetics for plants grown in environmental conditions similar to this research.

Phenotypic differences in total biomass accumulation were mainly related to longer durations of the acceleration and deceleration stages. Phenotype S1 showed the longest acceleration and deceleration stages, 45 and 30 days, respectively (Figure 2A). Besides, S1 formed leaves for 20 days more than the other phenotypes. S2 showed a faster acceleration stage (Figure 2B), but it only lasted 32 days, and its plants grew 11 days less than S1. Conversely, S3 showed the lowest biomass accumulation rate during its short acceleration stage (Figure 2C) and ended with the lowest total biomass. Phenotypes S4 and S5 showed similar trends to those of S3 (Figures 2D and 2E). These analyses demonstrate that the acceleration and deceleration stages are the most determinant growth stages for biomass accumulation in marigold plants.

Other important phenotypic differences occurred in biomass allocation among plant organs. Flower heads, the most economically important organ in marigold, represented only 3.34 to 6.67 % of total biomass. Phenotype S1 stood out by its highest stem biomass accumulation and S2 by its higher biomass accumulation in leaves and inflorescences ($p < 0.05$). On the other hand, S5 and S3 were distinguished by allocating more biomass to roots ($p < 0.05$); phenotype S4 always showed intermediate biomass allocation values (Table 2).

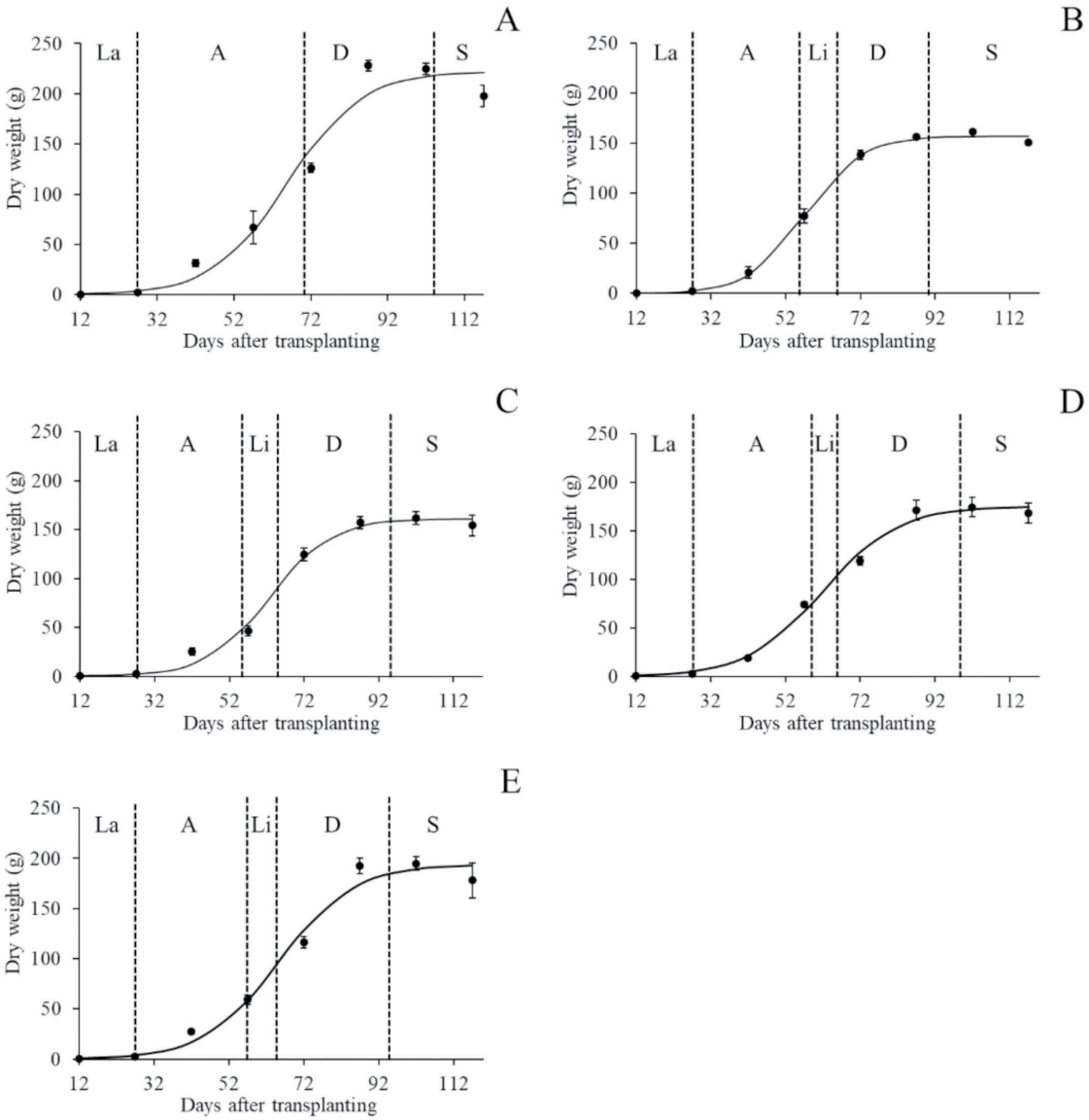

Figure 2. Growth curves of total biomass accumulation in five pot marigold (*Calendula officinalis* L.) selected phenotypes (S1 to S5), expressed in g plant^{-1}. A: phenotype S1; B: phenotype S2; C: phenotype S3; D: phenotype S4; E: phenotype S5. Growth stages L: lag; A: acceleration; Li: linear; D: deceleration; S: stationary. The data are averages of three replicates; vertical bars indicate ± standard error. The solid line represents predicted data, while solid points represent observed data.

Table 1. Values for growth parameters a, b, and c corresponding to the logistic equation $y = a/(1+be^{-cx})$ used to simulate the kinetics of total biomass accumulation in five selected phenotypes (S1 to S5) of Calendula officinalis L

Phenotype	a (g)	b	c (g g^{-1} d^{-1})	R^2
S1	2.220E+02	9.025E+02	1.033E-01	0.98
S2	1.574E+02	1.827+03	1.310E-01	0.99
S3	1.610E+02	2.014E+03	1.214E-01	0.99
S4	1.750E+02	4.467E+02	9.878E-02	0.99
S5	1.941E+02	7.187E+02	1.005E-01	0.99

a: initial weight; b: maximum weight or asymptotic weight; c: growth rate; R^2: determination coefficient per phenotype.

Table 2. Average distribution of biomass allocation among plant organs in five selected phenotypes (S1 to S5) of *Calendula officinalis* L.

Organ	S1 (g)	S2 (g)	S3 (g)	S4 (g)	S5 (g)
Stem	136.15 A	52.65 E	74.90 D	94.36 C	102.84 B
	60.12 %	33.10 %	46.97 %	54.67 %	53.10 %
Leaf	71.49 B	85.00 A	61.52 C	63.50 C	65.95 BC
	31.57 %	53.43 %	38.58 %	36.78 %	34.05 %
Root	11.24 B	10.79 B	16.82 A	7.38 C	18.08 A
	4.96 %	6.78 %	10.55 %	4.27 %	9.34 %
Flowers	7.57 B	10.64 A	6.22 C	7.38 B	6.79 BC
	3.34 %	6.69 %	3.90 %	4.27 %	3.51 %
Total	226.45 A	159.08 D	159.46 D	172.61 C	193.66 B

Values are average data (n = 6) of the sixth (87 DAT) and seventh (102 DAT) sampling dates, which correspond to the points with the highest biomass accumulation for all phenotypes. Percentage (%) of biomass assigned to each organ with respect to total biomass; S: phenotype. Phenotype mean values are compared in the same row by organs in a Tukey test ($p \leq 0.05$); different letters indicate significant differences between phenotypes.

Canopy size measured by the leaf area (LA) per plant was similar in the five phenotypes until 27 DAT; thereafter, the phenotypic differences in this trait became evident during the rest of the growing season, from 42 to 117 DAT, when S1 and S2 accumulated 14 123 and 14 601 cm^2 per plant, respectively (Figure 3). S5 only accumulated 58 % of the LA recorded in S2, with 8491 cm^2 per plant. When phenotypes S1 and S2 reached their largest LA, they already were at the stationary growth stage; their top LA (ca. 14 000 cm^2 $plant^{-1}$) was about four times higher than the one reported for marigold var. 'Bonina sortida' with 4470 cm^2 per plant (Honório *et al*., 2016). This quoted low LA

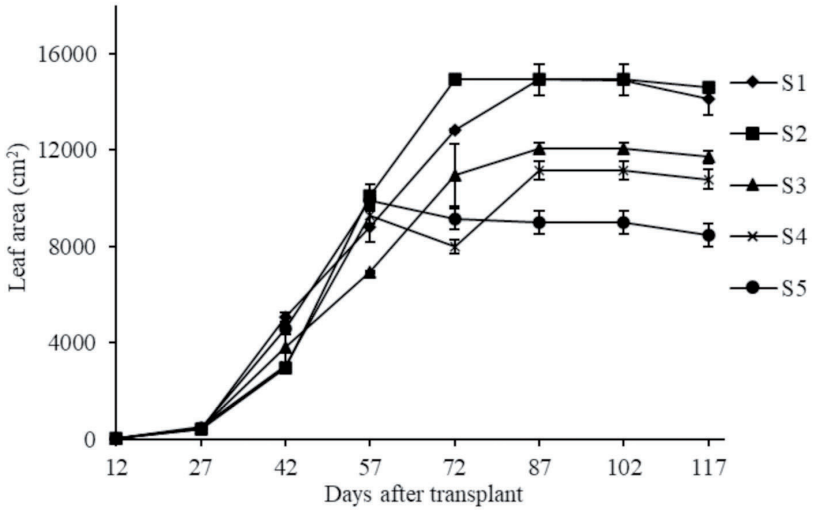

Figure 3. Kinetics of leaf area per plant in five pot marigold (*Calendula officinalis* L.) selected phenotypes (S1 to S5) measured through eight sampling dates. Data are averaged values (n = 3); vertical bars correspond to ± 1 standard deviation.

value seems to be due to the scarce flower harvestings done in that research, because it resulted in a lower branch and flower formation. Finley and Aarssen (2022) claim that periodical floral harvests in marigold promote sprouting of new shoot branches and thus a higher number of flowers.

Regarding other growth parameters of marigold, such as growth rate (GR) and relative growth rate (RGR), we found notorious contrasts among plant organs and phenotypes. For instance, the GR, which also estimates the sink strength, for the reproductive organs was about 10 times smaller than the GR for vegetative organs. This large difference between vegetative and reproductive organs may explain why calendula flowers received less than 7 % of the total biomass (Table 2). The vegetative organs reached the highest GR at 57 DAT in S2, while in the other phenotypes the peak occurred 15 days later (Figures 4A and 4B). As expected, the highest GR occurred at the end of the acceleration growth stage in all phenotypes. For the reproductive organs, the maximum GR occurred at 57 DAT in phenotypes S1, S2, S3, and S5, while in S4, the earliest phenotype, it occurred at 42 DAT. Considering all measured growth parameters, phenotypes S1 and S2 stood out for having the highest reproductive sink strength, which explains the highest biomass allocation in their flower heads (Figure 4B).

Contrary to the GR pattern, the RGR of the reproductive organs (Figures 4C and 4D) was similar to that of vegetative organs at the early stages of plant growth (up to 47 DAT). However, afterwards, the higher sink activity (i.e., higher RGR) occurred in

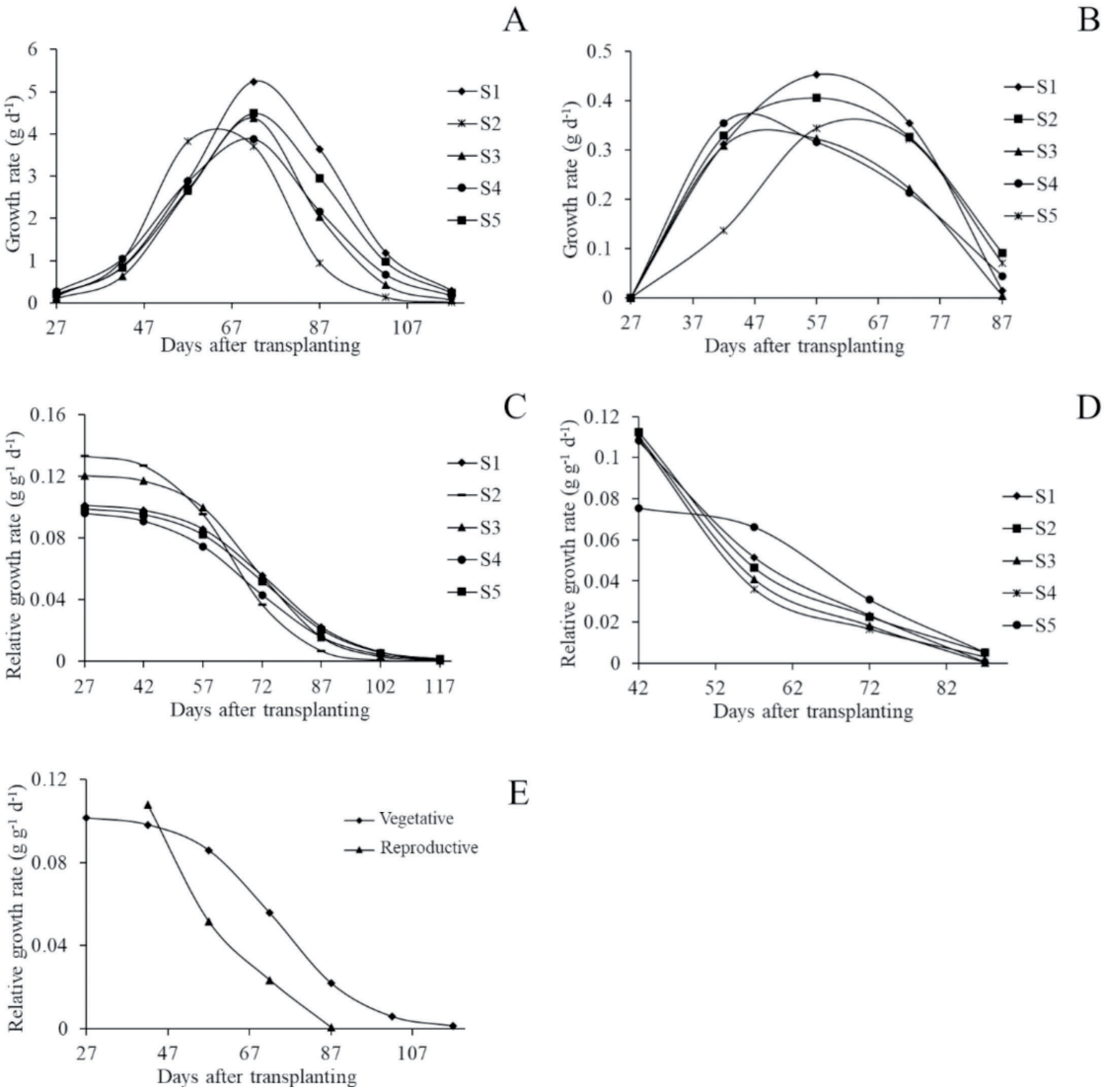

Figure 4. Growth efficiency indexes of vegetative and reproductive organs in five pot marigold (*Calendula officinalis* L.) contrasting phenotypes (S1 to S5). A: growth rates (GR) in vegetative organs; B: GR in reproductive organs; C: relative growth rates (RGR) in vegetative organs; D: RGR in reproductive organs; E: RGR of vegetative and reproductive organs in phenotype S1, which achieved the highest biomass accumulation among all phenotypes.

the vegetative organs during the rest of the growing season. This shift in sink organs may be attributed to the stem branching process, since to produce more new flower heads, new branches must be formed first. The internal competition among organs for photoassimilates clearly favors vegetative allocation, as was exemplified in phenotype S1 (Figure 4E). Moreover, at an early growth stage (42 DAT), phenotype S2 showed the highest vegetative and reproductive RGR values, 0.13 and 0.11 g g^{-1} d^{-1}, respectively. Considering that the RGR is an indicator of meristematic activity (Kumar *et al.*, 2018), then S2 is the phenotype with the most active shoot meristematic activity; in contrast, S5 had the lowest RGR value (30 % less than S2) for reproductive organs, associated with the smallest flower biomass in S5. Therefore, a high RGR value for reproductive organs might indicate a high potential to reach a higher yield. In this context, even though the RGR declines progressively as plants age, differences between phenotypes might explain the flower yield differences across harvesting dates. At the end of the growth season, the RGR phenotypic differences vanished due to a generalized decrease in the capacity to form new branches and new flowers (Figure 4D).

Photosynthetic parameters

Even though S1 was the best at biomass accumulation, this phenotype did not have the best photosynthetic features. In fact, S1 was the most limited phenotype regarding photosynthetic parameters. In general, the mathematical models obtained for the *A*/*Ci* curves of the five marigold phenotypes had good fittings between observed and predicted data (Figure 5). From these curves, it was evident that phenotype S1 has the lowest *Ci* saturation point of around 600 ppm (Figure 5A), while S2 got the highest *Ci* of c.a. 1200 ppm (Figure 5B). Phenotypes S3, S4, and S5 showed similar photosynthetic kinetics with A_{max} values in the range of 35 to 45 μmol CO_2 m^{-2} s^{-1} that occurred at *Ci* of c.a. 960 ppm (Figures 5C, D, and E).

Such photosynthetic trends allowed for the classification of the phenotypes into three groups: (1) S1 as the lowest in A_{max}; (2) S2 as the highest in A_{max}; and (3) S3, S4, and S5 with intermediate A_{max} values. The five phenotypes also showed contrasts in other photosynthetic parameters (Table 3). For instance, the CO_2 saturation point (*Psat*) needed for reaching A_{max} ranged from 30 to 74 Pa (384 to 947 ppm of *Ci*) among phenotypes, where S1 and S4, respectively, had the lowest and highest values. Therefore, S1 reached a lower *Amax* compared to the other phenotypes because of its lower ability to use high concentrations of CO_2; S1 also had the lowest rubisco efficiency among all five phenotypes (Table 3).

According to Sharkey *et al.* (2007), differences in A_{max} are associated with three limiting factors of the photosynthetic process: the maximum carboxylation rate (V_{cmax}), ribulose phosphate regeneration rate (J_{max}), and triose phosphate use (TPU_{max}). Among the five studied phenotypes, S1 had the lowest values on these three parameters (Table 4). Then, S1 may be regarded as the most limited phenotype in terms of photosynthetic potential. On the other hand, phenotypes S2 and S3 had the highest J_{max} rates; furthermore, S2 was also remarkable for its high TPU_{max}. Conversely, phenotype S3

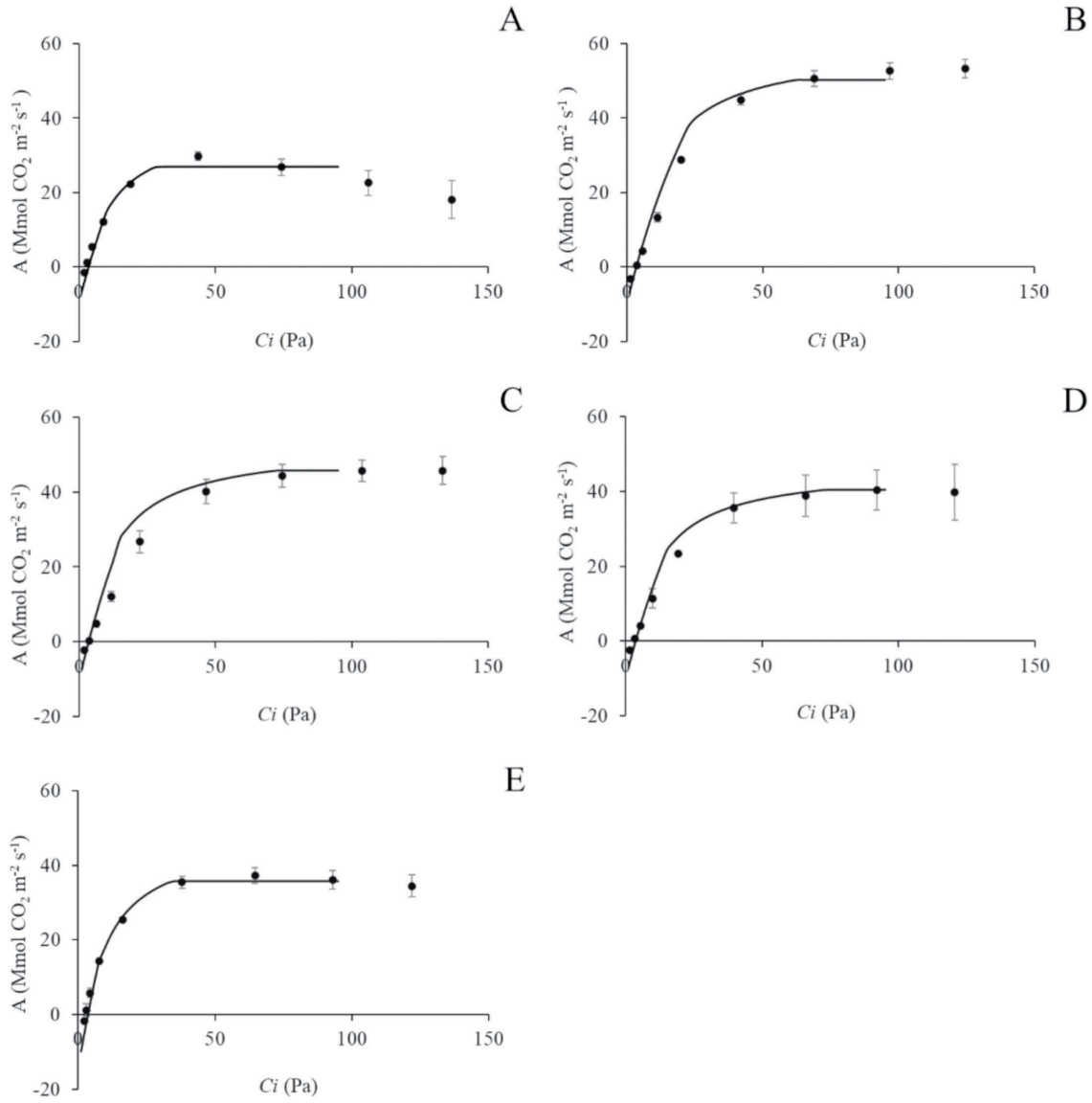

Figure 5. Kinetics of net photosynthesis rates in response to internal CO_2 concentration (*A*/*Ci* curves) of five pot marigold (*Calendula officinalis* L.) selected phenotypes (S1 to S5). A: S1; B: S2; C: S3; D: S4; E: S5. The *Ci* concentration scales are expressed in pascals (Pa); 50 Pa = 640 ppm of Ci, 100 Pa = 1280 ppm of *Ci*, and 150 Pa = 1920 ppm of *Ci*. The solid line in each graph represents predicted data by the models, while solid points represent observed data. The vertical bars on solid points represent ± standard deviation.

Table 3. Photosynthetic parameters (compensation (*PC*) and saturation (P_{sat}) points for CO_2, maximum photosynthetic rate (A_{max}), and rubisco efficiency (*REf*)) of five *Calendula officinalis* L. phenotypes (S1 to S5). The measurements were done at the blooming stage, from 77 to 84 days after transplant.

Phenotype	*PC* CO^a_2	*Psat* CO^b_2	*Amax*[c]	*Ref* [d]	SQ
S1	30.72	384	26.9	1.9	21.00
S2	42.24	793	50.1	2.0	3.02
S3	40.96	832	45.0	2.4	2.59
S4	37.12	960	40.4	2.0	7.91
S5	33.28	448	37.8	3.5	34.25

[a]expressed in ppm, [b]expressed in ppm, [c] and [d]expressed in μmol CO_2 m^{-2} s^{-1}; *SQ*: sum of squares of the model.

Table 4. Photosynthetic parameters at 25 °C calculated as proposed by Sharkey *et al.* (2007) in five selected phenotypes (S1 to S5) of pot marigold (*Calendula officinalis* L.). All measurements were done at the blooming stage, between 77 and 84 days after transplant.

Phenotype	Vc_{max}[a]	J_{max}[a]	TPU_{max}[a]	*gm*[b]
S1	127.0 ± 12.5	123.3 ± 4.6	7.6 ± 0.6	24.6 ± 0
S2	172.8 ± 7.5	279.5 ± 14.4	19.9 ± 0.9	12.6 ± 7.3
S3	204.5 ± 10.7	237 ± 14.3	17.4 ± 1.1	5.2 ± 1.5
S4	155.8 ± 12.5	211 ± 28.8	15.5 ± 2.1	24.6 ± 7.3
S5	215.8 ± 30.9	218 ± 6.9	14.8 ± 0.8	24.9 ± 9.3

Each value represents an average ± standard deviation (n = 4). V_{Cmax}: maximum carboxylation rate; J_{max}: ribulose regeneration rate; TPU_{max}: triose phosphate usage; *gm*: mesophyll conductance. [a]Data expressed in μmol m^{-2} s^{-1}, [b]data in μmol m^{-2} s^{-1} Pa^{-1}.

showed a low mesophyll conductance (*gm*), indicating a slow CO_2 diffusion into the chloroplasts, which might be a photosynthetic limitation (Evans, 2020). However, the poor condition of S3 was ameliorated by its high V_{cmax}, J_{max}, and TPU_{max} values (Table 4). Considering all the measured photosynthetic parameters, S2 may be regarded as the best phenotype for photosynthetic performance.

Compared to other plant species that have been subjected to this type of photosynthetic measurement, such as *Acacia mangium* Willd., *Buchanania arborescens* Blume, *Dillenia suffruticosa* (Griff.) Martelli, *Calophyllum inophyllum* L., and *Ploiarium alternifolium* Korth., in which the A_{max} values ranged between 10 and 13 μmol CO_2 m^{-2} s^{-1} (Benner *et al.*, 1988; Ibrahim *et al.*, 2021), our five pot marigold phenotypes showed much higher

A_{max} values (26.9 to 50.1 μmol CO_2 m^{-2} s^{-1}). The marigold A_{max} values were also higher than those of *Rubus* plant species (15 μmol CO_2 m^{-2} s^{-1}) (Mcdowell, 2002). Moreover, the V_{cmax} values of marigold phenotypes (127 to 215 μmol CO_2 m^{-2} s^{-1}) were much higher than the average V_{cmax} of herbaceous C3 plants (75 μmol m^{-2} s^{-1}) as reported by Wullschleger (1993). These comparisons indicate that pot marigold is, in general, a photosynthetically efficient species. The wide photosynthetic diversity registered in the five studied marigold phenotypes might be used for plant breeding in order to increase photosynthesis and biomass accumulation efficiency in marigold varieties. Other physiological parameters might be added to select the best progenies.

Flower and oil yield

As mentioned above, flower yield was measured only in mature open flowers, as they are commonly harvested. This means that all immature flowers were excluded for measuring flower yield, whereas for the plant growth analysis, all flowers were included, both mature and immature. According to this flower yield evaluation, S1 produced the highest flower yield among the five phenotypes (Table 5), as well as the highest biomass accumulation in the stem and in the whole plant. Since S1 also had the highest flower GR (Figure 3B), these flowers accumulated more biomass, and a larger amount of bloomed flower heads were collected at every harvest date, which explains why S1 reached the maximum flower yield among all five phenotypes.

Table 5. Flower yield of five selected phenotypes (S1 to S5) of pot marigold (*Calendula officinalis* L.) through eight harvesting dates, and the Phenotype (P) x Harvest Day (HD) interaction.

HD DAT	Phenotype S1 (kg ha^{-1})	S2 (kg ha^{-1})	S3 (kg ha^{-1})	S4 (kg ha^{-1})	S5 (kg ha^{-1})	$\bar{x}$ by HD (kg ha^{-1})
56	73.7 n…p	74.0 n…p	82.3 j…p	96.0 j…p	43.9 p	74.0 F
63	100.6 i…p	77.4 m…p	89.9 j…p	101.1 j…p	64.3 op	86.7 EF
70	127.5 h…o	80.9 l…p	97.5 i…p	106.3 i…p	84.8 j…p	99.4 E
77	264.4 a…c	217.8 b…f	232.5 b…e	173.2 e…h	185.6 d…h	214.7 B
84	235.4 b…e	236.1 b…e	237.2 b…e	179.8 d…h	184.0 d…h	214.5 B
91	309.2 a	257.0 a…c	282.2 ab	318.9 a	209.1 c…g	275.3 A
98	240.5 b…d	126.3 h…o	140.5 h…m	163.2 f…i	133.5 h…n	160.8 C
105	144.3 g…l	142.3 h…k	105.2 i…p	147.8 g…j	81.5 k…p	124.2 D
Cumulative yield per phenotype	1495.5 A	1211.9 B	1267.5 B	1286.3 B	986.7 C	
$\bar{x}$ yield by phenotype per HD	186.9 A	151.5 B	158.43 B	160.8 B	123.3 C	

Data represents the mean value across replications, expressed in kilograms of dry matter per hectare (kg ha^{-1}). Averages followed by different capital letters in a column or a row are statistically different in that column or row, according to the Tukey test ($p \leq 0.05$). Averages followed by different lowercase letters in a column or a row are statistically different in that column or row in a Tukey test ($p \leq 0.05$). DAT: days after transplant.

The second-highest flower-yielding phenotype was S2, a phenotype that also had a large leaf biomass and the lowest stem dry matter. These results suggest that the instant net photosynthesis rate (A) in all phenotypes was enough to supply sugars for plant and flower growth and for getting the highest flower yield in S1. Therefore, a high dry matter accumulation in the stem, the organ with branches where flowers are developed, is not essential to obtain a high flower yield, but stem branching is necessary for flower production, as observed in phenotype S2, which produced many flowers and obtained the second highest flower yield (Table 5). Phenotype S2 stands out for doubling the photosynthetic capacity (A_{max}) of S1.

Therefore, in marigold plants, the stem ability for branching is a trait closely associated with flower yield, and branching is promoted by periodical flower harvests. Other factors involved could be the plant architecture and leaf angle (traits not measured here), because they could modify the amount of photosynthetic active radiation (PAR) intercepted by the canopy, as pointed out by Emmel *et al.* (2020). By computing the stem biomass/leaf biomass ratio, the following morphological differences were detected between S1 and S2: S1 assigned about 60 % of total biomass to stems and 30 % to leaves (stem:leaf, 2:1), while S2 assigned around 30 % biomass to the stem and 54 % to leaves (stem:leaf, 1:2) (Table 2). This allocation comparison shows that phenotype S1 grows more branches per plant but with fewer leaves per branch, while S2 forms fewer branches but each branch has more leaves, which would probably cause differences in the intercepted PAR by each phenotype.

In pot marigold, the most valuable organs are the flowers because of their medicinal and industrial applications (Khalid and da Silva, 2012). Regarding the flower yield monitored through eight harvests across the season, there were statistical differences among phenotypes (P) and harvest dates (HD), as well as for the P x HD interaction ($p \leq 0.01$). These results clearly show that the five marigold phenotypes vary in flower yields through the cutting dates. S1 reached the highest mature flower yield accumulated through the growing season ($p < 0.05$). Interestingly, S2 allocated more biomass to flowers, including both mature and immature buds, thus possessing a higher sink strength (Table 2), a trait that could potentially be used to increase its flower yield. This phenotypic difference may be explained because S1 developed more mature flowers at each harvesting date, so with each harvest (i.e., pruning), the stem would be induced to develop a higher number of new lateral branches. On the contrary, S2 with a smaller number of mature flowers at each harvest date would induce a smaller stimulus for branching formation and, consequently, a lesser flower yield than S1.

Nonetheless, phenotype S2 has the physiological potential to reach the highest flower yield by accelerating flower development (faster maturation). Since continuous flower production across the growing season in marigold plants is prevented by apical dominance, which suppresses the development of lateral buds (required for branching). Therefore, when flowers are harvested, the apical dominance of that branch is temporarily suppressed, thus allowing the sprouting of axillary meristems for producing new branches (Finley and Aarssen, 2022). This means that each flower

harvest will promote the formation of new flowers. In marigold plants, each flower harvest also delays the leaf senescence process while promoting new secondary shoots (branches), so that periodical flower harvestings would result in a higher flower yield accumulated through the season. In pot marigold grown at Samsum, Turkey, on 24 harvesting dates over four months, the total flower yield was 566 kg ha^{-1} DW (Caliskan and Kurt, 2018), while in our study, the phenotype S1 yielded 1495 kg ha^{-1} DW in a harvesting period of only two months. Therefore, for pot marigold, the number of harvested flowers is more correlated to the flower yield than to the number of harvesting dates across the season.

Across the harvest dates, the sixth one (91 DAT) rendered the maximum flower production ($p < 0.05$). On this harvest, phenotypes S1 and S4 showed their highest yields, which are higher than those reported by Acosta-de la Luz *et al*. (2001) for pot marigold grown in Cuba (200 to 300 kg ha^{-1} DW). Considering the total flower production accumulated across the season, phenotype S1 outstands as the best in flower yield ($p < 0.05$). Interestingly, the phenotype ranking for flower yield (Table 5) matches the phenotype ranking for leaf area (Figure 2). This close association between leaf area and flower yield shows the importance of leaf surface as an important component of the source strength for suppling sugars and nutrients required for flower development and growth, considering flower yield as the most important sink strength in marigold in terms of sink-source relationships.

Essential oil content and chemical variation

The content of relevant compounds in the marigold flowers, such as carotenoids, flavonoids, and essential oils, is important because these flowers are used for medicinal and industrial purposes (Kurzawa *et al.*, 2022). The essential oils had received broad attention because of their diverse biological effects (Zengin *et al.*, 2021). In our study, phenotypes S1, S2, and S5 maintained constant oil content through the growing season, while S3 and S4 showed a notorious increment in oil yield from the first to the sixth harvest (Table 6). According to flower mass essential oil yield, phenotype S2 showed the highest oil yield. However, when combining the average floral yields (kg DW ha^{-1}) with their corresponding oil yields (g 100 g^{-1} DW) in each phenotype, the resulting oil yields for phenotypes S1, S2, S3, S4, and S5 were 6.73, 6.51, 6.18, 5.79, and 4.56 kg of oil per hectare (Table 6), respectively. In this rank, phenotypes S1, S2, and S3 stand as the best ones for oil production under the tested field conditions. S2 flowers possessed a higher content of oil, but S1 produced more flowers, thus yielding a higher amount of oil per hectare.

Regarding the types of essential oils, the chromatographic analyses showed important chemical variations among marigold phenotypes and harvesting dates. Phenotype S4 was the most diverse, with 26 identifiable volatile compounds. The metabolite diversity decreased in the other phenotypes as follows: S2 > S3 > S1 > S5, with 24, 23, 19, and 18 identified compounds, respectively (Table 7). The chemical composition of essential oils included aldehydes, monoterpenes, and sesquiterpenes. Only the

Table 6. Oil yield (relative content, %) in flowers of five selected phenotypes (S1 to S5) of pot marigold (*Calendula officinalis* L.) harvested through four dates and extracted by enfleurage.

	Phenotype					
DAT[a]	S1	S2	S3	S4	S5	$\bar{x}$ by harvest
56	3.5 ± 0.7	4.7 ± 1.4	3.7 ± 0.1	3.2 ± 0.06	3.5 ± 0.2	3.7 ± 0.52
70	3.8 ± 0.9	3.8 ± 0.4	3.3 ± 0.3	3.7 ± 0.2	3.9 ± 0.4	3.7 ± 0.21
84	3.7 ± 0.3	3.7 ± 0.3	4.0 ± 0.04	3.3 ± 0.7	3.7 ± 0.7	3.7 ± 0.22
91	3.6 ± 0.1	5.0 ± 0.1	4.6 ± 0.3	4.3 ± 0.6	3.7 ± 0.2	4.2 ± 0.53
$\bar{x}$ by phenotype	3.6 ± 0.1	4.3 ± 0.6	3.9 ± 0.5	3.6 ± 0.5	3.7 ± 0.2	

The data represent average values (n =3) ± standard deviation. [a]DAT, days after transplant.

sesquiterpenes copaene and δ-cadinene, was detected in all the phenotypes and harvesting dates (Table 7). S2 and S3 stand out as the phenotypes with the highest contents of δ-cadinene (30 to 45 % of the total oil content). This sesquiterpene has been reported as having antibacterial activity against *Streptococcus pneumoniae* (Pérez-López *et al*., 2011). According to Babahmad *et al.* (2018), essential oils with high content of cadinenes have been reported with a strong antimicrobial activity.

The chemical variation in essential oils through different harvesting dates has also been observed by other researchers (Okoh *et al*., 2007). Most compounds found here in phenotypes S1–S5 (Table 7) have been previously reported in the essential oils of pot marigold (Okoh *et al*., 2007; Gazim, 2008; Okoh *et al*., 2008; Muley *et al*., 2009; Król, 2012; Ourabia *et al*., 2019; Sahingil, 2019). In general, δ-cadinene was the most abundant volatile in all oils. This monoterpene has been previously reported in pot marigold grown in Brazil, representing 27 % of its essential oils (Gazim, 2008), which is about half the percentage found here in phenotype S3.

Moreover, three cadinene-like compounds (α-cadinene, 7-epi-α-cadinene, and α-cadinol) are also contained in our marigold oils at good percentages (Table 7). In S2, α-cadinene was present up to 7.5 % of the total oil content at the third and fifth harvesting dates. This compound has been reported to be as high as 13 % in pot marigolds (Okoh *et al*., 2008). The isomer 7-epi-α-cadinene was produced by phenotypes S2, S3, S4, and S5 on different harvesting dates, with percentages ranging from 5.5 to 7.5 %. According to Muley *et al.* (2009), this metabolite is a component of the marigold essential oil. In S5, α-cadinol reached almost 8 % of the oil composition extracted from the first harvesting date. This last metabolite is produced by other species such as *Syzygium aromatic* L. and *Juniperus communis* L. (Zheljazkov *et al*., 2017; Ayub *et al*., 2023), and it has been reported as an antifungal agent (Ho, 2011). Moreover, α-cadinol has been proposed as a cure for antibiotic-resistant tuberculosis (Bueno *et al*., 2011).

Table 7. Chemical composition of essential oils extracted from five pot marigold (*Calendula officinalis* L.) phenotypes through four harvesting dates, expressed in relative composition (%) compared to total content.

		Phenotype					Phenotype					Phenotype					Phenotype				
	KI*	S1	S2	S3	S4	S5	S1	S2	S3	S4	S5	S1	S2	S3	S4	S5	S1	S2	S3	S4	S5
		56 DAT					70 DAT					84 DAT					98 DAT				
Benzaldehyde	707	0.5	-	-	0.9	-	0.3	-	0.2	1	-	-	-	0.2	0.7	-	-	-	0.2	0.5	-
Octanal	801	-	-	-	-	-	-	-	-	1.1	-	-	-	-	-	-	-	-	-	-	-
Nonanal	1000	0.2	-	0.2	1.5	3.7	0.3	0.7	0.4	1.1	-	0.2	-	0.3	1	-	0.2	-	0.3	0.7	-
Carene	1048	0.6	-	-	-	-	-	-	-	-	-	-	-	-	-	-	-	-	-	-	-
γ-muurolene	1502	1.2	3	-	-	3.3	0.7	-	-	-	-	0.7	2.6	-	1.1	-	-	5	0.7	-	-
7-*epi*-α-cadinene	1507	-	-	1	2.9	-	-	7	2.8	7.4	6.3	-	7	2.9	5.1	4.8	-	-	0.9	6	5.5
Epizonarene	1507	-	7.5	-	-	-	-	-	-	0.2	-	-	8	-	0.2	-	-	-	-	0.2	-
Germacrene D	1510	-	-	0.2	-	-	-	-	0.2	0.9	-	-	1.5	0.1	0.5	-	-	-	0.1	-	-
Isoledene	1514	-	5.4	-	-	6.1	-	-	-	0.3	-	-	5.2	-	0.2	-	-	-	-	2.5	8.4
Viridiflorol	1514	-	-	-	-	-	-	3.1	-	-	-	-	-	-	-	-	-	-	-	-	-
α-muurolene	1515	-	-	0.5	-	-	-	-	1.3	3.7	8.4	-	1.5	-	-	7.3	-	-	-	-	-
Caryophyllene	1516	0.1	-	0.1	-	-	-	-	-	-	-	0.1	-	-	-	-	0.1	-	-	-	-
δ-cadinene	1519	5.6	29.3	2.4	3.7	32.9	6.8	41	4.7	8.2	45.8	4.5	39.9	3.9	8.4	40.8	2.4	39	1.7	7.2	44.9
α-cubebene	1520	0.4	-	0.2	-	0.7	0.7	3.7	0.4	0.5	2.9	0.4	1.7	0.2	-	1.8	0.2	2.3	0.2	-	2.4
α-cadinene	1528	2	-	-	-	-	2.4	7.6	1.1	2.4	-	1.3	-	1.2	-	-	-	7.1	-	-	-
Copaene	1533	0.6	2.2	0.3	0.5	2	0.8	3.6	0.6	0.9	3	0.6	2	0.5	1.3	2.8	0.3	2.1	0.3	0.6	3.1
Aromadendrene[b]	1547	-	-	-	0.8	-	-	-	-	-	-	-	1.8	-	0.1	-	-	-	-	0.3	1.3
β-cubebene	1550	0.7	3.7	0.3	-	2.4	1.2	5.9	0.8	0.5	5.8	0.1	3.4	0.5	-	4.7	0.3	4.1	0.3	-	5
Phellandrene[a]	1551	1.1	-	-	-	-	0.9	-	-	-	-	1	-	0.3	-	-	-	-	-	-	-
β-gurjenene	1555	0.4	-	-	-	-	-	-	-	-	-	-	-	-	-	-	-	-	-	-	-
Calarene	1556	-	-	-	-	-	-	-	-	-	-	-	-	-	0.3	-	-	-	-	0.4	-
Longifolene	1558	-	-	-	-	-	-	1.6	-	-	-	-	-	-	0.1	-	-	-	-	0.2	-
γ-gurjenene	1559	-	1.4	-	0.7	1.1	-	-	-	-	-	0.3	-	0.1	2.6	0.6	-	-	-	-	-
τ-cadinol	1560	-	-	0.2	-	6.1	-	-	0.4	-	3	0.6	3.8	0.3	-	-	0.2	-	0.1	-	3.1
τ-mururolol	1561	-	-	-	-	-	-	-	-	-	-	-	-	0.7	-	-	-	-	-	-	-
β-patchoulene	1562	-	-	-	-	-	-	-	0.1	-	-	-	-	-	-	-	-	-	-	-	-
Aromadendrene	1563	-	0.3	0.1	-	-	-	-	-	-	-	-	-	0.1	-	-	-	-	-	-	-
Valencene	1563	-	-	-	0.5	-	0.9	-	0.1	0.3	0.8	-	-	0.1	0.8	-	-	-	-	0.2	-
α-cadinol	1564	0.9	-	-	-	7.8	0.9	-	0.5	-	-	0.8	4.3	-	-	-	-	-	-	-	-
Viridiflorene	1567	-	-	-	6	-	-	-	1	-	-	-	-	-	-	-	-	-	-	3.6	-
Cedrene	1578	-	-	-	-	-	-	-	-	-	-	0.2	-	-	-	-	-	-	-	-	-
Sesquirofuran	1578	-		-	-	-	-	-	-	-	-	-	0.7	-	-	-	-	-	-	-	-
α-elemene	1584	-	-	-	-	-	-	-	-	0.2	2.6	-	1.2	-	5.2	-	-	-	-	-	-
γ-selinene	1600	-	-	-	-	-	-	-	-	0.2	-	-	-	-	-	-	-	-	-	-	4.8
α-eremofilene	1612	-	-	-	1.8	-	-	-	0.3	-	-	-	-	-	0.1	-	-	-	-	-	-

*Retention index; [a]epi-bicyclosesquiphellandrene; [b]alloaromadendrene; [c]DAT: days after transplant.

CONCLUSIONS

Five phenotypes derived from a single common variety of pot marigold showed large contrasts in plant growth, photosynthetic parameters, flower yield, essential oil content, and metabolite composition through eight harvesting dates. Phenotypic differences in total biomass accumulation were positively associated with the duration of the acceleration and deceleration growth phases. That is, longer acceleration and deceleration phases provided higher total biomass accumulation. Phenotype S1 stands out as the most efficient for total biomass accumulation, flower yield, and essential oils yield. Regarding growth parameters, high growth rates (GR) serve as a selection parameter for high biomass accumulation phenotypes. On the other hand, high relative growth rate (RGR) values in vegetative organs might serve as a selection criterion for obtaining phenotypes that would produce more branches where flowers are generated, while selecting phenotypes with higher GR in reproductive organs would lead to select marigold plants able to allocate more biomass to individual flowers (bigger flowers).

The marigold phenotypic differences in photosynthetic potential are mainly determined by high values of max rates of carboxylation (V_{cmax}), ribulose regeneration (J_{max}), and triose phosphate usage (TPU_{max}) S2 stood out as the most efficiente phenotype in several photosynthesis parameters, contrasting with S1, which was the least efficient in this process. The apparent contradiction of phenotype S1 possessing the highest total biomass accumulation and flower yield while having the worst photosynthetic parameters could be explained by a larger total leaf area, a high branching rate, and a convenient branch/leaf architecture. Therefore, physiological parameters are useful traits for selecting efficient pot marigold varieties. Phenotypes S1 and S2 are the best candidates for breeding programs as they combine several important physiological traits, such as net photosynthetic rate, growth rate, and flower and oil yields.

ACKNOWLEDGEMENTS

To the *Colegio de Postgraduados* (Mexico) for financing all the research expenses, and to CONACYT-Mexico for providing a M. Sc. Scholarship to the first author.

REFERENCES

Acosta-de la Luz L, Rodríguez-Ferradá C, Sánchez-Govín E. 2001. Instructivo técnico de *Calendula officinalis*. Revista Cubana de Plantas Medicinales 6 (1): 23–27.

Aguilar-León MG, Carrillo-Salazar JA, Rivera-Peña A, González-Hernández VA. 2006. Análisis de crecimiento y de relaciones fuente-demanda en dos variedades de papa (*Solanum tuberosum* L.). Revista Fitotecnia Mexicana 29 (2): 145–156. https://doi.org/10.35196/rfm.2006.2.145

Ashwlayan VD, Kumar A, Verma M, V Kumar, Garg SK, Gupta M. 2018. Therapeutic potential of *Calendula officinalis*. Pharmacy and Pharmacology International Journal 6 (2): 149–155. https://doi.org/10.15406/ppij.2018.06.00171

Ayub MA, Goksen G, Fatima A, Zubair M, Abid MA, Starowicz M. 2023. Comparison of conventional extraction techniques with superheated steam distillation on chemical characterization and biological activities of *Syzygium aromaticum* L. essential oil. Separations 10 (1): 27. https://doi.org/10.3390/separations10010027

Babahmad RA, Aghraz A, Boutafda A, Papazoglou EG, Tarantilis PA, Kanakis C, Hafidis M, Ouhdouch Y, Outzourhit A, Ouhammou A. 2018. Chemical composition of essential oil of *Jatropha curcas* L. leaves and its antioxidant and antimicrobial activities. Industrial crops and products 121: 405–410. https://doi.org/10.1016/j.indcrop.2018.05.030

Baciu AD, Pamfil D, Mihalte L, Sestras AF, Sestras RE. 2013. Phenotypic variation and genetic diversity of *Calendula officinalis* (L). Bulgarian Journal of Agricultural Science 19 (1): 143–151.

Benner P, Sabel P, Wild A. 1988. Photosynthesis and transpiration of healthy and diseased spruce trees in the course of three vegetation periods. Trees 2 (4): 223–232. https://doi.org/10.1007/bf00202377

Bueno J, Escobar P, Martínez JR, Leal SM, Stashenko EE. 2011. Composition of three essential oils, and their mammalian cell toxicity and antimycobacterial activity against drug resistant-tuberculosis and nontuberculous mycobacteria strains. Natural Product Communications 6 (11): 1743–1748. https://doi.org/10.1177/1934578x1100601143

Caliskan O, Kurt D. 2018. Flower yields of pot marigold (*Calendula officinalis* L.) plants as effected by flowering durations and number of harvests. Journal of Medicinal Plants Studies 6 (6): 159–161.

Cruceriu D, Balacescu O, Rakosy E. 2018. *Calendula officinalis*: potential roles in cancer treatment and palliative care. Integrative Cancer Therapies 17 (4): 1068–1078. https://doi.org/10.1177/1534735418803766

Emmel C, D'Odorico P, Revill A, Hörtnagl L, Ammann C, Buchmann N, Eugster W. 2020. Canopy photosynthesis of six major arable crops is enhanced under diffuse light due to canopy architecture. Global Change Biology 26 (9): 5164–5177. https://doi.org/10.1111/gcb.15226

Evans JR. 2021. Mesophyll conductance: walls, membranes and spatial complexity. New Phtologist 229 (4): 1864–1876. https://doi.org/10.1111/nph.16968

Finley JV, Aarssen LW. 2022. No evidence of a generalized potential 'cost' of apical dominance for species that have strong apical dominance. Journal of Plant Ecology 15 (6): 1168–1184. https://doi.org/10.1093/jpe/rtac053

Gazim ZC, Rezende CM, Fraga SR, Filho BPD, Nakamura CV, Cortez DAG. 2008. Analysis of the essential oils from *Calendula officinalis* growing in Brazil using three different extraction procedures. Brazilian Journal of Pharmaceutical Sciences 44 (3): 391–395. https://doi.org/10.1590/s1516-93322008000300008

Givol O, Kornhaber R. Visentin D, Cleary M, Haik J, Harats M. 2019. A systematic review of *Calendula officinalis* extract for wound healing. Wound Repair and Regeneration 27 (5): 548–561. https://doi.org/10.1111/wrr.12737

Ho CL, Liao PC, Wang EIC, Su YC. 2011. Composition and antifungal activities of the leaf essential oil of *Neolitsea parvigemma* from Taiwan. Natural Product Communications 6 (9): 1357–1360. https://doi.org/10.1177/1934578x1100600935

Honório ICG, Bonfim FPG, Montoya SG, Casali VWD, Leite JPV, Cecon PR. 2016. Growth, development and content of flavonoids in calendula (*Calendula officinalis* L). Acta Scentiarum Agronomy 38 (1): 69–75. https://doi.org/10.4025/actasciagron.v38i1.25976

Ibrahim MH, Sukri RS, Tennakoon KU, Le QV, Metali, F. 2021. Photosynthetic responses of invasive *Acacia mangium* and coexisting native heath forest species to elevated temperature and CO_2 concentrations. Journal of Sustainable Forestry 40 (6): 573–593. https://doi.org/10.1080/10549811.2020.1792317

Jabborova D, Davranov K, Egamberdieva D. 2019. Antibacterial, antifungal, and antiviral properties of medical plants. *In* Egamberdieva D, Tiezzi A. (eds.), Microorganisms for Sustainability. Springer: Singapore, pp: 51–65. https://doi.org/10.1007/978-981-13-9566-6_3

Jan N, Majeed U, Andrabi KI, John R. 2018. Cold stress modulates osmolytes and antioxidant system in *Calendula officinalis*. Acta Physiologiae Plantarum 40 (4): 1–16. https://doi.org/10.1007/s11738-018-2649-0

Khalid KA, da Silva JT. 2012. Biology of *Calendula officinalis* Linn.: focus on pharmacology, biological activities and agronomic practices. Medicinal and Aromatic Plant Science and Biotechnology 6 (1): 12–27.

Król B. 2012. Yield and chemical composition of flower heads of selected cultivars of pot marigold (*Calendula officinalis* L). Acta Scientiarum Polonorum Hortorum Cultus 11 (1): 215–225.

Kumar V, Singh J, Chopra AK. 2018. Assessment of plant growth attributes, bioaccumulation, enrichment, and translocation of heavy metals in water lettuce (*Pistia stratiotes* L.) grown in sugar mill effluent. International Journal of Phytoremediation 20 (5): 507–521. https://doi.org/10.1080/ 15226514.2017.1393391

Kurzawa M, Wilczyńska E, Brudzyńska P, Sionkowska A. 2022. Total phenolic content, antioxidant capacity and UV radiation protection properties of marigold (*Calendula officinalis*), carrot (*Daucus carota*), tomato (*Solanum lycopersicum*) and hop (*Humulus lupulus*) Extracts. Cosmetics 9 (6): 134. https://doi.org/10.3390/cosmetics9060134

McDowell SCL. 2002. Photosynthetic characteristic of invasive and non-invasive species of *Rubus* (Rosaceae). American Journal of Botany 89 (9): 1431–1438. https://doi.org/10.3732/ajb.89.9.1431

Muley BP, Khadabadi SS, Banarase NB. 2009. Phytochemical constituents and pharmacological activities of *Calendula officinalis* Linn (Asteraceae): A review. Tropical Journal of Pharmaceutical Research 8 (5): 455–465. https://doi.org/10.4314/tjpr.v8i5.48090

Mur R, Langa E, Pino-Otín MR, Urieta JS, Mainar AM. 2021. Concentration of antioxidant compounds from *Calendula officinalis* through sustainable supercritical technologies, and computational study of their permeability in skin for cosmetic use. Antioxidants 11 (1): 96. https://doi.org/10.3390/antiox11010096

Okoh OO, Sadimenko AP, Asekun OT, Afolayan AJ. 2008. The effects of drying on the chemical components of essential oils of *Calendula officinalis* L. African Journal of Biotechnology 7 (10): 1500–1502.

Okoh OO, Sadimenko AP, Afolayan AJ. 2007. The effects of age on the yield and composition of the essential oils of *Calendula officinalis*. Journal of Applied Sciences 7 (23): 3806–3810. https://doi.org/10.3923/jas.2007.3806.3810

Ourabia I, Djebbar R, Tata S, Sabaou N, Fouial-Djebbar D. 2019. Determination of essential oil composition, phenolic content, and antioxidant, antibacterial and antifungal activities of marigold (*Calendula officinalis* L.) cultivated in Algeria. Carpathian Journal of Food Science and Technology 11 (2): 93–110. https://doi.org/10.34302/crpjfst/2019.11.2.8

Pérez-López A, Cirio AT, Rivas-Galindo VM, Aranda RS, de Torres NW. 2011. Activity against *Streptococcus pneumoniae* of the essential oil and δ-cadinene isolated from *Schinus molle* fruit. Journal of Essential Oil Research 23(5): 25–28. DOI: 10.1080/10412905.2011.9700477

Sahingil D. 2019. GC/MS-olfactometric characterization of the volatile compounds, determination antimicrobial and antioxidant activity of essential oil from flowers of calendula (*Calendula officinalis* L.). Journal of Essential Oil Bearing Plants 22 (6): 1571–1580. https://doi.org/10.1080/0972060x.2019.1703829

Salomé-Abarca LF, Soto-Hernández RM, Cruz-Huerta N, González-Hernández VA. 2015. Chemical composition of scented extracts obtained from *Calendula officinalis* by three extraction methods. Botanical Sciences 93 (3): 633–638. https://doi.org/10.17129/botsci.143

Samatadze TE, Zoshchuk SA, Hazieva FM, Yurkevich OY, Svistunova NY, Morozov AI, Amosova AV, Muravenk OV. 2019. Phenotypic and molecular cytogenetic variability in calendula (*Calendula officinalis* L) cultivars and mutant lines obtained via chemical mutagenesis. Scientific Reports 9 (1): 9155. https://doi.org/10.1038/s41598-019-45738-3

Sharkey TD, Bernacchi CJ, Farquhar GD, Singsaas EL. 2007. Fitting photosynthetic carbon dioxide response curves for C3 leaves. Plant, Cell and Environment 30 (9): 1035–1040. https://doi.org/10.1111/j.1365-3040.2007.01710.x

Silva D, Ferreira MS, Sousa-Lobo JM, Cruz MT, Almeida IF. 2021. Anti-Inflammatory activity of *Calendula officinalis* L. flower extract. Cosmetics 8 (2): 31. https://doi.org/10.3390/cosmetics8020031

Soto-Hernández RM, Palma-Tenango M, González-Hernández VA. 2013. Carotenoid content in six genotypes of *Calendula officinalis* L. through harvesting dates in Mexico. Planta Medica 79 (10): PS8. https://doi.org/10.1055/s-0033-1348822

Wullschleger SD. 1993. Biochemical limitations to carbon assimilation in C3 plants-A retrospective analysis of the A/Ci curves from 109 Species. Journal of Experimental Botany 44 (5): 907–920. https://doi.org/10.1093/jxb/44.5.907

Zengin G, Mahomoodally MF, Sinan KI, Sadeer N, Maggi F, Caprioli G, Angeloni S, Mollica A, Stefanucci A, Ak G, Cakılcıoglu U, Polat R., Akan H. 2021. Evaluation of chemical constituents and biological properties of two endemic *Verbascum* species. Process Biochemistry 108: 110–120. https://doi.org/10.1016/j.procbio.2021.06.007

Zheljazkov VD, Astatkie T, Jeliazkova EA, Heidel B, Ciampa L. 2017. Essential oil content, composition and bioactivity of Juniper species in Wyoming, United States. Natural Product Communications 12 (2): 201–204.

Zitterl-Eglseer K, Reznicek G, Jurenitsch J, Novak J, Zitterl W, Franz C. 2001. Morphogenetic variability of faradiol monoesters in marigold *Calendula officinalis* L. Phytochemical Analysis 12 (3): 199–201. https://doi.org/10.1002/pca.582.

Agrociencia

PHYSICAL CHARACTERIZATION AND MASS MODELING BY GEOMETRICAL ATTRIBUTES OF BLACK SAPOTE (*Diospyros nigra* (J.F.Gmel.) Perr.)

Guadalupe **Olmedo-Obrero**[1], Carlos Alberto **Villaseñor-Perea**[2*], Arturo **Mancera-Rico**[3], Emigdio **de la Cruz-de la Cruz**[4], Ma. del Rosario **Venegas-Ordoñez**[2], Gilberto de Jesús **López-Canteñs**[2], Cynthia **Serna-Abascal**[1]

[1]Universidad Autónoma Chapingo. Postgraduate in Agricultural Engineering and Integral Water Use. Carreteta Mexico-Texcoco km 38.5, Chapingo, Texcoco, State of Mexico, Mexico. C. P. 56230.
[2]Universidad Autónoma Chapingo. Department of Agricultural Mechanical Engineering. Carreteta Mexico-Texcoco km 38.5, Chapingo, Texcoco, State of Mexico, Mexico. C. P. 56230.
[3]Universidad Autónoma Agraria Antonio Narro. Department of Plant Breeding. Calzada Antonio Narro 1923, Buenavista, Saltillo, Coahuila, Mexico. C. P. 25315.
[4]Universidad Tecnológica de la Huasteca Hidalguense. Department of Agrobiotechnology. Carretera Huejutla-Chalahuiyapa S/N, Colonia Tepoxteco, Huejutla de Reyes, Hidalgo, Mexico. C. P. 43000.
* Author for correspondence: cvillasenorp@chapingo.mx

Citation: Olmedo-Obrero G, Villaseñor-Perea CA, Mancera-Rico A, de la Cruz-de la Cruz E, Venegas-Ordoñez M del R, López-Canteñs G de J, Serna-Abascal C. 2024. Physical characterization and mass modeling by geometrical attributes of black sapote (*Diospyros nigra* (J.F.Gmel.) Perr.). **Agrociencia** 58(4): 427-443. https://doi.org/ 10.47163/agrociencia.v58i4.2972

Editor in Chief: Dr. Fernando C. Gómez Merino

Received: February 22, 2023.
Approved: June 02, 2024.
Published in Agrociencia: June 13, 2024.

ABSTRACT

The fruit of black sapote (*Diospyros nigra* (J.F.Gmel.) Perr.) has been consumed in Mexico and Central America since pre-Hispanic times. They contain antioxidant compounds, minerals, and vitamins, making them valuable for nutraceutical and agro-industrial applications. Despite this, there is no scientific information on the physical and mechanical characterization of the fruit that helps in the design and development of protocols and equipment for storage, handling, processing, and added value for a better use of the fruit. In the present work, the physical and mechanical qualities of physiologically ripe black sapote fruit from the State of Hidalgo, Mexico, were characterized after one day of storage after harvest under environmental storage conditions. Models were also determined for the prediction of the mass of the fruit using their dimensional characteristics, finding that the quadratic models based on the volume of the ellipsoid (R^2 = 0.8919) and width of the fruit (R^2 = 0.8252) were the most appropriate to predict their mass. Likewise, a maximum compressive load force of 869.99 N and an apparent modulus of elasticity of 0.0.088 MPa were determined.

Keywords: mechanical properties, modulus of elasticity.

INTRODUCTION

The black sapote (*Diospyros nigra* (J.F.Gmel.) Perr.) is a fruit native to Mesoamerica. It is a member of the Ebenaceae family and has been consumed since prehispanic times (García-Díaz *et al.*, 2015). Its high phenolic compound content and nutritional value (Morton, 1987; Moo-Huchin *et al.*, 2014) make it ideal for use in nutraceutical

and agro-industrial applications. However, its high perishability has limited its commercialization outside of the production regions, so it is currently underutilized. This is due to its architecture and intense metabolic activity, causing farmers to lose up to 40 % of its value before they reach the consumer (Kitinoja *et al.*, 2011). In this regard, in Mexico, a sown area of 2488 ha was recorded in 2021, with a production of 18 482 Mg (SIAP, 2023).

The study of the physical characteristics of fruits and their relationships is necessary for the design, development, and optimization of various equipment suitable for harvesting, post-harvest processing, and material handling (Miraei Ashtiani *et al*., 2014; Jaiswal *et al.*, 2017). The determination of the mass, length, width, thickness, volume, and projected areas of the fruits is essential in the development of calibration systems and marketing since fruits with similar weight and uniform shape have a high acceptance by the consumer in the market (Panda *et al*., 2020).

Fruit classification systems could be optimized by knowing the relationship between their physical properties and mass (Vivek *et al*., 2018), since their geometric properties are easily measurable and their modeling could reduce classification time as well as work and costs in industries (Demir *et al*., 2020). Several studies have shown the advantage of modeling the mass of fruits, as it has been for *Neolamarckia cadamba* (Roxb.) Bosser, *Fragaria x Ananasa* Duch., *Laurocerasus officinalis* Roem., *Euryale ferox* Salisb., *Phyllanthus emblica* L., *Haematocarpus validus* (Miers) Bakh.f. ex Forman, *Psidium guajava* L., *Flacourtia jangomas* (Lour.) Raeusch., *Diospyros melanoxylon* Roxb., *Terminalia chebula* Retz, and *Citrus reticulata* L. (Mahawar *et al*., 2019; Pathak *et al*., 2019; Barbhuiya *et al*., 2020; Panda *et al*., 2020; Altuntas and Mahawar, 2021; Bibwe *et al*., 2022; Birania *et al*., 2022; Gaurav *et al*., 2022; Tomar and Pradhan, 2022; Panda *et al*., 2022; Sasikumar *et al*., 2021).

Fruits bruise during the transfer and storage stages due to the pressure exerted by heavy loads. Such damage reduces the quality of the product and increases the waste rate (Jahanbakhshi *et al*., 2018). Because of this, it is important to study the mechanical properties of the fruits, which are defined as those that are related to the behavior of the materials when applying forces characteristic of deformation stress under static and dynamic loads. It is necessary to determine the physical-mechanical properties of each particular fruit due to the close relationship between these properties and their degree of susceptibility to different types of mechanical damage (Pérez-López *et al*., 2014). In this sense, the American Society of Agricultural Engineers of the United States has developed guidelines such as Standard S368.4 DEC00 (ASAE, 2005), which deals with the compression test of agricultural products and served as the basis for the tests in the present study.

According to the Food and Agriculture Organization (FAO, 2003), there is a general demand for quality food in terms of nutritional value and safety, as well as appearance, freshness, and presentation. The fruit of *D. nigra* has a high nutritional value for its vitamin, mineral, and antioxidant content. However, their physical and mechanical properties are unknown, limiting proper post-harvest management. Also, *D. nigra*

fruit has a ripening process with climacteric behavior (Arellano-Gómez *et al*., 2005), so the fruit is harvested before ripening, which should be completed in a warehouse under controlled conditions of temperature and humidity.

The objective of this work was to characterize the physical and mechanical properties of freshly harvested *D. nigra* fruit in physiological maturity, in particular the dimensions, color, maximum compression load, maximum deformation by compression, and apparent modulus of elasticity, in addition to determining models that allow the estimation of its mass. The results of the research can be applied to the design of post-harvest processes that allow the reduction of damage and waste in the fruit of *D. nigra*, particularly those from the State of Hidalgo, Mexico.

MATERIALS AND METHODS

For the present study, 108 physiologically ripe and undamaged *D. nigra* fruit were collected; 46 were harvested 270 days after anthesis on January 26, 2022, and the remaining 62 were picked 260 days after anthesis on January 10, 2023. The fruit was obtained from a single wild tree incorporated into a family orchard, provided with no agronomic management (only weed control) in the Municipality of Atlapexco, Hidalgo, Mexico (21° 2′ 22.34″ N, 98° 20′ 48.55″ W), where the climate is humid semi-warm with rains all year round (72.1 %) and humid semi-warm with abundant rains in summer (27.9 %). After each harvest, the fruit was immediately packed in plastic nets and transported to the Materials Laboratory of Chapingo Autonomous University in the municipality of Texcoco, State of Mexico, Mexico, where the measurements were made.

Physical property characterization

The physical and mechanical properties of the fruit were characterized at a temperature of 21.19 ± 0.42 °C and a relative humidity (RH) of 39.39 ± 4.93 % on January 26, 2022. On January 10, 2023, the harvested fruit was characterized at a temperature of 19.76 ± 0.31 °C and a relative humidity (RH) of 45.12 ± 4 %. The moisture content was determined following the AOAC Method 925.10 (AOAC, 2005) using a digital balance (Ohaus; NJ, USA) with a sensitivity of 0.001 g. Mass was calculated using an Ohaus digital balance with a sensitivity of 1 g.

Color was determined with a portable colorimeter (X-rite; MI, USA), obtaining the luminosity L* (100 = white, 0 = black), a* (positive = red, negative = green), and b* (positive = blue, negative = yellow) values. The average values of three records reported in the equipment were considered the reported coordinates of each sample. The data was captured and processed in Adobe Photoshop® CS3 Extended (ASI, 2007) to determine the red, green, and blue (RGB) coordinate model. Subsequently, the data was processed to obtain the polar coordinates C* and H° using Microsoft Excel through the following equations (McGuire, 1992):

for a* and b* positives:

$$Tono\ (h^o) = arctan\frac{b^*}{a^*}$$

for a* negative and b* positive:

$$Tono\ (h^o) = 180 + arctan\frac{b^*}{a^*}$$

$$Croma\ (C^*) = (a^2 + b^2)^{1/2}$$

A digital Vernier (Truper, Mexico) with 0.01 millimeters (mm) accuracy was used to obtain the dimensions of length (L), width (W), and thickness (T) of the fruit (Figure 1). The results were expressed in terms of mm.

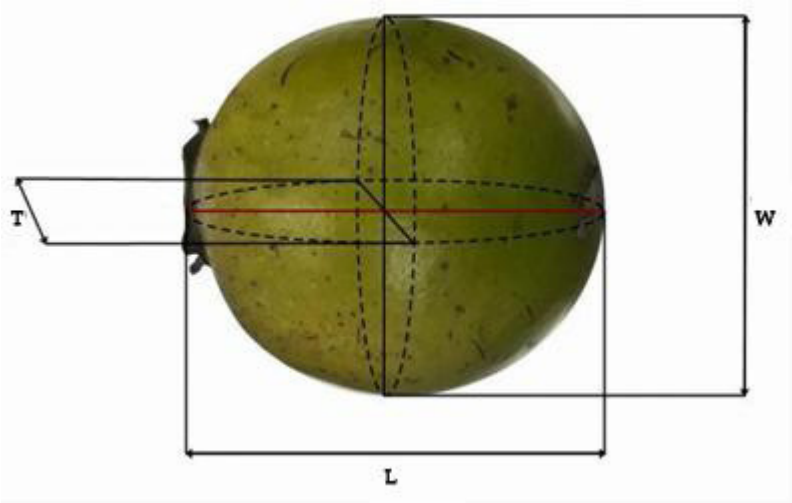

Figure 1. Length (L), width (W), and thickness (T) of black sapote (*Diospyros nigra* (J.F.Gmel.) Perr.) fruit.

The dimensional parameters were calculated using the following equations (Panda *et al*., 2020):

$$d_g = (L * W * T)^{1/3}$$

where d_g represents the geometric mean diameter (mm);

$$d_a = \frac{L + W + T}{3}$$

where d_a represents the arithmetic mean diameter (mm); and

$$d_e = \left[\frac{L * (W + T)^2}{4} \right]^{1/3}$$

where d_e represents the equivalent average diameter (mm).

The shape of the fruit was determined by calculating the sphericity, the aspect ratio of the fruit, the relationship between the thickness and width of the fruit (F_R), and the relationship between length and width (E_R), using the following equations:

$$\varphi = \frac{(L * W * T)^{1/3}}{L} * 100$$

where φ represents sphericity;

$$A_R = \frac{W}{L}$$

where A_R represents the aspect ratio;

$$F_R = \frac{T}{W}$$

where F_R represents the flaking index; and

$$E_R = \frac{L}{W}$$

where E_R represents the elongation index.

Projected areas perpendicular to thickness, length, and width were calculated using the following equations (Vivek *et al*., 2018):

$$P_T = \frac{\pi * W * T}{4}$$

where P_T represents the projected area perpendicular to the thickness (mm^2) of the fruit;

$$P_T = \frac{\pi * L * W}{4}$$

where P_L represents the projected area perpendicular to the length (mm^2) of the fruit;

$$P_W = \frac{\pi * W * W}{4}$$

where P_W represents the projected area perpendicular to the width (mm^2) of the fruit; and

$$CPA = \frac{P_L * P_T * P_W}{3}$$

where *CPA* represents projected area criteria (mm^2).

The fruit surface was calculated by reference to the following expression:

$$S_a = \pi * d_g^{\,2}$$

where S_a represents the surface area (mm^2) of the fruit.

The volume was calculated as a measure of a flattened spheroid, an elongated spheroid, and ellipsoid volume referring to the following equations (Shahbazi and Rahmati, 2013):

$$V_{obl} = \frac{4\pi}{3} * \left(\frac{W}{2}\right)^2 * \left(\frac{T}{2}\right)$$

where V_{obl} is the volume of the flattened spheroid (mm^3) of the fruit;

$$V_{prl} = \frac{4\pi}{3} * \left(\frac{L}{2}\right)^2 * \left(\frac{W}{2}\right)$$

where V_{prl} is the volume of the prolonged spheroid (mm^3) of the fruit; and

$$V_{ellip} = \frac{4\pi}{3} * \left(\frac{L}{2}\right) * \left(\frac{W}{2}\right) * \left(\frac{T}{2}\right)$$

where V_{ellip} represents the ellipsoid volume (mm^3) of the fruit.

Mass modeling of fruit

The mass modeling of the *D. nigra* fruit, according to their physical properties, was performed using six empirical models: linear, quadratic, power, S-curve, exponential, and multiple linear (equations 1 to 6, respectively), which have been previously reported for the modeling of fruit mass (Mahawar *et al.*, 2019; Pathak *et al.*, 2019; Barbhuiya *et al.*, 2020; Panda *et al.*, 2020; Altuntas and Mahawar, 2021; Bibwe *et al.*, 2022; Birania *et al.*, 2022; Gaurav *et al.*, 2022; Tomar and Pradhan, 2022; Panda *et al.*, 2022; Sasikumar *et al.*, 2021).

$$M = \beta_0 + \beta_1 X \quad (1)$$

$$M = \beta_0 + \beta_1 X + \beta_2 X^2 \quad (2)$$

$$M = \beta_0 X^{\beta 1} \quad (3)$$

$$M = \beta_0 + \beta_1 \frac{1}{X} \quad (4)$$

$$M = \beta_0 e^{\beta 1 X} \quad (5)$$

$$M = \beta_0 + \beta_1 L + \beta_2 W + \beta_3 T \quad (6)$$

where M is the mass (g), X is the physical property of the *D. nigra* fruit, and β_0, β_1, β_2, and β_3 are the adjustment constants of the curves.

Mechanical properties

Compression tests were applied within parallel plates of 15 cm in diameter to determine the mechanical properties of the maximum compression load (N), Hencky deformation, and apparent modulus of elasticity (MPa) of the fruit (Bourne, 2002). The equipment used was an INSTRON (Universal Testing Machine) model 3382 (INSTRON, Norwood, MA, USA) with a crosshead speed of 50 mm min^{-1} (ASAE, 2005) and a load cell of 100 kN. The fruit was placed in horizontal orientation (transverse axis) on a platform. The load was applied until the fracture. The INSTRON machine was simultaneously connected to a computer with BLUEHILL® Software, which provides the compression load and compression extension values for each fruit evaluated.

From this data, the instantaneous compression stress-Hencky deformation curve was generated for each sample, taking into consideration the radial height of the fruit and the surface area of the compression plate. The apparent modulus of elasticity and Hencky deformation were calculated according to the following equations (Nedomová *et al.*, 2017):

$$E = \frac{\sigma}{\varepsilon_H} = \frac{\frac{F}{A_{instant}}}{\varepsilon_H}$$

$$\varepsilon_H = -ln\left(1 - \frac{compression\ extension}{h}\right)$$

$$A_{instant} = \frac{A * h}{h - compression\ extension}$$

where E is the apparent modulus of elasticity of the fruit, ε is the fruit tension, ε_H is the Hencky deformation in the fruit, F is the force applied during compression, A is

the area of the disc that makes contact with the surface of the fruit, $A_{instant}$ is the instant area, and h is the radial height of the fruit.

Statistical analysis

Statistical indices, including mean, minimum, maximum, standard deviation, and coefficient of variation, were calculated using R programming (version 4.1.2) (R Core Team, 2017). The raw data on physical properties were used to obtain mass models (regression models between mass and physical characteristics), regression coefficients (R^2), and standard error of estimates (SEE). All model coefficients were analyzed with F-tests and t-tests with $\alpha = 0.05$. The best model fit was decided based on the highest R^2 value and lowest SEE.

RESULTS AND DISCUSSION

Physical characteristics

The moisture content determined for the fruit of *D. nigra* harvested on January 26, 2022, was 80.62 ± 1.68 %. For the fruit harvested on January 10, 2023, the moisture content was 76.45 % ± 3.77 %. These moisture values match those of 71 to 83 % moisture previously reported by Morton (1987).

The average results of color measurement of the fruit in the CIE-L*a*b* color space, as well as the color palette of epicarps, mesocarps, and seeds (Table 1) show a bright green and light-yellow color were observed in the epicarp and mesocarp, respectively, which coincides with Ledesma and Campbell (2001), who mentioned that the color of the pulp of the unripe fruits of *D. nigra* is golden-yellow. Regarding the seeds, an average of 6 ± 3 seeds per fruit of a dark brown color were obtained (Table 1), with an average weight of 1.23 ± 0.14 g and a length of 22.07 ± 2.57 mm, which coincides with Morton (1987), who mentions that there can be from 1 to 10 seeds per fruit, which are flat, smooth, brown, and 1.9–2.54 cm long.

The physical parameters of the fruit (Table 2), as well as the distributions obtained for the mass (M), length (L), width (W), and thickness (T) of the analyzed lot of *D. nigra* fruit (Figure 2), showed a natural variation in the dimensions of the fruit of up to 30.68 %. This variation is important to know and consider in the design of postharvest processes such as drying and packaging, among others (Pathak *et al.*, 2020).

Table 1. Rectangular chromatic coordinates and color palette of black sapote (*Diospyros nigra* (J.F.Gmel.) Perr.).

Part of the fruit	Parameters					
	L*	a*	b*	Tone (h°)	Croma (C*)	Color
Epicarp	51.46 ± 4.40	-5.91 ± 2.14	38.95 ± 4.81	278.82 ± 3.35	39.47 ± 4.70	
Mesocarp	55.12 ± 7.20	7.31 ± 2.39	40.60 ± 7.22	259.93 ± 1.81	41.27 ± 8.09	
Seed	21.57 ± 5.83	11.95 ± 1.28	12.27 ± 1.95	224.76 ± 6.63	17.08 ± 2.16	

Table 2. Black sapote (*Diospyros nigra* (J.F.Gmel.) Perr.) fruit dimensions.

Property	Minimum	Maximum	Mean	Standard deviation	Coefficient of variation (%)
M (g)	74.74	318.55	160.70	43.55	27.10
L (mm)	56.10	106.60	81.05	8.74	10.70
W (mm)	50.50	88.20	66.94	6.88	10.28
T (mm)	54.95	91.70	70.30	6.76	9.62
d_e (mm)	39.10	90.53	72.30	7.00	9.68
d_g (mm)	54.42	90.13	72.34	6.18	8.54
d_a (mm)	54.50	90.80	72.69	6.18	8.50
P_L (mm^2)	2225.07	6781.60	4284.25	743.69	17.36
P_W (mm^2)	2002.96	6109.80	3555.94	738.64	20.77
P_T (mm^2)	2256.80	6352.25	3729.67	740.20	19.85
CPA (mm^2)	2161.61	6035.91	3851.43	707.60	18.37
S_A (mm^2)	9305.24	25 521.64	16 557.42	2832.61	17.11
V_{ellip} (mm^3)	84 404.41	383 386.40	203 389.88	51 900.63	25.52
V_{ops} (mm^3)	75 979.01	373 512.49	169 734.38	52 075.70	30.68
V_{prl} (mm^3)	83 217.70	481 945.63	235 110.24	63 840.41	27.15
f	79.51	106.78	89.89	7.26	8.08
A_R	0.70	1.08	0.83	0.10	12.13
F_R	1.00	1.18	1.05	0.04	3.84
E_R	0.92	1.44	1.22	0.14	11.36

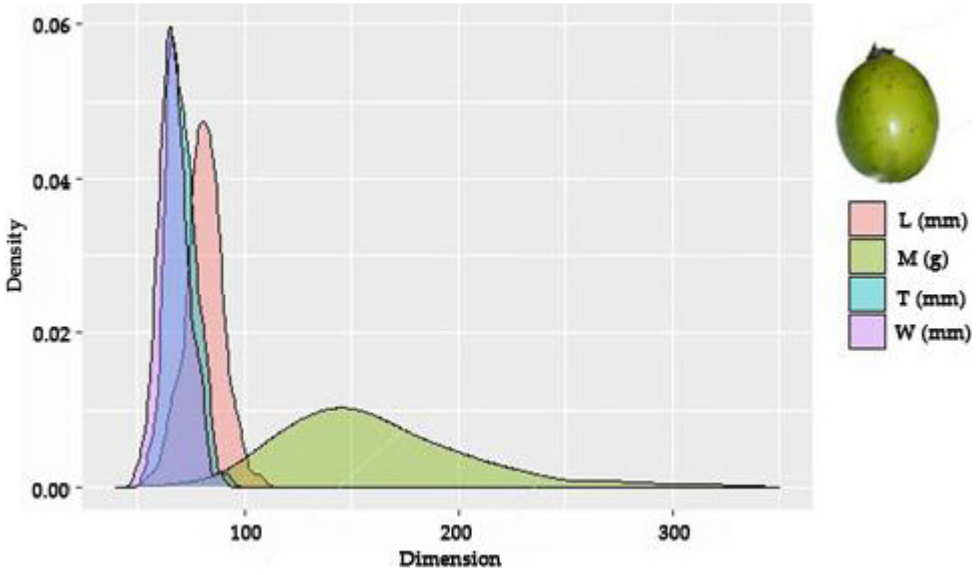

Figure 2. Distributions of mass (M), length (L), thickness (T), and width (W) of black sapote (*Diospyros nigra* (J.F.Gmel.) Perr.) fruit.

Mass modeling of the fruit

The quadratic (Equation 1) and multiple linear (Equation 4) models were selected as the best models for all physical attributes due to their high coefficients of determination (R^2) and low standard error of estimates (SEE) (Table 3). The F test values for these models were also significant ($p < 0.05$).

Table 3. Coefficients and the standard error of estimates (SSEs) of the models tested for the calculation of the black sapote (*Diospyros nigra* (J.F.Gmel.) Perr.) fruit mass.

Independent parameter(s)	Model	R^2	SSE	β_0	β_1	β_2	β_3
W	Quadratic	0.8252	18.41	$7.85x10^{1}$	$-3.19x10^{0}$	$6.53x10^{-2}$*	--
T	Quadratic	0.7979	19.80	$1.19x10^{2}$	$-4.40x10^{0}$	$7x10^{-2}$*	--
d_e	Quadratic	0.8798	15.27	$6.21x10^{2}$*	$-1.92x10^{1}$*	$1.75x10^{-1}$*	--
d_g	Quadratic	0.8780	15.38	$5.12x10^{2}$*	$-1.62x10^{1}$*	$1.6x10^{-1}$*	--
d_a	Quadratic	0.8644	16.22	$5.21x10^{2}$*	$-1.63x10^{1}$*	$1.55x10^{-1}$*	--
P_L	Quadratic	0.7627	21.57	$7.16x10^{1}$	$8.84x10^{-3}$	$6.71x10^{-6}$*	--
P_w	Quadratic	0.8251	18.42	$-3.57x10^{0}$	$3.92x10^{-2}$*	$1.88x10^{-6}$	--
P_T	Quadratic	0.8381	17.72	$1.66x10^{1}$	$4.16x10^{-2}$*	$1.53x10^{-6}$	--
CPA	Quadratic	0.8914	14.51	$4.84x10^{1}$	$1.48x10^{-3}$	$6.96x10^{-2}$*	--
SA	Quadratic	0.8763	15.32	$8.01x10^{1}$*	$-4.28x10^{-3}$	$5.37x10^{-7}$*	--
V_{ellip}	Quadratic	0.8919	14.55	$3.40x10^{1}$	$4.64x10^{-4}$*	$7.38x10^{-10}$*	--
V_{osp}	Quadratic	0.8393	17.65	$1.67x10^{1}$	$9.23x10^{-4}$*	$-4.01x10^{-10}$	--
L, W, and T	Multiple linear	0.8852	15.08	$-3.12x10^{2}$*	$1.21x10^{0}$*	2.50*	2.94*

*Model coefficients (βi) are significant ($p < 0.05$) according to the t-test obtained in the R programming environment.

The model that uses the ellipsoid volume (V_{ellip}) as the independent variable has the highest R^2 value and lowest SEE (Equation 7 and Figure 3A); therefore, it is suggested as the best fit.

$$M = 4.639\ x\ 10^{-4}\ V_{ellip} + 7.375\ V^2_{ellip};\ R^2 = 0.891,\ SEE = 14.55 \quad (7)$$

Similar results regarding the estimation of fruit mass based on ellipsoid volume (V_{ellip}) within a quadratic model have been reported as a suitable physical property for mass modeling of the fruit *Haematocarpus validus, Euryale ferox*, *Diospyros melanoxylon, Terminalia chebula,* and *Citrus reticulata* (Mahawar *et al.*, 2019; Pathak *et al.*, 2019; Panda *et al.*, 2020; Sasikumar *et al.*, 2021; Gaurav *et al.*, 2022), with R^2 values of 0.945, 0.879, 0.955, 0.970, and 0.955, respectively.

Likewise, the model that uses only fruit width (W) as an independent variable shows R^2 values of 0.8252 and SSE of 18.41 (Equation 8 and Figure 3B), which could also be

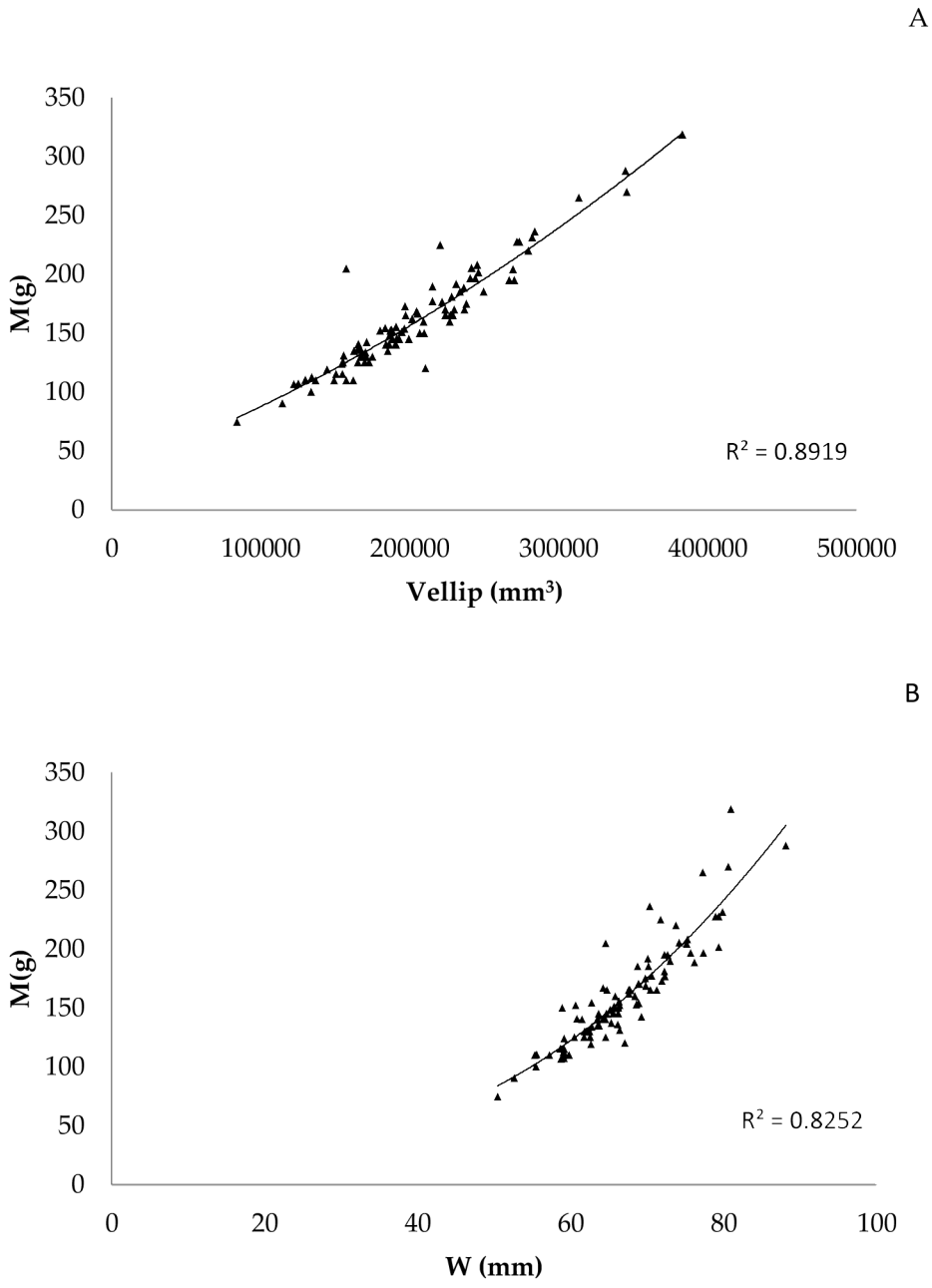

Figure 3. Quadratic mass models of black sapote (*Diospyros nigra* (J.F.Gmel.) Perr.) fruit. A: model based on ellipsoid volume (V_{ellip}); B: based on width (W).

considered a suitable model if a higher speed and lower processing costs of *D. nigra* fruit and data are sought.

$$M = 0.065\ W^2;\ R^2 = 0.825,\ SEE = 18.41 \quad (8)$$

Fruit width was reported as a suitable physical property for mass modeling in the case of *Prunus avium* fruit by being the most appropriate model among the three one-dimensional models they tested, with an R^2 value of 0.825 (Khadivi-Khub and Naderiboldaji, 2013).

Mechanical properties

The obtained values for maximum compression load, maximum Hencky deformation, and apparent elasticity (Table 4) show that freshly harvested nigra fruits are not damaged when the compression force is less than 399.7 N. Likewise, the compression load vs. extension and the instantaneous compressive stress vs. Hencky deformation curves obtained for a sample showed that *D. nigra* fruits present a typical linear viscoelastic behavior (Figure 4) (Severa, 2008).

Table 4. Values obtained for the mechanical properties of black sapote (*Diospyros nigra* (J.F.Gmel.) Perr.) fruit.

	Maximum compressive load (N)	Maximum Hencky's strain (%)	Apparent modulus of elasticity (MPa)
Minimum	399.72	21.82	$4.75x10^{-2}$
Maximum	1623.75	54.69	$1.50x10^{-1}$
Average	869.99	41.77	$8.77x10^{-2}$
Standard deviation	234.80	5.01	$2.53x10^{-2}$
Coefficient of variation (%)	26.99	12.18	$2.88x10^{+1}$

The results show that the force that the physiologically mature fruit of *D. nigra* with one day of post-harvest storage can tolerate, up to the breaking point, is approximately 869.99 N, which is higher than the force reported for other fruits such as banana (*Musa acuminata* var. *Cavendish*), with a value of 194 N (Jahanbakhshi *et al*., 2020), and tomato (*Solanum lycopersicum*) (V. Canyon, Early Ch), with a value of 57.85 N (Lak *et al*., 2018). The value obtained for the apparent elastic modulus is 0.088 MPa, which is higher than other fruits, such as banana with a value of 0.007 MPa (Jahanbakhshi *et al*., 2020), and tomato (*Solanum lycopersicum*) (V. Canyon, Early Ch) with 0.05 MPa (Lak *et al*., 2018), and lower than fruits such as orange, with a reported value of 0.584 MPa (Gharaghani and Maghsoudi, 2018).

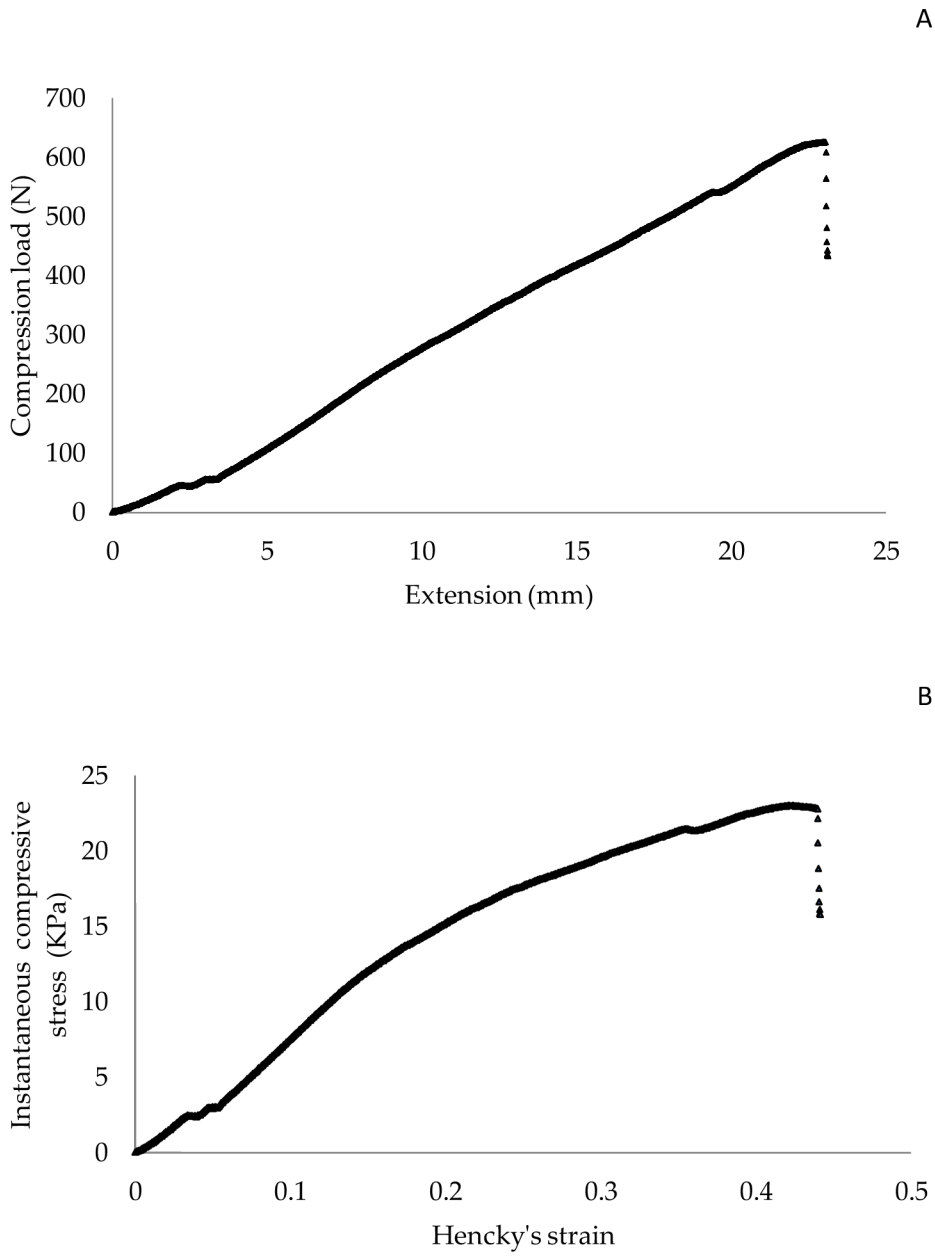

Figure 4. Compression test graphs for *Diospyros nigra* (J.F.Gmel.) Perr. A: compression load vs. extension; B: instantaneous compressive stress vs. Hencky's strain.

CONCLUSIONS

The physical and mechanical properties of black sapote (*Diospyros nigra* (J.F.Gmel.) Perr.) fruit at physiological maturity with one day of storage from the State of Hidalgo, Mexico, were characterized. In the models evaluated, all physical properties and their

coefficients were statistically significant. The second-order polynomial model was the most suitable, with the highest R^2 values, indicating a strong correlation between the characterized physical variables and fruit mass. The models that use the ellipsoid volume (V_{ellip}) and the fruit's thickness (W) as independent variables are recommended for modeling mass; the latter requires fewer resources and only requires determining one dimension of the fruit. Black sapote fruit withstands a maximum compression load of 869.99 N at breakage. The data obtained can be used to design, develop, and manufacture different sorting, packing, transport, and processing machines for this fruit. However, due to morphological variation between locations, it is still necessary to study the mechanical, physical, and chemical characteristics as well as the compounds present in *D. nigra* fruits, including fruit from other areas. This will help identify any correlations between the various existing morphologies.

ACKNOWLEDGMENTS

The authors gratefully acknowledge the *Consejo Nacional de Ciencia y Tecnología* (CONACYT) for Grant (90726) which provided support for the first author.

REFERENCES

Altuntas E, Mahawar MK. 2021. Mass prediction of cherry laurel genotypes based on physical attributes using linear regression models. Journal of Agricultural Faculty of Gaziosmanpasa University 38 (2): 87–94. https://doi.org/10.13002/jafag4765

AOAC (Association of Official Analytical Chemists). 2005. Official Methods 925.10 (32.1.03) – solids (total) and moisture in flour – air oven methods: Official methods of analysis of AOAC International (15th edition). Association of Official Analytical Chemists: Washington, DC, USA.

ASI (Adobe Systems Incorporated). 2007. The lab color mode in Photoshop. Adobe Photoshop CS3. https://helpx.adobe.com/mx/photoshop/using/converting-color-modes.html (Retrieved: January 2023).

Arellano-Gómez LA, Saucedo-Veloz C, Arévalo-Galarza L. 2005. Cambios bioquímicos y fisiológicos durante la maduración de frutos de zapote negro (D*iospyros digyna* Jacq.). Agrociencia 39 (2): 173–181.

ASAE (American Society of Agricultural Engineers). 2005. Standard S368.4 DEC00: Compression test of food materials of convex shape. *In* ASAE Standards: Standards, Engineering Practices and Data Adopted by the American Society of Agricultural Engineers. American Society of Agricultural Engineers: St. Joseph, MI, USA, pp: 600–608.

Barbhuiya RI, Nath D, Singh SK, Dwivedi M. 2020. Mass modeling of Indian coffee plum (Flac*ourtia Jan*gomas) fruit with its physicochemical properties. International Journal of Fruit Science 20 (3): S1110–S1133. https://doi.org/10.1080/15538362.2020.1775161

Bibwe B, Mahawar MK, Jalgaonkar K, Meena VS, Kadam DM. 2022. Mass modeling of guava (cv. *Allahabad safeda*) fruit with selected dimensional attributes: Regression analysis approach. Journal of Food Process Engineering 45 (3): e13978. https://doi.org/10.1111/jfpe.13978

Birania S, Attkan AK, Kumar S, Kumar N, Singh VK. 2022. Mass modeling of strawberry (*Fragaria x Ananasa*) based on selected physical attributes. Journal of Food Process Engineering 45 (5): e14023. https://doi.org/10.1111/jfpe.14023

Bourne MC. 2002. Food texture and viscosity: Concept and measurement (Second edition). Academic Press: New York, NY, USA. 423 p.

Demir B, Eski İ, Gürbüz F, Kuş ZA, Sesli Y, Ercişli S. 2020. Prediction of walnut mass based on physical attributes by Artificial Neural Network (ANN). Erwerbs-Obstbau 62 (1): 47–56. https://doi.org/10.1007/s10341-019-00468-8

FAO (Food and Agriculture Organization). 2003. Manual para la preparación y venta de frutas y hortalizas. Food and Agriculture Organization. Rome, Italy. http://www.fao.org/3/y4893s/y4893s08.htm (Retrieved: January 2023).

García-Díaz R, Cuevas-Sánchez JA, Segura-Ledesma S, Basurto-Peña F. 2015. Análisis panbiogeográfico de *Diospyros* spp. (Ebenaceae) en México. Revista Mexicana de Ciencias Agrícolas 6 (1): 187–200.

Gaurav A, Nath D, Barbhuiya RI, Pradhan RC. 2022. Physical characterization and mass modeling of traditionally Popped Makhana (*Euryale ferox* Salisbury) variety: Sabour-1 Makhana. Journal of Food Process Engineering 45 (6): e13927. https://doi.org/10.1111/jfpe.13927

Gharaghani BN, Maghsoudi H. 2018. Free fall analysis of orange fruit using numerical and experimental methods. International Journal of Food Properties 21 (1): 484–495. https://doi.org/10.1080/10942912.2018.1446148

Jahanbakhshi A, Abbaspour-Gilandeh Y, Gundoshmian TM. 2018. Determination of physical and mechanical properties of carrot in order to reduce waste during harvesting and post-harvesting. Food Science and Nutrition 6 (7): 1898–1903. https://doi.org/10.1002/fsn3.760

Jahanbakhshi A, Yeganeh R, Shahgoli G. 2020. Determination of mechanical properties of banana fruit under quasi-static loading in pressure, bending, and shearing tests. International Journal of Fruit Science 20 (3): 314–322. https://doi.org/10.1080/15538362.2019.1633723

Jaiswal SG, Dole BR, Satpathy SK, Naik SN. 2017. Physical attributes and modelling of trans-Himalayan seabuckthorn berries. Current Research in Nutrition and Food Science 5 (3): 391–397. https://doi.org/10.12944/crnfsj.5.3.25

Khadivi-Khub A, Naderiboldaji M. 2013. Predicting models for mass and volume of the sweet cherry (*Prunus avium* L.) fruits based on some physical traits. Canadian Journal of Plant Science 93 (5): 831–838. https://doi.org/10.4141/cjps2013-007

Kitinoja L, Saran S, Roy SK, Kader AA. 2011. Postharvest technology for developing countries: Challenges and opportunities in research, outreach and advocacy. Journal of the Science of Food and Agriculture 91 (4): 597–603. https://doi.org/10.1002/jsfa.4295

Lak M, Minaei S, Soufizadeh S, Banakar A. 2018. Modeling rupture force based on physical properties. A case study for Roma tomato (*Solanum lycopersicum*) fruits. Agricultural Engineering International: CIGR Journal 20 (3): 221–226.

Ledesma N, Campbell J. 2001. Reseña histórica, cultivares y propagación del zapote prieto (*Diospyros digyna* Jacq.) en el sur de la Florida. Proceedings of the Interamerican Society for Tropical Horticulture 45: 12–14.

Mahawar MK, Bibwe B, Jalgaonkar K, Ghodki BM. 2019. Mass modeling of kinnow mandarin based on some physical attributes. Journal Food Process Engineering 42 (5): e13079. https://doi.org/10.1111/jfpe.13079

McGuire RG. 1992. Reporting of objective color measurements. HortScience 27 (12): 1254–1255. https://doi.org/10.21273/hortsci.27.12.1254

Miraei Ashtiani SH, Baradaran MJ, Emadi B, Aghkhani MH. 2014. Models for predicting the mass of lime fruits by some engineering properties. Journal of Food Science and Technology 51 (11): 3411–3417. https://doi.org/10.1007/s13197-012-0862-1

Moo-Huchin VM, Estrada-Mota I, Estrada-León R, Cuevas-Glory L, Ortiz-Vazquez E, Vargas M de LV, Betancur-Ancona D, Sauri-Duch E. 2014. Determination of some physicochemical characteristics, bioactive compounds and antioxidant activity of tropical fruits from Yucatan, Mexico. Food Chemistry 152: 508–515. https://doi.org/10.1016/j.foodchem.2013.12.013

Morton JF. 1987. Fruits of warm climates. Echo Point Books and Media: Miami, FL, USA. 550 p.

Nedomová Š, Kumbár V, Pytel R, Buchar J. 2017. Mechanical properties of sugar beet root during storage. International Agrophysics 31 (4): 507–513. https://doi.org/10.1515/intag-2016-0081

Panda G, Vivek K, Mishra S. 2020. Physical characterization and mass modeling of Kendu (*Diospyros melanoxylo*n Roxb.) fruit. International Journal of Fruit Science 20 (3): S2005–S2017. https://doi.org/10.1080/15538362.2020.1851339

Panda TC, Thota, N, Dwivedi M, Pradhan RC, Seth D. 2022. Mass modeling of engineering properties and characterization of Kadamb fruit (*Neolamarckia cadamba*): An underutilized fruit. Journal of Food Process Engineering 45 (11): e14160. https://doi.org/10.1111/ jfpe.14160

Pathak SS, Pradhan RC, Mishra S. 2019. Physical characterization and mass modeling of dried *Terminalia chebula* fruit. Journal of Food Process Engineering 42 (3): e12992. https://doi.org/10.1111/jfpe.12992

Pathak SS, Pradhan RC, Mishra S. 2020. Mass modeling of Belleric Myrobalan and its physical characterization in relation to post-harvest processing and machine designing. Journal of Food Science and Technology 57 (4): 1290–1300. https://doi.org/10.1007/s13197-019-04162-1

Pérez-López A, Chávez-Franco SH, Villaseñor-Perea CA, Espinosa-Solares T, Hernández-Gómez LH, Lobato-Calleros C. 2014. Respiration rate and mechanical properties of peach fruit during storage at three maturity stages. Journal of Food Engineering 142: 111–117. https://doi.org/10.1016/j.jfoodeng.2014.06.007

R Core Team. 2017. R: A language and environment for statistical computing, R Foundation for Statistical Computing. Vienna, Austria. https://www.R-project.org/

Sasikumar R, Vivek K, Chakkaravarthi S, Deka SC. 2021. Physicochemical characterization and mass modeling of blood fruit (Haematocarpus Validus) – An underutilized fruit of Northeastern India. International Journal of Fruit Science 21 (1): 12–25. https://doi.org/10.1080/15538362.2020.1848752

Severa L. 2008. Behaviour of the peach under underwater shock wave loading. Acta Universitatis Agriculturae et Silviculturae Mendelianae Brunensis 56 (4): 151–160. https://doi.org/10.11118/actaun200856040151

Shahbazi F, Rahmati S. 2013. Mass modeling of fig (Ficus carica L.) fruit with some physical characteristics. Food Science and Nutrition 1 (2): 125–129. https://doi.org/10.1002/fsn3.20

SIAP (Servicio de Información Agroalimentaria y Pesquera). 2023. Cierre de la producción agrícola por cultivo, modalidad riego + temporal. Gobierno de México. Secretaría de Agricultura y Desarrollo Rural. Servicio de Información Agroalimentaria y Pesquera. Ciudad de México, México. https://nube.siap.gob.mx/cierreagricola/ (Retrieved: January 2023).

Tomar MS, Pradhan RC. 2022. Prediction of mass-based process designing parameters of amla fruit using different modeling techniques. Journal of Food Process Engineering 45 (8): e14039. https://doi.org/10.1111/jfpe.14039

Vivek K, Mishra S, Pradhan RC. 2018. Physicochemical characterization and mass modelling of Sohiong (*Prunus nepalensis* L.) fruit. Journal of Food Measurement and Characterization 12: 923–936. https://doi.org/10.1007/s11694-017-9708-x

Agrociencia

ANTIOXIDANT AND ANTIBACTERIAL EFFECT OF MESQUITE HONEY ON PORK SAUSAGES DURING STORAGE

Rosa Isela **Castillo-Zamudio**[1], Nohemí **Soto-Reyes**[2], Rey David **Vargas-Sánchez**[3], Brisa del Mar **Torres-Martínez**[3], Gastón Ramón **Torrescano-Urrutia**[3], Armida **Sánchez-Escalante**[3*]

[1]Colegio de Postgraduados Campus Veracruz. Carretera Xalapa-Veracruz km 88.5, Xalapa, Veracruz, Mexico. C. P. 91690.
[2]Instituto Tecnológico de Estudios Superiores de Monterrey. Escuela de Ingeniería y Ciencias. Avenida Eugenio Garza Sada 2501 Sur, Monterrey, Nuevo León, Mexico. C. P. 64849.
[3]CONAHCyT - Centro de Investigación en Alimentación y Desarrollo A. C. Coordinación de Tecnología de Alimentos de Origen Animal. Carretera Gustavo Enrique Astiazarán Rosas 46, Hermosillo, Sonora, Mexico. C. P. 83303.
* Author for correspondence: armida-sanchez@ciad.mx

Citation: Castillo-Zamudio RI, Soto-Reyes N, Vargas-Sánchez RD, Torres-Martínez B del M, Torrescano-Urrutia GR, Sánchez-Escalante A. 2024. Antioxidant and antibacterial effect of mesquite honey on pork sausages during storage. **Agrociencia** 58(4): 444-458. https://doi.org/ 10.47163/agrociencia.v58i4.3029

Editor in Chief:
Dr. Fernando C. Gómez Merino

Received: June 11, 2023.
Approved: May 17, 2024.
Published in Agrociencia: May 21, 2024.

ABSTRACT

Lipid oxidation and microbial growth are factors associated with meat product quality loss. Different synthetic additives are used to reduce both processes, but their use has been linked to health risks. Thus, the use of natural ingredients has been suggested as a strategy to prevent these factors. The aim of this study was to investigate the effect of mesquite honey on the oxidative stability and microbial growth of uncooked and cooked pork sausages during refrigerated storage. Pollen origin, moisture, and phenolic compound content of collected honey were evaluated, and the data were only presented as descriptive statistics. The effect of a natural additive (mesquite honey at 5 and 10 %) and two synthetic additives (caffeic acid phenethyl ester at 100 and 200 ppm and butylhydroxytoluene at 0.02 %) on oxidative stability and microbial growth were also measured, and the data were subjected to a two-way analysis of variance. All data were obtained from three independent experiments. Results showed that honey samples had a moisture content of 15.8 %, and *Prosopis juliflora* (Sw.) DC. (mesquite) was the dominant pollen identified (> 45 %). In addition, kaempferol, pinocembrin, caffeic acid, and luteolin were the major phenolic compounds in mesquite honey. The inclusion of mesquite honey in uncooked and cooked pork sausages increased oxidative stability by reducing pH and thiobarbituric acid reactive substances (TBARS) and decreased microbial growth by reducing mesophilic and psychrophilic counts. The addition of mesquite honey to uncooked pork sausages reduced color changes and MMb development. Furthermore, during storage, the concentration of caffeic acid phenethyl ester (CAPE) decreased. This study found that mesquite honey has greater potential as a natural antioxidant and antibacterial ingredient for uncooked and cooked pork sausages than synthetic additives.

Keywords: phenolic compounds, biological activity, meat quality.

INTRODUCTION

The appearance of meat and meat products is one of the most important sensory attributes that influence the consumer's intention to purchase a product (Papuc *et al*., 2017). Lipid oxidation and microbial growth have been considered the primary factors that determine food quality loss during storage and changes in sensory attributes. They also cause the degradation of macronutrients (lipids and proteins) and create consumer health problems (Pateiro *et al*., 2021). Therefore, the reduction of these factors is key to improving the quality of meat products and prolonging their shelf life (Papuc *et al*., 2017; Pateiro *et al*., 2021). Synthetic additives have been used to reduce quality loss, increase consumer acceptance, and reduce human health risks (Papuc *et al*., 2017).

Synthetic antioxidants such as butylhydroxytoluene, butylhydroxyanisole, butylhydroxyquinone, and propyl gallate are widely used to reduce catalytic chain reactions, which initiate and spread lipid peroxidation. However, it has been reported that synthetic antioxidants pose safety concerns when used in doses not permitted by the corresponding legal authority (Bensid *et al*., 2022). Therefore, several investigations regarding the use of non-toxic natural preservatives with antioxidant and antimicrobial activity have increased (Pateiro *et al*., 2021).

Honey (produced by *Apis mellifera* bees) is considered a valuable food due to its nutritional components, including macronutrients and micronutrients, as well as bioactive substances like phenolic compounds (Mărgăoan *et al*., 2021). The presence of phenolic acids and flavonoids has been associated with bioactive attributes such as antiviral, anti-inflammatory, antimutagenic, antioxidant, and antibacterial activity. Thus, honey has been previously proposed as a natural food additive to reduce lipid oxidation in raw and cooked turkey breast meat and frozen chicken patties (Antony *et al*., 2000; Alabdulkarim *et al*., 2012), as well as an antimicrobial ingredient in chicken slices (El-Kalyoubi *et al*., 2014). Nevertheless, it has also been reported that the phenolic composition and bioactivity of honeys depend on their floral origin (Salvador *et al*., 2019; Viteri *et al*., 2021). Based on the above, the use of mesquite honey as a natural additive for the meat industry is still limited.

Therefore, the aim of this study was to evaluate the effect of mesquite honey on the oxidative stability and microbial growth of cooked and uncooked pork sausages during storage.

MATERIALS AND METHODS

Honey collection

Honey was collected during the period of maximum mesquite flowering (April–June 2020) in the Ures municipality of central Sonora, Mexico (29° 27′ N, 110° 22′ W; altitude 413 m). In terms of temperature (20–22 °C) and annual rainfall (400–500 mm), the climate in the region may be defined as semi-arid (SMN, 2018). The honey samples

were collected directly from the apiary in order to avoid any type of processing. Five racks were randomly chosen from the strongest hives (25 000 bees per hive), centrifuged (homemade equipment), and stored in 1 L plastic jars at -20 °C in the dark until use.

Honey characterization

Moisture content

The moisture content was determined by the 969.38 method (AOAC, 2020a), with minor changes. The honey sample was homogenized with distilled water at a 1:10 ratio (Vortexer 2, Bohemi, USA), and 100 µL of the obtained solution were transferred to the prism surface of a refractometer. Subsequently, the ratio of the refractive index and the percentage of humidity were registered.

Pollen analysis

Pollen analysis was determined using the acetolysis method (Sereia *et al*., 2011), with minor changes. The honey sample (40 mL) was homogenized with 60 mL of boiling water and centrifuged at 4000 ×g at 4 °C for 10 min (Allegra® X-12R; Palo Alto, CA, USA). The resultant sediment was dehydrated in glacial acetic acid, mixed with an anhydride/sulphuric acid solution at a 9:1 ratio, and subsequently centrifuged. The obtained sediment was mixed with 0.5 mL of glycerine, and 100 µL of the suspension was transferred onto a microscope slide. An optical microscope (Olympus CX31; Tokyo, Japan) was used to register the pollen types (at least 1000 counts). Results were assigned to four percentage classes: above 45 % (predominant), between 15–45 % (secondary), between 3–15 % (important minor), and under 3 % (minor). Plant pollen slides were used to identify floral origins.

Phenolic compounds extraction

The phenolic compounds were extracted using the column separation method (Yung An *et al*., 2016), with minor changes. The honey sample (100 g) was mixed with 500 mL of acidic water at pH 2. The resultant solution was filtered with cotton to remove solid particles, and phenolic compounds were retained in an Amberlite XAD-2 column (pore size 9 mm and particle size 1.2–3 mm). Phenolic compounds were recovered using ethanol, concentrated at 40 °C at 120 rpm (BÜCHI R-200; Flawil, Switzerland) under high vacuum (10–4 mm Hg). The obtained extract was mixed with 5 mL of distilled water, re-extracted with diethyl ether (1:10 ratio), concentrated, and stored at -20 °C in the dark.

Phenolic compounds identification

The phenolic compounds were identified by the HPLC-DAD method (Yung An *et al*., 2016), with minor changes. An HPLC system (Varian ProStar 320; CA, USA) equipped with a diode array detector (DAD) and an Agilent C18 column (150 × 4.6 mm, 5 µm)

were used. The assignment of peaks was performed by comparing the retention time and by skipping the samples with the respective standard, monitored at 290 and 340 nm. Phenolic compound quantification was performed using calibration curves at 15.6–250 μg mL^{-1} ($r \geq 0.99$). The injection volume was set to 20 μL at 1.5 mL min^{-1}, while formic acid (5 %) and methanol were used as elution solvents (A and B, respectively). The gradient program was as follows: 0 % B (0 min), 30 % (10–15 min), 40 % (15–20 min), 45 % (30–50 min), 60 % (50–52 min), 80 % (52–62 min), 100 % (65–70 min), and 0 % (70–71 min).

Caffeic acid phenethyl ester (CAPE) synthesis

CAPE synthesis was carried out by esterification of caffeic acid catalyzed with *p*-toluenesulfonic acid (Nakanishi *et al*., 1991), with minor changes. The reaction mixture contained caffeic acid and phenethyl alcohol (1:15 molar ratio). The resultant solution and catalyst (*p*-toluenesulfonic acid) were dissolved in anhydrous toluene and kept at reflux for four days. The water formed during the esterification reaction was removed using a Dean-Stark trap. Toluene was removed under reduced pressure (0.1 mm Hg) to obtain concentrated CAPE. In addition, column chromatography was used for CAPE purification. Subsequently, CAPE was crystallized, characterized by ^{1}H, ^{13}C, and IR nuclear magnetic resonance (data not shown).

Pork sausages manufacture

Pork meat (*Semimembranosus* m., 48 h *postmortem*) was acquired from a local processor (Norson®). Visible extra-muscular fat was removed. The pork meat was minced through a 4.8 mm orifice plate (Hobart Dayton 4152; OH, USA) and mixed in separate batches with back fat (40 %) and NaCl (1.5 %). The mass was divided into six different treatments: negative control, sausages without additives (T0); natural additive, sausages with 5 and 10 % mesquite honey (T1 and T2, respectively); synthetic additive #1, sausages with 100 and 200 ppm (fat basis) of CAPE (T3 and T4, respectively); synthetic additive #2, sausages with 0.02 % (fat basis) of butylhydroxytoluene (BHT) (T5). The batches were stuffed (Smith RS-2050; NJ, USA) in a natural lamb casing of 15 mm diameter. This process was maintained at low temperatures (< 5 °C). In addition, some samples were cooked until they reached an internal temperature of 71 °C (George Foreman®, USA). Uncooked and cooked pork sausages were placed on a Styrofoam® tray and wrapped with polyvinyl chloride film (17 400 cm^3 O_2 m^{-2}, at 23 °C for 24 h). Uncooked and cooked pork sausages were stored at 2 °C in the dark and opened for subsequent analysis at each sampling point (days 0, 4, 8, 12, and 16).

Physicochemical analysis of pork sausages

pH measurement

Each sampling day, uncooked and cooked pork sausages were homogenized with distilled water (1:10 ratio) at 4500 rpm at 5 °C for 1 min (T25 IKA®; Wilmington, DE,

USA) and pH was measured with a potentiometer (Ion Analyzer 255; New York, NY, USA) according to method 981.12 (AOAC, 2020b).

Lipid oxidation measurement

Lipid oxidation was determined using the thiobarbituric acid reactive substances method (Pfalzgraf *et al*., 1995). Each sampling day, uncooked and cooked pork sausages (10 g) were homogenized at 4500 rpm at 5 °C for 1 min with 20 mL of trichloroacetic acid solution (10 %). The slurry was centrifuged at 3500 ×g at 4 °C for 20 min, and 2 mL of supernatant were homogenized with 2 mL of 2-thiobarbituric acid (TBA) solution (0.02 M). The obtained mixture was incubated at 97 °C for 20 min, and the absorbance was recorded at 531 nm (Genesys 5; Madison, WI, USA). Results were calculated from a 1,1,3,3,-tetramethoxypropane standard curve ($r \geq 0.99$) and expressed as mg of malondialdehyde (MDA) kg^{-1}.

Color changes and metmyoglobin formation

The color changes and metmyoglobin (MMb) formation of uncooked pork sausages were measured by the spectrophotometric method (AMSA, 2012). Each sampling day, uncooked pork sausages were extracted from their packaging and exposed to atmospheric oxygen at 5 °C for 30 min. After that, lightness (L*), redness (a*), and yellowness (b*) were acquired to measure color changes, while the quotient K/S_{525} nm and K/S_{572} nm parameters were recorded to determine the MMb (CM 508d, Konica Minolta Inc.; Tokyo, Japan).

Microbial analysis of sausages

Mesophilic and psychrophilic bacterial growth was measured by the pour plate method (DOF, 1994). Uncooked and cooked pork sausages were homogenized with peptone water (0.1 %) at a 1:9 ratio at 25 °C for 1 min (Seward Stomacher® 400; FL, USA). After that, 1 mL of the resultant dilution was inoculated in a PCA plate and incubated for mesophilic (37 °C for 2 d) and psychrophilic growth (7 °C for 10 d). Results were expressed as $\log_{10}$ colony-forming units (CFU) g^{-1}.

CAPE content of sausages

The CAPE content was determined for uncooked and cooked pork sausages during storage. In this context, 5 g of each sausage was mixed with 100 mL of ethanol, heated in a water bath (60–70 °C for 5 h), and filtered through Whatman filter paper No. 4. The filtrate obtained was concentrated in a rotary evaporator at 64 °C under high vacuum (10–4 mm Hg). The concentrate was homogenized in 10 mL of hexane, and the solvent was evaporated under high vacuum. Subsequently, the concentrate was mixed with 5 mL of methanol, and CAPE was monitored in HPLC equipment under the aforementioned program conditions. The calibration curves were prepared using a mixture of each pork sausage (5 g) with CAPE (200 ppm) for quantification, and linear ranges were determined ($r \geq 0.99$).

Statistical analysis

The data were obtained from at least three independent experimental trials and expressed as the mean ± standard deviation. Pork sausage quality measurements were subjected to a two-way analysis of variance, considering the treatments at six levels (T0–T5) and storage time at five levels (days 0, 4, 8, 12, and 16) as the main effects and a two-way interaction. The Tukey HSD test was carried out for multiple comparisons of means at $p \leq 0.05$ (IBM SPSS Statistics, version 21).

RESULTS AND DISCUSSION

Honey characterization

Moisture content is a quality parameter related to honey maturity, production and harvest method, environmental condition, and nectar source. This parameter is also associated with the granulation and fermentation processes during storage (Rodríguez *et al*., 2012). In this study, the refractive index of the studied honey sample was 1.487, which was used to calculate the humidity percentage (15.8 %). This value is below the limit (20 % of moisture) established by Mexican regulations (DOF, 2018). In addition, the floral origin has also been associated with honey quality (Rodríguez *et al*., 2012; DOF, 2018). Several pollen types were found in the studied honey sample (Table 1). Eight pollen types that belong to three families were identified, mainly from the Fabaceae family (95 % of total pollen grains). While the most common pollen type identified was *Prosopis juliflora* (> 45 %), the honey sample was classified as either monofloral or mesquite honey. In agreement with this study, it has been reported that the mesquite tree (*Prosopis* spp.), which belongs to the Fabaceae family, is one of

Table 1. Pollen type frequencies identified in the honey samples for use in the evaluation of the oxidative stability and microbial growth of pork sausages.

Pollen type	Common name	Family	%
Prosopis juliflora	Mesquite	Fabaceae	67
Olneya tesota	Ironwood	Fabaceae	16
Desmodium spp.	--	Fabaceae	7
Cercidium floridum	Palo Verde	Fabaceae	2
Acacia spp.	--	Fabaceae	2
Brassica spp.	--	Brassicaceae	2
Dalea spp.	--	Fabaceae	1
Citrus spp.	--	Rutaceae	1
Unidentified*	--	--	2
Total	--	--	100

**Ambrosia* spp., Acanthaceae, Malvaceae, and Cactaceae (counts < 1 %).

the primary sources of pollen for honey production in semi-arid regions of Mexico (Medina-Cuéllar *et al*., 2018).

The results showed that mesquite honey is an important source of phenolic acids, esterified phenolic acids, flavones, flavonols, and flavanone compounds. Caffeic acid, kaempferol, pinocembrin, and luteolin were the most abundant in this honey (Table 2). In agreement with this study, it has been reported that there is the presence of caffeic acid, caffeic acid phenethyl ester (CAPE), acacetin, chrysin, galangin, kaempferol, myricetin, pinobanksin, pinocembrin, and luteolin in several mono-floral honeys,

Table 2. Identified and quantified phenolic compounds in mesquite (*Prosopis juliflora)* honey for use in the evaluation of the oxidative stability and microbial growth of pork sausages.

#	Compounds	Retention time (min)	μg 100 g^{-1}
1	Caffeic acid	7.7	157.7 ± 3.12
2	Myricetin	16.2	76.50 ± 1.73
3	Pinobanksin	20.0	(+)
4	Luteolin	23.5	126.25 ± 1.44
5	Kaempferol	25.4	347.70 ± 3.12
6	Apigenin	27.2	33.60 ± 1.62
7	Pinocembrin	30.2	168.10 ± 2.19
8	Chrysin	35.6	11.10 ± 1.27
9	Galangin	36.1	4.75 ± 0.29
10	CAPE	37.0	2.70 ± 0.35
11	Acacetin	38.5	3.35 ± 0.17

(+) compound identified but not quantified. CAPE: caffeic acid phenethyl ester.

although the type of compound and its concentration will depend on the vegetation surrounding the collection area, climate, and geographic region (Mărgăoan *et al*., 2021). Also, it has been demonstrated that honey is an important source of bioactive compounds that exert antioxidant and antimicrobial activity (Salvador *et al*., 2019; Viteri *et al*., 2021). In this regard, the findings obtained highlight that mesquite honey may be employed as a possible antioxidant and antibacterial additive to enhance oxidative stability and reduce the microbial growth of meat products.

Oxidative stability

In this study, a significant effect on pH and thiobarbituric acid reactive substances (TBARS) values ($p \leq 0.001$) was found by the treatment x storage time interaction. At the beginning of the experiment (day 0), pH values (Figure 1A) of uncooked and

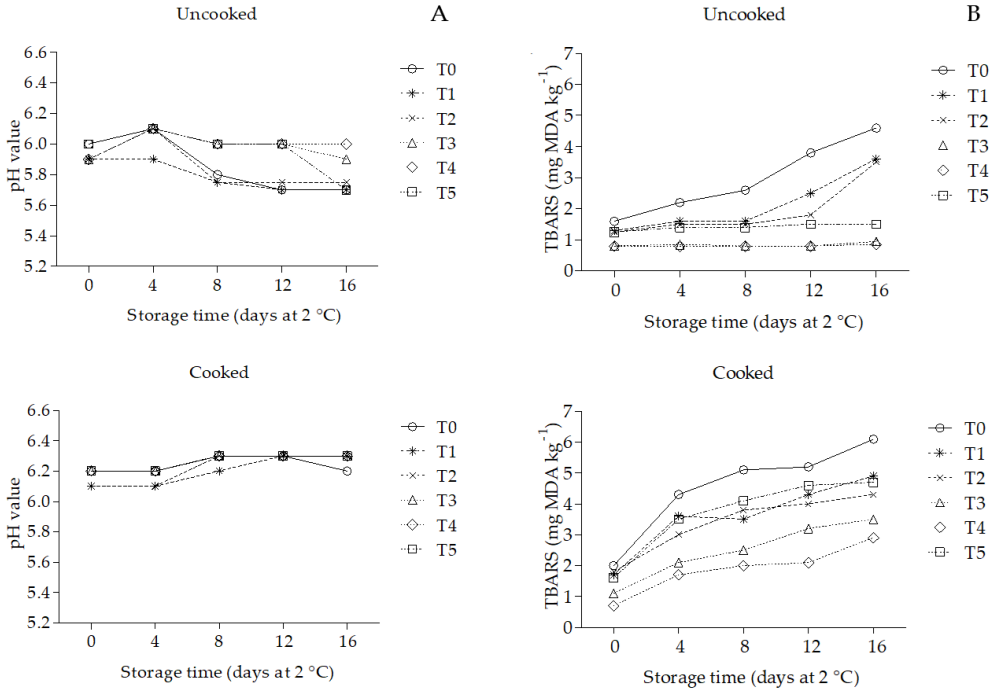

Figure 1. Effect of treatment and storage time on pH and thiobarbituric acid reactive substances (TBARS) values in uncooked and cooked pork sausages. A: effect on pH; B: effect on TBARS. T0: negative control, sausages without additives; T1: natural antioxidant, sausages with 5 % of mesquite honey; T2: natural antioxidant, sausages with 10 % of mesquite honey; T3: synthetic additive #1, sausages with 100 ppm of caffeic acid phenethyl ester (CAPE); T4: synthetic additive #1, sausages with 200 ppm of CAPE; T5: synthetic additive #2, sausages with 0.02 % of butylhydroxytoluene (BHT).

cooked pork sausages were not affected ($p \geq 0.05$) by the inclusion of T1 and T2, as well as T3 and T4 (average pH values of 5.9 and 6.2, respectively). In addition, these values decreased ($p \leq 0.05$) only for uncooked samples during storage. At the end of the experiment (day 16), uncooked and cooked pork sausages treated with T3 and T4 showed the highest ($p \leq 0.05$) pH values compared to T0 (an increase of 3.4 % in this parameter). Additionally, at the beginning of the experiment (day 0), the TBARS values (Figure 1B) of uncooked and cooked pork sausages were reduced ($p \leq 0.05$) by the inclusion of additives (T3 and T4 > T1 and T2 > T5); however, these values increased ($p \leq 0.05$) during storage. At the end of the experiment (day 16), uncooked pork sausages treated with T3 and T4 (80.4 % inhibition), T1 and T2 (22.8 % inhibition), and T5 (67.4 % inhibition) showed lower TBARS values than T0 ($p \leq 0.05$). Cooked pork sausages treated with T3 and T4 (47.5 % inhibition), T1 and T2 (24.6 % inhibition), and T5 (23 % of inhibition) showed lower TBARS values than T0 ($p \leq 0.05$).

Although pH and TBARS data on the effect of the inclusion of mesquite honey in pork sausages during storage is still limited, it has been reported that a natural additive obtained from a honeybee product reduces pH and TBARS changes in an uncooked and cooked meat product during storage, which is associated with the antioxidant effect of the identified phenolic compounds, mainly attributed to the presence of CAPE (Vargas-Sánchez *et al*., 2015, 2019). In disagreement with this study, Yücel *et al*. (2005) reported a not significant effect on pH values of marinated cooked chicken breast incorporated with honey (20 and 30 %; undeclared floral origin) and stored at 4 °C for 7 d; however, a reduction in pH values of chicken meat was observed during storage. Also, a not significant effect was observed on pH values of cooked turkey slices incorporated with 5 and 15 % of dry honey (undeclared floral origin) and stored at 4 °C for 12 weeks under vacuum (Antony *et al*., 2006).

In agreement with this study, a reduction in TBARS values was reported on cooked ground turkey incorporated with 5 % of acacia, clover, soy, and buckwheat honey (53.2, 61.6, 65.1, and 79.4 %, respectively) stored at 4 °C for 3 d (McKibben and Engeseth, 2002). Also, clover and wildflower honey decreased TBARS values of beef patties stored at 4 °C for 12 d and at -18 °C for 45 d (Johnston *et al*., 2005). Sampaio *et al*. (2012) reported a higher reduction in TBARS values for chicken thigh and breast (70 and 82 % inhibition, respectively) incorporated with 5 and 10 % of orange honey than BHT (28.6 and 30 % inhibition, respectively) stored at 4 °C for 4 d. Another study demonstrated that the incorporation of acacia honey (5 and 10 %) reduced TBARS values of fried chicken patties stored at -18 °C for 60 d (Alabdulkarim *et al*., 2012). Similarly, a decrease in TBARS values (26.7 %) was reported in pork sausages incorporated with honey (1.15 %, multifloral origin) stored at 2 °C for 20 d in the dark, which was associated with an increase in phenolic compounds and antiradical activity during storage (Półtorak *et al*., 2018). Recently, a reduction of TBARS values was reported in chicken sausages treated with 2 and 4 % of honey (undeclared floral origin) stored at -20 °C for 30 d (Ali *et al*., 2022).

Meat color is a sensory attribute that has a primary influence on consumers' propensity to purchase it, as it changes from red to brown during storage, reducing its acceptability. (Passetti *et al*., 2019). Also, MMb formation has been associated with color changes in meat and meat products due to high MMb values related to the oxidation process. Nevertheless, these parameters can be affected by changes in the pH and TBARS values of meat and meat products during storage (Khan *et al*., 2015; Passetti *et al*., 2019). In our study, a significant effect ($p \leq 0.001$) on color and MMb formation values (Figure 2) was found by the treatment x storage time interaction. No significant effect ($p \geq 0.05$) was shown in L* and b* values during storage (average values of 60.8 and 18.3, respectively) for uncooked pork sausages. However, a* and MMb formation values decreased and increased during storage, respectively ($p \leq 0.05$). At the end of the experiment (day 16), samples incorporated with antioxidants T1 and T2 (29.4 %) > T3, T4, and T5 (18.1 %) increased a* values compared to T0 ($p \leq 0.05$). In addition, T1 and T2 (32.1 %) > T3, T4, and T5 (12.3 %) reduced MMb formation values compared to T0 ($p \leq 0.05$).

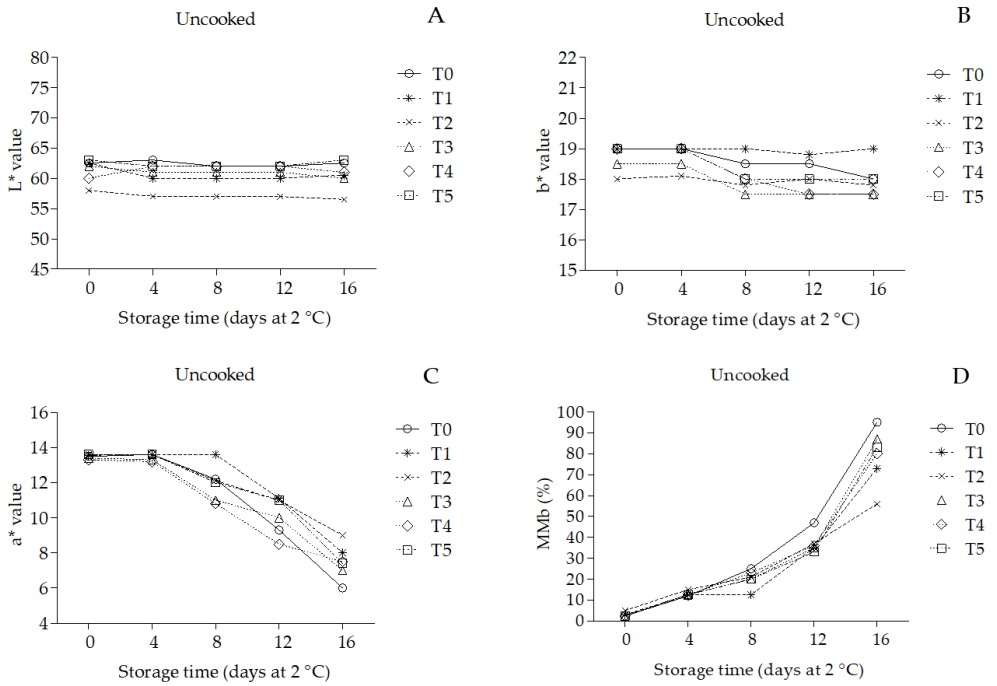

Figure 2. Effect of treatment and storage time on color changes and MMb formation values of uncooked pork sausages. A–D: effect on color changes; D: effect on MMb formation values. T0: negative control, sausages without additives; T1: natural antioxidant, sausages with 5 % of mesquite honey; T2: natural antioxidant, sausages with 10 % of mesquite honey; T3: synthetic additive #1, sausages with 100 ppm of caffeic acid phenethyl ester (CAPE); T4: synthetic additive #1, sausages with 200 ppm of CAPE; T5: synthetic additive #2, sausages with 0.02 % of butylhydroxytoluene (BHT).

Although color and MMb formation data on the effect of the inclusion of mesquite honey in pork sausages during storage is still limited, it has been reported that a natural additive obtained from a honeybee product reduces the color and MMb formation changes of uncooked meat products during storage, which is associated with the antioxidant effect of the identified phenolic compounds (Vargas-Sánchez *et al*., 2015, 2019). In disagreement with this study, Yücel *et al*. (2005) reported that the inclusion of honey (20 and 30 %; undeclared floral origin) in marinated chicken breast reduced color changes (b* value) during storage at 4 °C for 7 d. Although certain phenolic compounds were found in greater concentrations in mesquite honey, a previous study revealed through computational methods (DFT, density functional theory) that CAPE exerted the highest antiradical potential when compared with other phenolic compounds (Vargas-Sánchez *et al*., 2015).

Microbial growth

In this study, a significant effect ($p \leq 0.001$) on mesophilic and psychrophilic counts (Figure 3) was found by the treatment x storage time interaction. At the beginning of the experiment (day 0), no significant effect ($p \geq 0.05$) was found. However, microbial growth increased during storage ($p \leq 0.05$). At the end of the experiment (day 16), samples treated with T1 and T2 reduced mesophilic counts ($p \leq 0.05$) for uncooked and cooked pork sausages (13.3 and 15.2 %, respectively) when compared to T0, while samples treated with T4 also reduced mesophilic growth in uncooked and cooked pork sausages (8.1 and 7.1 %, respectively). Furthermore, samples treated with T1 and T2 showed the lowest ($p \leq 0.05$) psychrophilic counts in uncooked (20.6 and 33.8 %, respectively) and cooked pork sausages (36.4 and 58.2 %, respectively).

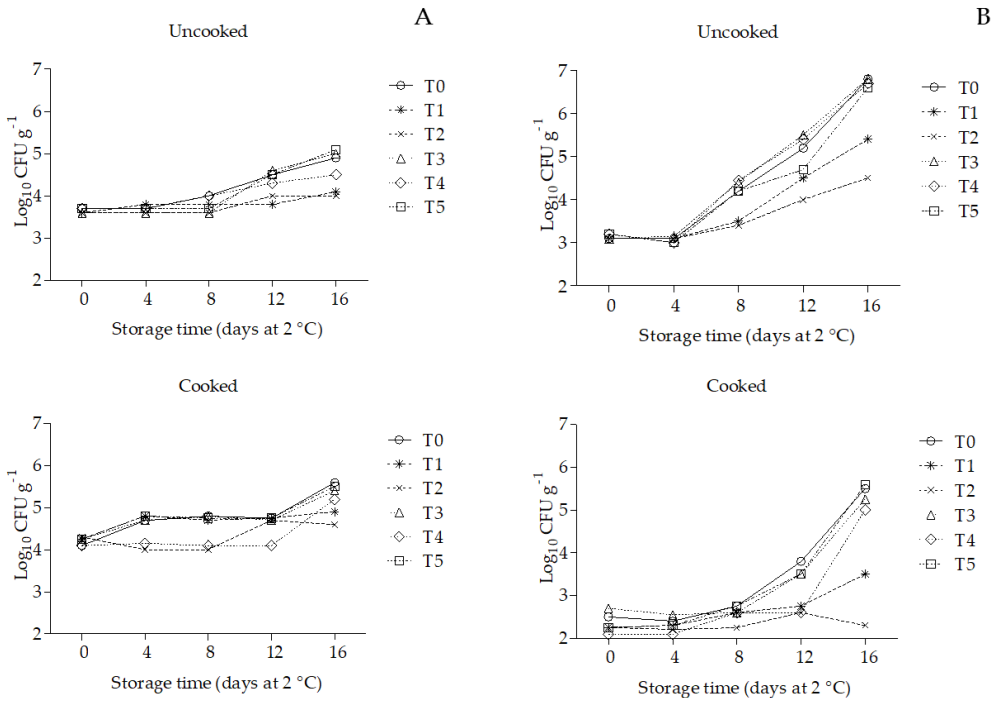

Figure 3. Effect of treatment and storage time on microbial growth values of uncooked and cooked pork sausages. A: mesophilic counts; B: psychrophilic counts. T0: negative control, sausages without additives; T1: natural antioxidant, sausages with 5 % of mesquite honey; T2: natural antioxidant, sausages with 10 % of mesquite honey; T3: synthetic additive #1, sausages with 100 ppm of caffeic acid phenethyl ester (CAPE); T4: synthetic additive #1, sausages with 200 ppm of CAPE; T5: synthetic additive #2, sausages with 0.02 % of butylhydroxytoluene (BHT).

In agreement with this study, a decrease in mesophilic counts (19.1 %) was reported in pork sausages incorporated with 1.15 % of honey (multifloral origin) stored at 2 °C for 20 d in the dark (Półtorak *et al*., 2018). El-Kalyoubi *et al*. (2014) reported that the

incorporation of 5, 10, and 20 % of honey (undeclared floral origin) into chicken slices reduced mesophilic counts (4.0, 3.4, and 5.5 %, respectively) stored at 4 °C for 14 d. Also, McKibben and Engeseth (2002) reported that Chinese milk vetch, acacia, mixed-breed, and buckwheat honey decreased by 82.7, 84.5, 81.8, and 83.6 % the mesophilic counts of raw beef stored at 10 °C for 7 days in the dark. A significant effect was observed in mesophilic counts of marinated cooked chicken breast with honey (20 and 30 %) during storage (Yücel *et al*., 2005). In addition, the literature indicates that the antimicrobial effects of CAPE are probably based on RNA polymerase and cellular protein inhibition (Arasoglu *et al*., 2015).

CAPE content in pork sausages

In this study, a significant effect ($p \leq 0.001$) on CAPE content (Figure 4) was found by the treatment x storage time interaction. At the beginning of the experiment (day 0), uncooked and cooked pork sausages incorporated with T4 showed the highest ($p \leq 0.05$) CAPE values (87 and 130.6 ppm, respectively). However, CAPE content decreased ($p \leq 0.05$) during storage. No detectable CAPE content ($p \geq 0.05$) was shown in the rest of the treatments. At the end of the experiment (day 16), uncooked and cooked pork sausages incorporated with T4 showed the highest ($p \leq 0.05$) CAPE content (62.6 and 89.4 ppm, respectively). In agreement with this study, it was demonstrated that the incorporation of honey and other natural sources rich in phenolic compounds increases phenolic bioavailability in meat products, and storage influenced this content (Półtorak *et al*., 2018; Vargas-Sánchez *et al*., 2019).

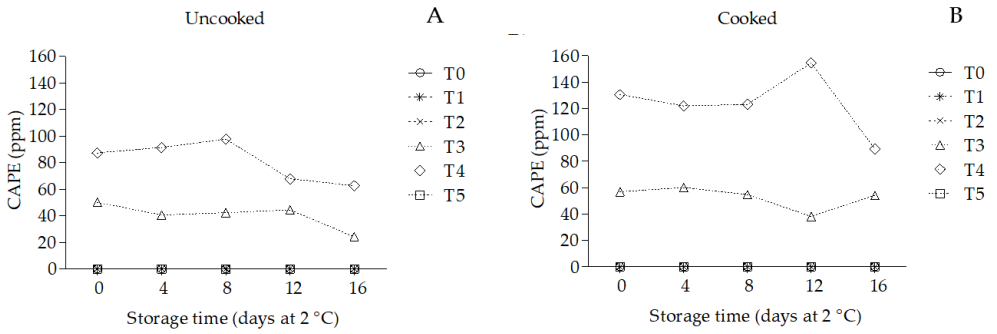

Figure 4. Effect of treatment and storage time on caffeic acid phenethyl ester (CAPE) content of pork sausages. A: cooled sausages; B: uncooked sausages. T0: negative control, sausages without additives; T1: natural antioxidant, sausages with 5 % of mesquite honey; T2: natural antioxidant, sausages with 10 % of mesquite honey; T3: synthetic additive #1, sausages with 100 ppm of CAPE; T4: synthetic additive #1, sausages with 200 ppm of CAPE; T5: synthetic additive #2, sausages with 0.02 % of butylhydroxytoluene (BHT).

CONCLUSIONS

The evaluated honey samples revealed acceptable humidity levels that complied with Mexican regulations. According to the pollen analysis, the floral origin of the sample was mesquite (*Prosopis juliflora*). Mesquite honey showed the presence of phenolic compounds, including phenolic acids and flavonoids. The inclusion of mesquite honey in uncooked and cooked pork sausages increased oxidative stability by reducing pH and thiobarbituric acid reactive substances and decreased microbial growth by reducing mesophilic and psychrophilic counts. A reduction in color changes and metmyoglobin formation was also observed in uncooked pork sausages. In addition, a reduction in caffeic acid phenethyl ester content was observed during storage. In comparison to artificial additives, this study found that mesquite honey has great potential as a natural addition to both cooked and uncooked pork sausages.

ACKNOWLEDGEMENTS

The authors gratefully acknowledge CONAHCyT (*Investigadoras e Investigadores por México*) for the fellowship of the project No. 739.

REFERENCES

Alabdulkarim B, Bakeet ZAN, Arzoo S. 2012. Effect of frying oils on quality characteristics of frozen chicken patties incorporated with honey. African Journal of Biotechnology 11 (12): 2985–2992. https://doi.org/10.5897/ajb11.3389

Ali MS, Rahman MM, Habib M, Kabir MH, Hashem MA, Azad MAK. 2022. Quality of spent hen sausages incorporated with bee honey. Meat Research 2 (1). https://doi.org/10.55002/mr.2.1.9

AMSA (American Meat Science Association). 2012. AMSA meat color measurement guidelines. American Meat Science Association: Champaign, IL, USA. 136 p.

Antony S, Rieck JR, Dawson PL. 2000. Effect of dry honey on oxidation in turkey breast meat. Poultry Science 79 (12): 1846–1850. https://doi.org/10.1093/ps/79.12.1846

Antony S, Rieck JR, Acton JC, Han IY, Halpin EL, Dawson PL. 2006. Effect of dry honey on the shelf life of packaged turkey slices. Poultry Science 85 (10): 1811–1820. https://doi.org/10.1093/ps/85.10.1811

AOAC (Association of Official Analytical Chemists). 2020a. AOAC 969.38-1969, Moisture in honey. Gaitherburg, MD, USA. http://www.aoacofficialmethod.org/index.php?main_page=product_info&products_id=2876 (Retrieved: January 2023).

AOAC (Association of Official Analytical Chemists). 2020b. AOAC 981.12-1982, pH in acidified foods. Gaitherburg, MD, USA. http://www.aoacofficialmethod.org/index.php?main_page=product_info&products_id=1159 (Retrieved: January 2023).

Arasoglu T, Derman S, Mansuroglu B. 2015. Comparative evaluation of antibacterial activity of caffeic acid phenethyl ester and PLGA nanoparticle formulation by different methods. Nanotechnology 27 (2): 025103. https://doi.org/10.1088/0957-4484/27/2/025103

Bensid A, El Abed N, Houicher A, Regenstein JM, Özogul F. 2022. Antioxidant and antimicrobial preservatives: Properties, mechanism of action and applications in food–a review. Critical

Reviews in Food Science and Nutrition 62 (11): 2985–3001. https://doi.org/10.1080/10408398.2020.1862046

El-Kalyoubi MH, Khalaf MM, Nadir AS., Wafaa MA, Mansour ME. 2014. Bee honey effect against microbial and oxidation in chicken slices. Middle East Journal of Applied Sciences 4 (4): 884–893.

Johnston JE, Sepe HA, Miano CL, Brannan RG, Alderton AL. 2005. Honey inhibits lipid oxidation in ready-to-eat ground beef patties. Meat Science 70 (4): 627–631. https://doi.org/10.1016/j.meatsci.2005.02.011

Khan A, Allen K, Wang X. 2015. Effect of Type I and Type II antioxidants on oxidative stability, microbial growth, pH, and color in raw poultry meat. Food and Nutrition Sciences 6 (16): 1541. https://doi.org/10.4236/fns.2015.616159

Mărgăoan R, Topal E, Balkanska R, Yücel B, Oravecz T, Cornea-Cipcigan M, Vodnar DC. 2021. Monofloral honeys as a potential source of natural antioxidants, minerals and medicine. Antioxidants 10 (7): 1023. https://doi.org/10.3390/antiox10071023

McKibben J, Engeseth NJ. 2002. Honey as a protective agent against lipid oxidation in ground turkey. Journal of Agricultural and Food Chemistry 50 (3): 592–595. https://doi.org/10.1021/jf010820a

Medina-Cuéllar SE, Tirado-González DN, Portillo-Vázquez M, López-Santiago MA, Franco-Olivares VH. 2018. Environmental implications for the production of honey from mesquite (*Prosopis laevigata*) in semi-arid ecosystems. Journal of Apicultural Research 57 (4): 507–515. https://doi.org/10.1080/00218839.2018.1454377

Nakanishi K, Oltz EM, Grunberger D. 1991. Caffeic acid esters and methods of producing and using same. U.S. Patent No. 5,008,441. Washington, DC, USA. 12 p.

DOF (Diario Oficial de la Federación). 1994. NORMA Oficial Mexicana NOM-110-SSA1-1994. Preparación y dilución de muestras de alimentos para su análisis microbiológico. Gobierno de México. Secretaría de Salud. Ciudad de México, México. http://www.salud.gob.mx/unidades/cdi/nom/110ssa14.html (Retrieved: May 2020).

DOF (Diario Oficial de la Federación). 2018. NORMA Oficial Mexicana NOM-004-SAG/GAN-2018. Producción de miel y especificaciones. Gobierno de México. Secretaría de Agricultura y Desarrollo Rural. Ciudad de México, México. http://dof.gob.mx/nota_detalle.php?codigo=5592435&fecha=29/04/2020 (Retrieved: July 2021).

Papuc C, Goran GV, Predescu CN, Nicorescu V, Stefan G. 2017. Plant polyphenols as antioxidant and antibacterial agents for shelf-life extension of meat and meat products: Classification, structures, sources, and action mechanisms. Comprehensive Reviews in Food Science and Food Safety 16 (6): 1243–1268. https://doi.org/10.1111/1541-4337.12298

Passetti RAC, Resconi VC, Çakmakçı C, Campo MM, Kirinus JK, Passetti LCG, Guerrero A, do Prado IN, Sañudo C. 2019. Number of consumers and days of display necessary for the assessment of meat colour acceptability. Food Research International 121: 387–393. https://doi.org/10.1016/j.foodres.2019.03.036

Pateiro M, Domínguez R, Lorenzo JM. 2021. Recent research advances in meat products. Foods 10 (6): 1303. https://doi.org/10.3390/foods10061303

Pfalzgraf A, Frigg M, Steinhart H. 1995. Alpha-tocopherol contents and lipid oxidation in pork muscle and adipose tissue during storage. Journal of Agricultural and Food Chemistry 43 (5): 1339–1342. https://doi.org/10.1021/jf00053a039

Półtorak A, Marcinkowska-Lesiak M, Lendzion K, Moczkowska M, Onopiuk A, Wojtasik-Kalinowska I, Wierzbicka A. 2018. Evaluation of the antioxidant, anti-inflammatory and

antimicrobial effects of catuaba, galangal, roseroot, maca root, guarana and polyfloral honey in sausages during storage. LWT-Food Science and Technology 96: 464–370. https://doi.org/10.1016/j.lwt.2018.05.035

Rodríguez BA, Mendoza S, Iturriga MH, Castaño-Tostado E. 2012. Quality parameters and antioxidant and antibacterial properties of some Mexican honeys. Journal of Food Science 77 (1): C121–C127. https://doi.org/10.1111/j.1750-3841.2011.02487.x

Salvador L, Guijarro M, Rubio D, Aucatoma B, Guillén T, Vargas-Jentzsch P, Ciobotă V, Stolker L, Ulic S, Vásquez L *et al*. 2019. Exploratory monitoring of the quality and authenticity of commercial honey in Ecuador. Foods 8 (3): 105. https://doi.org/10.3390%2Ffoods8030105

Sampaio GR, Saldanha T, Soares RAM, Torres EAFS. 2012. Effect of natural antioxidant combinations on lipid oxidation in cooked chicken meat during refrigerated storage. Food Chemistry 135 (3): 1383–1390. https://doi.org/10.1016/j.foodchem.2012.05.103

Sereia MJ, Alves EM, Toledo VA, Marchini LC, Serine ES, Faquinello P, de Almeida D, Moreti AC. 2011. Physicochemical characteristics and pollen spectra of organic and non-organic honey samples of *Apis mellifera* L. Anais da Academia Brasileira de Ciências 83 (3): 1077–1090. https://doi.org/10.1590/S0001-37652011000300026

SMN (Servicio Meteorológico Nacional). 2018. Temperature report in Mexico. Gobierno de México. Comisión Nacional del Agua. Servicio Meteorológico Nacional. Ciudad de México, México. https://smn.conagua.gob.mx/es/climatologia/pronostico-climatico/temperatura-form (Retrieved: May 2020).

Vargas-Sánchez RD, Mendoza-Wilson AM, Torrescano-Urrutia GR Sánchez-Escalante A. 2015. Antiradical potential of phenolic compounds fingerprints of propolis extracts: DFT approach. Computational and Theoretical Chemistry 1066: 7–13. https://doi.org/10.1016/j.comptc.2015.05.003

Vargas-Sánchez RD, Torrescano-Urrutia GR, Torres-Martínez BDM, Pateiro M, Lorenzo J M, Sánchez-Escalante A. 2019. Propolis extract as antioxidant to improve oxidative stability of fresh patties during refrigerated storage. Foods 8 (12): 614. https://doi.org/10.3390/foods8120614

Viteri R, Zacconi F, Montenegro G, Giordano A. 2021. Bioactive compounds in *Apis mellifera* monofloral honeys. Journal of Food Science 86 (5): 1552–1582. https://doi.org/10.1111/1750-3841.15706

Yücel B, Önenç A, Bayraktar H, Açikgöz Z, Altan Ö. 2005. Effect of honey treatment on some quality characteristics of broiler breast meat. Journal of Applied Animal Research 28 (1): 53–56. https://doi.org/10.1080/09712119.2005.9706788

Yung An C, Hossain MM, Alam F, Islam MA, Khalil MI, Alam N, Gan SH. 2016. Efficiency of polyphenol extraction from artificial honey using C18 cartridges and Amberlite® XAD-2 resin: A comparative study. Journal of Chemistry: 8356739. https://doi.org/10.1155/2016/8356739

Agrociencia

CHIA SEED GERMINATION AND EXTRUSION TO INCREASE NUTRITIONAL VALUE, PHENOLIC COMPOUNDS, GABA, ANTIOXIDANT ACTIVITY, AND *in vitro* ANTIHYPERTENSIVE POTENTIAL

Luisa Fernanda **Madrigales-Reátiga**[1], Yazmín Alejandra **Castro-Montoya**[1], Cuauhtémoc **Reyes-Moreno**[1], Roberto **Gutiérrez-Dorado**[1], Fernando **Salas-López**[2], Janitzio Xiomara Korina **Perales-Sánchez**[1*]

[1]Universidad Autónoma de Sinaloa. Facultad de Ciencias Químico-Biológicas (FCQB). Calzada de las Américas Nte, 2771, Ciudad Universitaria, Burócrata, Culiacán, Sinaloa, Mexico. C. P. 80030.
[2]Universidad Autónoma de Occidente. Departamento de Ciencas de la Salud. Blvd. Lola Beltrán y Blvd. Rolando Arjona, 4 de Marzo, Culiacán, Sinaloa, Mexico. C. P. 80020.
* Author for correspondence: janitzio.perales@uas.edu.mx

Citation: Madrigales-Reátiga LF, Castro-Montoya YA, Reyes-Moreno C, Gutiérrez-Dorado R, Salas-López F, Perales-Sánchez JXK. 2024. Chia seed germination and extrusion to increase nutritional value, phenolic compounds, GABA, antioxidant activity, and *in vitro* antihypertensive potential. **Agrociencia** 58(4): 459-473. https://doi.org/ 10.47163/agrociencia.v58i4.3043

Editor in Chief:
Dr. Fernando C. Gómez Merino

Received: July 09, 2023.
Approved: May 16, 2024.
Published in Agrociencia: May 29, 2024.

ABSTRACT

A functional ingredient derived from extruded, germinated chia seeds would be an excellent substitute to improve the nutritional and nutraceutical quality of widely consumed foods in Mexico. The aim of this study was to create a functional ingredient with outstanding nutritional and nutraceutical value and microbiological safety by processing chia seeds using a combined germination and extrusion process under optimal conditions. The implementation of optimized germination and extrusion techniques was hypothesized to boost the nutritional value, phenolic compounds, γ-aminobutyric acid (GABA), antioxidant activity, *in vitro* antihypertensive potential, and microbiological stability of the functional flour obtained from chia seeds. Germinated chia flour (GCF) was produced under optimized germination conditions (21 °C for 157 h). To determine the optimal conditions for GCF extrusion, the response surface methodology was used. A central composite rotatable design was applied with two factors [extrusion temperature (ET, 50–160 °C) and screw velocity (SV, 50–240 rpm)] and five levels. Total phenolic compounds (TPC), antioxidant activity (AoxA), and *in vitro* protein digestibility (IVPD) were selected as response variables. The best combination of extrusion process variables to produce extruded germinated chia flour (EGCF) with maximum TPC, AoxA, and IVPD values was ET = 147 °C and SV = 170 rpm. EGCF had higher protein content (88 %), total dietary fiber (13 %), phenolic compounds (57 %), GABA (933 %), and antioxidant activity (2,2'-azino-bis(3-ethylbenzothiazoline-6-sulfonic) acid (ABTS), 110 %; 2,2-diphenyl-1-picrylhydrazyl (DPPH), 114 %) than raw chia flour (RCF). Regarding *in vitro* antihypertensive potential, germinated-extruded chia flour presented the best IC_{50} value. The main findings of this research show that extrusion processing applied in combination with germination is a promising strategy for increasing the nutritional value, bioactive compound content, antioxidant and antihypertensive potential, and microbiological stability of functional flours obtained from pseudocereal seeds.

Keywords: Functional ingredient, optimization, nutraceutical, microbiological stability.

INTRODUCTION

Chia (*Salvia hispanica*) is a flowering herbaceous plant from the Lamiaceae family. Its seeds, which have a high nutritional and nutraceutical value, are considered functional foods. Chia seeds are a good source of proteins (15–24 %) and lipids (25–40 %). They also contain B vitamins and have a higher mineral content than cereals. In addition, due to their dietary fiber content (35 %), they have a positive effect on insulinemic and glycemic responses, reducing cholesterolemia and some chronic disorders (CD), such as cardiovascular diseases. Chia seeds contain bioactive compounds such as polyphenolic compounds (phenolic acids, flavonols, and isoflavones) that are associated with antioxidant properties and prevention against CD (Ghafoor *et al*., 2020; Hernández-Pérez *et al*., 2020).

Germination is an inexpensive and sustainable process suitable for the development of functional foods and ingredients. This process offers several advantages, including improved nutritional value (increased digestibility of nutrients) and increased content of bioactive compounds (γ-aminobutyric acid (GABA) and phenolic compounds) that improve antioxidant activity (Bermejo and Munné-Bosch, 2023). Chia sprouts have enormous potential in the agri-food industry as an ingredient in new food products. Their use is an effective strategy to improve food nutritional and nutraceutical value (Abdel-Aty *et al*., 2021). Germinated seeds are consumed fresh, without any process that eradicates pathogenic organisms that may proliferate due to processing conditions.

The ingestion of sprouts has been associated with the appearance of disease outbreaks transmitted by food consumption. Due to this microbiological problem, it is necessary to apply technologies that ensure microbiological quality and preserve the high content of bioactive compounds and nutraceutical properties generated during seed germination. Among the processing techniques that have this potential, extrusion stands out because, in addition to ensuring the microbiological stability of the sprouts, it improves the nutritional, physicochemical, and techno-functional properties, as well as the palatability of the foods (Paucar-Menacho *et al*., 2022). Extrusion also applies high temperatures, pressure, and shear force for a brief period of time and is extremely effective in reducing energy usage and water pollution.

It is increasingly evident that the adoption of a healthy diet is necessary to prevent the risk of diseases as well as to maintain environmental sustainability and food security. Germination-extrusion has been used as a combined process to produce functional foods, such as functional flours, with better nutritional, nutraceutical, and sensory properties, as well as higher microbiological quality by eliminating the microbial load of the sprouts when applying the extrusion process. The use of germinated-extruded flours for partial or total replacement of common cereals represents an opportunity for the development of new foods (Albarracín *et al*., 2019; Paucar-Menacho *et al*., 2022).

This study had the objective to develop a functional ingredient with high nutritional and nutraceutical value through the combination of germination and extrusion technologies in chia seeds. The working hypothesis was that the combination of procedures (germination and extrusion) used on chia seeds increases nutritional value, bioactive chemicals, antioxidant activity, and *in vitro* antihypertensive potential.

MATERIALS AND METHODS

Chia seed germination and extrusion

Chia seeds were purchased at the "Rafael Buelna" market in Culiacán, Sinaloa, Mexico. Chia germination was carried out according to Gómez-Favela *et al*. (2017). Seed lots weighing 200 g were distributed on sterilized trays and placed in germination chambers (germination temperature: 21 °C, germination time: 157 h). Light and dark periods (50/50 %) were used during the germination process. The sprouts were dried at 50 °C for 8 h) and ground (US 80 mesh) to obtain germinated chia flour (GCF).

To obtain extruded flour, GCF lots weighing 500 g were defatted using an oil press (lipids up to 8 % dry weight (DW)). Water was added to the defatted GCF until a humidity of 17 % was achieved (4–8 °C, 12 h). Extrusion was carried out in a Mod 20 DN single screw extruder (Brabender Instruments, Inc.; NJ, USA). The operating conditions of the extruder were: extrusion temperature (ET) = 50–160 °C and screw velocity (SV) = 50–240 rpm. The extrudates were cooled, ground (80 mesh), and packaged in plastic bags.

Response surface methodology (RSM)

RSM was used to find the best combination of extrusion process variables to obtain extruded germinated chia flour (EGCF) with maximum total phenolic compounds (TPC), antioxidant activity (AoxA), and *in vitro* protein digestibility (IVPD) values. A central composite rotatable experimental design was selected with two factors (ET: 50, 66.1, 105, 143.9, and 160 °C; SV: 50, 77.8, 14.5, 212.2, and 240 rpm) and five levels of variation. The regression procedure was applied, non-significant terms ($p > 0.1$) were eliminated, and a new polynomial was used to obtain a prediction model for each response variable. The conventional graphic method was applied as an optimization technique to obtain maximum TPC, AoxA, and IVPD values. The prediction models were used to graphically represent the system. The contour plots of each variable response were superimposed to obtain a contour plot for the observation and selection of the optimal combination of ET and SV to produce EGCF. For RSM analyses, Design Expert statistical software (Stat-Ease; Minneapolis, MN, USA) was used.

Free and bound phenolic compounds extraction

Free and bound phenolic compounds were extracted in accordance with Salas-López *et al*. (2018). One gram of dry sample was mixed with an ethanol-water solution (80–20 v/v) and agitated for 10 min. The supernatant was recovered by centrifugation (3000 xg, 10 min) (Sorvall RC5C, Sorvall Instruments, Dupont; Wilmington, DE, USA). The pellets from the extraction of free phenolic compounds were hydrolyzed (2 M NaOH) and neutralized (HCl). The final solution was extracted with ethyl acetate and evaporated. Extracts were reconstituted in 2 mL of 50 % methanol and stored at -20 °C. All extractions were performed in triplicate.

Chemical characterization

The chemical composition of chia flour was determined using the AOAC (2012) chemical methods. The TPC content of free and bound phenolic extracts was determined colorimetrically (Folin-Ciocalteu reagent) according to Servín de la Mora-López *et al*. (2018). AoxA was assessed using the 2,2′-azino-bis(3-ethylbenzothiazoline-6-sulfonic) acid (ABTS) (Salas-López *et al*., 2018) and 2,2-diphenyl-1-picrylhydrazyl (DPPH) assays (Servín-de la Mora-López *et al*., 2018). The extracts were evaluated against gallic acid and Trolox standards, respectively. The TPC content results were expressed as mg of gallic acid equivalents (GAE) 100 g^{-1} (DW). The AoxA was expressed as μmol of Trolox equivalents (TE) 100 g^{-1} (DW). The γ-aminobutyric acid (GABA) content was determined using the methodology reported by Watchararparpaiboon *et al*. (2010) and expressed as mg of GABA 100 g^{-1} sample (DW). All measurements were performed in triplicate.

Nutritional properties

The essential amino acid composition, IVPD, and protein efficiency ratio were determined in accordance with Salas-López *et al*. (2018). The essential amino acid composition was determined using an analytical scale (4.6 × 250 mm) hypersil ODS C18 column (SGE; Dandenong, Australia) kept at 38 °C and connected to an HPLC system (GBC; Dandenong, Australia) equipped with a fluorescence detector > LC 5100 set at 270 and 316 nm for excitation and emission, respectively. Tryptophan was detected at 280 nm with an ultraviolet detector. IVPD was evaluated using a multienzyme system. The chemical score (CS) was calculated as follows:

$$CS = (\text{Content of the most limiting } EAA/REAAR) \times 100$$

where *EAA* is the essential amino acid, and *REAAR* is the recommended amino acid requirement for three-year old children and older, adolescents, and adults (FAO, 2013). The calculated protein efficiency ratio (C-PER) is based on the IVPD and the essential amino acid composition of the optimized mixture. All determinations were made in triplicate.

Antihypertensive potential (IC_{50})

Angiotensin-converting enzyme (ACE) inhibitory activity, recognized as antihypertensive potential (IC_{50}), was evaluated in free and bound phenolic extracts using the Dojindo ACE Kit-WST test kit (Dojindo Laboratories; Kumamoto, Japan). This method is based on the detection of a colorimetric indicator after a redox reaction at an absorbance of 450 nm measured with a microplate reader (Synergy™ HT Multi-Detection, BioTek, Inc.; Winooski, VT, USA). The ACE inhibitory activity of the phenolic extracts was calculated using the following equation:

$$\% \text{ inhibition} = \left[\frac{(\text{Abs control} - \text{Abs extract})}{\text{Abs control}}\right] \times 100$$

where Abs_{450} extract is the absorbance of the reaction solution containing phenolic extract, Abs_{450} control is the absorbance of the reaction solution without phenolic extract, and Abs_{450} blank is the absorbance of the reaction solution with enzyme and without substrate and phenolic extract. IC_{50} values were calculated from different concentrations of the phenolic extracts and ACE inhibitory activity values using the Prism v5 software (GraphPad Prism) (Argüelles-López *et al*., 2018).

Microbiological stability

The evaluation of the microbiological stability of raw chia flour (RCF), GCF, and EGCF required the preparation of a flour suspension in 1 % peptone water (10 g of flour in 90 mL peptone water) for each sample. The count of total coliforms was carried out according to NOM-113-SSA1-1994 (DOF, 1994c). Decimal dilutions up to 10^{-5} were prepared, inoculating 1 mL in violet-red bile glucose agar by the mass seeding method. The plates were incubated at 35 °C for 24 h. The count of aerobic mesophilic microorganisms was carried out according to NOM-092-SSA1-1994 (DOF, 1994a) using plate count agar (Biokar). Plates were inoculated with 1 ml of the corresponding dilutions and incubated at 35 °C for 48 h. The mold count was carried out according to NOM-111-SSA1-1994 (DOF, 1994b); decimal dilutions up to 10^{-3} were prepared, inoculating 1 mL in 10 mL of acidified potato dextrose agar (PDA) by the mass homogenization method. The plates were incubated for 3–4 d at 25 °C. The counts were performed in triplicate, and the results were expressed as colony-forming units per gram (CFU g^{-1}).

Statistical analysis

The experimental results of the chemical composition, physicochemical and functional properties, and microbiological stability of the flours were subjected to a one-way analysis of variance (ANOVA), followed by Tukey's multiple range test ($p \leq 0.05$). These analyses were conducted using Statgraphics Plus 6.0 software.

RESULTS AND DISCUSSION

Prediction models for response variables

The experimental values for total phenolic content (TPC), antioxidant activity (AoxA), and *in vitro* protein digestibility (IVPD) varied from 584 to 650 mg GAE 100 g^{-1} (DW), 9067 to 13 940 μmol TE 100 g^{-1} (DW), and 70 to 78.2 %, respectively. The prediction models included linear, quadratic, and interaction terms of ET and SV ($p \leq 0.05$) for each response variable. The prediction models for each of the response variables were:

$$TPC = 588.34 + 15.19\,(ET) + 9.49\,(SV) + 11.35\,(ET)\,(SV) + 14.53\,(ET)^2 + 13.40\,(SV)^2$$

$$AoxA = 9408.20 + 815.63\ (ET) + 1083.53\ (SV) + 367.50\ (ET)\ (SV) + 1257.65\ (ET)^2 + 1246.65\ (SV)^2$$

$$IVPD = 76.75 + 0.73\ (ET) - 2.15\ (ET)^2 - 2.82\ (SV)^2$$

The regression models explained 95.46, 96.96, and 85.97 % of the total variability ($p \leq 0.0001$) of TPC, AoxA, and IVPD, respectively. The lack of fit ($p > 0.05$) and the relative dispersion of the experimental points of the model predictions (CV) were found to be < 10 %. These values indicated that the experimental models were adequate and reproducible. The TPC values of EGCF increased with ET and SV until reaching values of 682.20 mg GAE 100 g^{-1} (DW) at 150 °C and 240 rpm (Figure 1A). In the same way, AoxA increased as ET and SV increased, obtaining a maximum value of 16 128 µmol

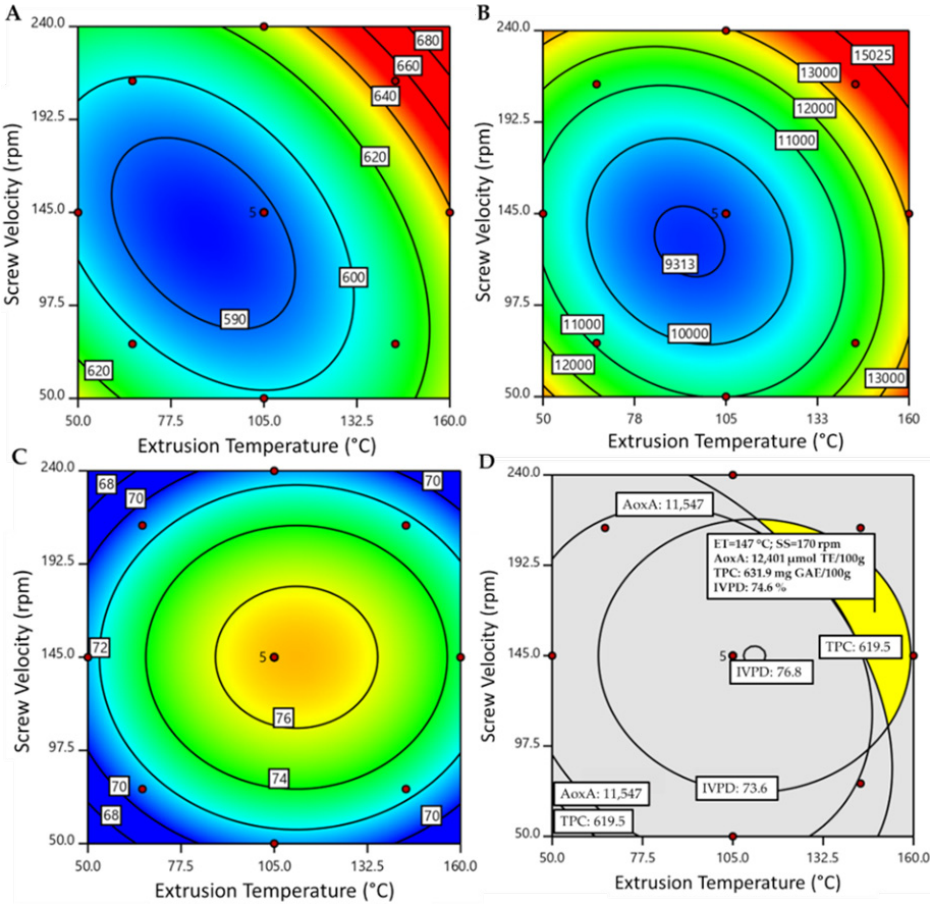

Figure 1. Contour plots showing the effect of the process variables (ET and SV). A: total phenolic compounds; B: antioxidant activity; C: *in vitro* protein digestibility; D: overlay graph showing the region with the best combination of process variables to obtain an optimized extruded germinated chia flour (EGCF).

TE 100 g^{-1} (DW) at 150 °C and 240 rpm (Figure 1B). In the case of IVPD, the highest value (78.2 %) was obtained at 145 °C and 105 rpm (Figure 1C).

AoxA and TPC decreased quadratically with ET and SV (Figures 1A and 1B). The reactions tended to reach a minimum stationary point, as evidenced by the positive sign of the quadratic impact of ET and SV (data not shown); the minimal values of this response are undesirable. The desired values of these responses (AoxA, TPC) were the highest, which were located in a range of 135–160 °C and 145–240 rpm for ET and SV, respectively. It was observed that IVPD increased quadratically with ET and SV. The negative sign of the quadratic effect of ET and SV (data not shown) indicated that the responses tended to reach a maximum stationary point. The maximum values of this response are desired, in a range of 100–120 °C and 120–160 rpm for ET and SV, respectively.

Process condition optimization

The TPC, AoxA, and IVPD values of EGCF are affected by ET and SV (Figures 1A, 1B, and 1C). The superposition of these graphs (Figure 1D) indicates the ideal combination of process variables to produce an EGCF with maximum values for TPC, AoxA, and IVPD. With this combination of process variables (ET = 147 °C and SV = 170 rpm), it is possible to predict the following values: TPC = 631.9 mg GAE 100 g^{-1} of sample (DW), AoxA = 12 401 μmol TE 100 g^{-1} of sample (DW), IVPD = 74.6 %. The experimental values of AoxA, TPC, and IVPD of EGCF were similar to the predicted values. This means that the optimal extrusion conditions were appropriate and reproducible.

Chemical composition and nutritional properties of chia flours

The chemical composition and nutritional properties of RCF, GCF, and EGCF (Table 1) show that germination under optimized conditions led to an increase ($p < 0.05$)

Table 1. Chemical composition of chia flours[†].

Property	Raw chia f lour (RCF)	Germinated chia flour (GCF)	Extruded germinated chia flour (EGCF)
Chemical composition (%, DW)			
Proteins	18.47 ± 0.15^{C}	22.78 ± 0.30^{B}	34.74 ± 0.45^{A}
Lipids	32.64 ± 0.23^{A}	18.48 ± 0.29^{B}	7.71 ± 0.11^{C}
Ashes	3.74 ± 0.12^{C}	5.87 ± 0.17^{B}	6.17 ± 0.08^{A}
Dietary fiber			
Soluble	3.99 ± 0.043^{C}	3.45 ± 0.01^{B}	4.78 ± 0.05^{A}
Insoluble	38.53 ± 0.47^{C}	40.51 ± 0.12^{B}	43.30 ± 0.71^{A}
Total	42.52 ± 0.43^{C}	43.96 ± 0.05^{B}	47.85 ± 0.33^{A}
Carbohydrates	2.82 ± 0.04^{C}	9.35 ± 0.18^{A}	3.6 ± 0.24^{B}

[†] Means with different letters per row are different (Tukey, $p \leq 0.05$). DW: dry weight. A, B, C mean values per column with different letters are statistically different ($p \leq 0.05$).

in protein content (23 %). The result coincides with reports from other researchers on different pseudocereals and legumes (Gómez-Favela *et al*., 2017; Salas-López *et al*., 2018). This is mainly attributed to the loss of nutrients, particularly carbohydrates, through the respiration process to produce CO_2 and water, as well as the activation of enzymes (α-amylase) that break down starch into simple sugars. Extrusion caused an increase in protein content (52 %); however, this is attributed to a concentration effect due to the partial defatting of the GCF before extrusion.

RCF and GCF showed lipid contents of 32.64 and 18.48 % (DW), respectively (Table 1). During germination, lipids are used as an energy source to perform various metabolic activities (synthesis of DNA, RNA, enzymes, and structural proteins) necessary for seedling development using nutrient reserves (starch and lipids). Gómez-Favela *et al.* (2017) and Salas-López *et al*. (2018) reported a decrease in lipid content during the germination of pseudocereals and legumes.

The total dietary fiber content (TDF) of raw and germinated chia flours was 42.52 and 43.96 % (DW), respectively (Table 1). During the germination process, the structure of the polysaccharides of the seed cell wall is modified, producing an increase in hemicellulose, cellulose, and polysaccharides. These results coincide with Salas-López *et al*. (2018). When applying the extrusion process to chia sprouts, the TDF content increased ($p \leq 0.05$), presenting a value of 47.85 %. This is due to the "nutrient concentration" effect of defatting the GCF as pre-extrusion conditioning and to the release of oligosaccharides due to the breaking of the glycosidic bonds of the polysaccharides by mechanical stress, as well as the formation of materials resistant to enzymatic degradation, such as starch and protein-polysaccharide complexes caused by heating.

The essential amino acid (EAA) content of RCF was higher than the standard of EAA recommended by FAO (2013) for children, adolescents, and adults, except for Leu and Lys (Table 2).

Sandoval-Oliveros and Paredes-López (2013) reported similar values in EAA content in chia seeds. The EAA content of GCF and EGCF was higher than that recommended by FAO (2013), with Lys acting as a limiting EAA in both processed seed flours. The extrusion process caused a slight decrease ($p < 0.05$) in the EAA content of the GCF; however, both flours (GCF and EGCF) presented a high chemical score (98.12, 96.88).

The IVPD of the RCF, GCF, and EGCF were 65.1, 72.9, and 83.2 %, respectively (Table 2). Ohanenye *et al*. (2022) reported on the increase in protein digestibility of legume seeds as a consequence of germination. The improvement of IVPD during germination may be due to the hydrolysis of compounds that contain organic phosphates and release inorganic phosphates, which are used for plant growth (Gamel *et al*., 2007). The extrusion increases protein digestibility and favors their denaturation, making them more accessible to the action of proteases. The protein digestibility values of the extruded products are higher than RCF and GCF; this is possible due to the shear cut and high temperatures, causing protein denaturation and the inactivation of anti-nutritional factors that hinder digestion (Salas-López *et al*., 2018).

Table 2. Protein characteristics of chia flours[†].

Property	Raw chia flour (RCF)	Germinated chia flour (GCF)	Extruded germinated chia flour (EGCF)	FAO (2013)[¶]
His	2.14 ± 0.03^{B}	4.07 ± 0.02^{A}	4.05 ± 0.03^{A}	1.6
Ile	3.35 ± 0.03^{C}	6.59 ± 0.03^{A}	6.42 ± 0.04^{B}	3.0
Leu	5.41 ± 0.03^{C}	7.85 ± 0.02^{A}	7.78 ± 0.03^{B}	6.1
Lys	3.49 ± 0.02^{C}	4.71 ± 0.02^{A}	4.65 ± 0.03^{B}	4.8
Met+Cys	2.67 ± 0.02^{C}	5.91 ± 0.03^{A}	5.74 ± 0.04^{B}	2.3
Phe+Tyr	4.51 ± 0.03^{B}	7.28 ± 0.03^{A}	7.26 ± 0.03^{A}	4.1
Thr	2.65 ± 0.02^{B}	3.20 ± 0.02^{A}	3.18 ± 0.04^{A}	2.5
Trp	1.78 ± 0.02^{C}	2.17 ± 0.02^{A}	2.11 ± 0.03^{B}	0.66
Val	4.04 ± 0.02^{B}	6.92 ± 0.03^{A}	6.93 ± 0.03^{A}	4.0
Total	30.04	48.70	48.12	29.06
Chemical score	72.70	98.12	96.88	
Limited EAA	Lys	Lys	Lys	
IVPD	65.1 ± 1.50^{C}	72.9 ± 0.89^{B}	83.2 ± 0.77^{A}	
C-PER	1.10	2.03	2.27	

[†] Means with different letters per row are different (Tukey, $p \leq 0.05$). A, B, C mean values per column with different letters are statistically different ($p \leq 0.05$). [¶]Amino acid requirements for children (three years and older), adolescents, and adults. EAA: essential amino acid; IVPD: *in vitro* protein digestibility; C-PER: calculated protein efficiency ratio.

The combined germination-extrusion processes, both under optimized conditions, increased ($p < 0.05$) the IVPD by 19.81 % (Table 2). El-Hady and Habiba (2003) reported an increase of 6.21 % in the IVPD of legumes (peas, chickpeas, and beans) processed sequentially by soaking and extrusion. Regarding C-PER, its content improved when applying the combined processes (germination and extrusion) due to the increase in IVPD, despite the slight decrease in EAA due to the extrusion process.

Phenolic compounds, gamma aminobutyric acid, and antioxidant properties

The content of free phenolic compounds in ungerminated chia seeds was 489 mg GAE 100 g^{-1} sample (DW) (Table 3). Germination increased ($p < 0.05$) the contents of free (44.24 %), bound (14.48 %), and total (32.92 %) phenolic compounds. Khang *et al*. (2016) reported that the concentration of phenolic compounds increased in soybeans and peanuts after germination; this could be due to the release and biosynthesis of phenolic compounds, such as hydroxycinnamates, that bind to non-starch polysaccharides in the cell walls of grains through ester and ether linkages. The action of cell wall-degrading enzymes (esterases) on these bonds contributes to the release of bound phenolic compounds (Perales-Sánchez *et al*., 2014).

On the other hand, the extrusion caused a 17.84 % increase in TPC levels. This is associated with the destruction of cell walls and the release of phenolic compounds,

Table 3. Content of phenolic compounds, γ-aminobutyric acid (GABA), and antioxidant activity of chia flours[†].

Property	Raw chia flour (RCF)	Germinated chia flour (GCF)	Extruded germinated chia flour (EGCF)
		Phenolic compounds[¶]	
Free	226 ± 3^{C}	326 ± 4^{B}	401 ± 6^{A}
Bound	283 ± 2^{B}	324 ± 2^{B}	365 ± 9^{A}
Total	489 ± 4^{C}	650 ± 3^{B}	766 ± 8^{A}
GABA[§]	13.08 ± 0.55^{C}	138.28 ± 0.82^{A}	135.16 ± 0.75^{B}
		Antioxidant activity[Þ]	
		ABTS	
Free phenolics	2515 ± 92^{C}	9475 ± 137^{B}	13 905 ± 198^{A}
Bound phenolics	8642 ± 167^{C}	12 747 ± 131^{A}	9568 ± 171^{B}
Total phenolics	11 157 ± 182^{C}	22 222 ± 122^{B}	23 473 ± 182^{A}
		DPPH	
Free phenolics	2370 ± 136^{C}	6620 ± 140^{B}	8825 ± 154^{A}
Bound phenolics	4738 ± 117^{C}	7095 ± 123^{A}	6440 ± 134^{B}
Total phenolics	7108 ± 72^{C}	13 716 ± 108^{B}	15 265 ± 121^{A}
		Antihypertensive potential (IC_{50})	
Ace inhibition	0.62 ± 0.03^{A}	0.45 ± 0.07^{B}	0.22 ± 0.03^{C}

[†] Means with different letters per row are different (Tukey, $p \leq 0.05$). A, B, C mean values per column with different letters are statistically different ($p \leq 0.05$). [¶]mg GAE 100 g^{-1} sample (DW). [§]mg γ aminobutyric acid 100 g^{-1} sample (DW). [Þ]μmol TE 100 g^{-1} sample (DW).

as well as the formation of Maillard reaction products that are quantified as phenolic compounds. Some researchers have observed that the combined processes (germination and extrusion) in rice (Albarracín *et al*., 2015) and corn (Gong *et al*., 2018) increase the content of phenolic compounds.

γ-aminobutyric acid (GABA), a non-protein essential amino acid, functions as the predominant inhibitory neurotransmitter in the central nervous system. It is also effective in lowering blood pressure and treating epilepsy. The GABA content in RCF was 13.08 mg 100 g^{-1} (DW); after germination under optimal conditions (21 °C for 157 h), chia seeds showed an increase ($p < 0.05$) in GABA (10.6 times) (Table 3). Germination causes the partial hydrolysis of proteins, increasing the availability of free glutamic acid. GABA is mainly produced by the decarboxylation of L-glutamic acid and is catalyzed by glutamate decarboxylase. These results coincide with what was reported by Paucar-Menacho *et al*. (2022), who reported increases in GABA content during the germination of pseudocereals. The extrusion caused a decrease in GABA content; this can be attributed to the heat and shear used during processing. However, it can be

seen that the GABA content of EGCF is higher than that of unprocessed chia. Zhu *et al*. (2017) reported that extrusion could be a suitable processing technology to produce grain-based products with high GABA content.

The total AoxA was determined using the ABTS and DPPH methodologies. The AoxA evaluated using the ABTS assay was 11 157, 22 222, and 23 473 μmol TE 100 g^{-1} of sample (DW) for RCF, GCF, and EGCF, respectively (Table 3). The increase in AoxA is one of the many metabolic changes that occur when germinating seeds, due to an increase in the content of phenolic compounds caused by the action of endogenous hydrolytic enzymes. Extrusion caused a 46.75 % AoxA increase ($p < 0.05$) in free phytochemicals and a 33.22 % decrease ($p < 0.05$) in bound phytochemicals. The AoxA of TPC increased by 10.13 % (Table 3). The increase in the total hydrophilic AoxA could be the result of the release of antioxidant phenolic compounds during the extrusion, the prevention of oxidation of the phenolic compounds in the extruded product by enzymatic inactivation during processing, and the presence of Maillard reaction products with antioxidant activity generated during the extrusion of raw materials containing amino acids and reducing sugars (Argüelles-López *et al*., 2018).

Combined processes (germination and extrusion) increased the total hydrophilic AoxA of RFC by 110 and 115 % ($p < 0.05$), as evaluated by the ABTS and DPPH methodologies, respectively (Table 3). Albarracín *et al.* (2015) reported an 86 % increase in total AoxA, evaluated by ABTS, in whole rice flours sequentially processed by germination-extrusion. Hegazy *et al.* (2017) reported a 19 % increase in AoxA (DPPH) in extruded germinated maize and chickpea mixtures.

Antihypertensive potential of phenolic extracts

The antihypertensive potential (IC_{50}) is defined as the concentration (mg of extract per mL) required to inhibit 50 % of angiotensin-converting enzyme (ACE) activity. The phenolic extracts of RCF, GCF, and EGCF had antihypertensive potential corresponding to an IC_{50} of 0.62, 0.45, and 0.22 mg extract mL^{-1}, respectively (Table 3). The improvement in the antihypertensive potential of germinated chia seeds is due to the increase in the total content of phenolic compounds and GABA (Salgado *et al*., 2022). The improvement in IC_{50} values during extrusion could be due to the release and formation of bioactive compounds (phenolic compounds, Maillard reaction products) with antihypertensive potential. The degree of inhibition of the ACE activity depends on the absorption and metabolism of these compounds, their mode of action related to the class (subclass), and the structure of the phenolic compound that is used. According to this research, the phenolic compounds present in RCF, GCF, and EGCF are suitable for use as functional food supplements or natural medicines to treat hypertension.

Microbiological stability of chia flours

The RCF is within the NOM-147-SSA1-1996 guidelines (DOF, 1996) since the indicator microorganisms were evidenced in amounts less than those established as the maximum allowed limit (Figure 2).

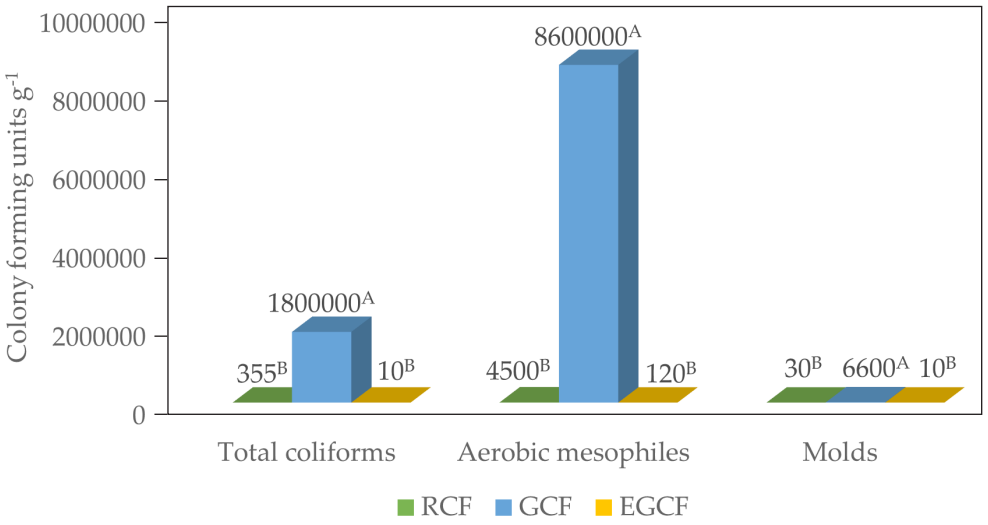

Figure 2. Total coliforms, aerobic mesophiles, and molds in chia flours. Means with different letters for the same type of microorganism present statistical differences (Tukey, $p \leq 0.05$).

The GCF has a low microbiological quality, with total coliforms, aerobic mesophiles, and molds at 18 x 10^5, 86 x 10^5, and 65 x 10^5 CFU g^{-1}, respectively (Figure 2). This represents an increase of 4, 3, and 2 log units, respectively, compared to RCF. These amounts exceed the maximum allowable limit (500, 500 000, and 500 CFU g^{-1} for total coliforms, aerobic mesophiles, and molds, respectively) established by NOM-147-SSA1-1996. This may be due to the characteristic conditions of the germination, such as the high humidity of the seed and the environment, temperature, pH close to neutrality, and availability of carbohydrates and other nutrients, which favor the growth of the bacteria inside or outside the seed (Cava *et al*., 2009).

To improve the microbiological stability of GCF and preserve and/or increase its nutritional and nutraceutical quality, extrusion was applied under optimized conditions as a combined process. As a result, a reduction was observed in the proliferation of microorganisms compared to RCF ($p > 0.05$). Bacterial reductions of up to five logarithms were obtained for total coliforms and aerobic mesophiles (Figure 2). Cava *et al*. (2009) reported an increase of five (coliforms) and six (aerobic mesophiles) logarithms in germinated bean grains compared to ungerminated grains. In the EGCF, the microorganisms were within the specifications of the Official Mexican Standard NOM-147-SSA1-1996 (DOF, 1996).

Microbiological safety is an important factor that determines the quality, shelf life, and effects on human health. In extrusion, thermal processing is designed to kill mesophilic organisms. Shear stress may be involved in reducing the microbial load during the extrusion process, which predicts that mechanical forces may cause cell

rupture. Most of the pathogenic organisms in food can be inactivated by extrusion if the process conditions are previously optimized (Temgire *et al*., 2021).

CONCLUSIONS

The combined germination-extrusion processes of chia seeds under optimized conditions allowed the generation of a new functional ingredient (flour) with nutritional value, high nutraceutical properties, and adequate microbiological stability. The extruded germinated chia flour can be used as a functional ingredient in highly consumed foods to improve their nutritional and nutraceutical quality. This work concluded that it is possible to produce an ingredient with health benefits through the combination of optimized processes in pseudocereals. For the development of new foods that incorporate the use of germinated seed flour, the use of extrusion technology is recommended as an efficient process after germination that ensures the microbiological stability of these flours, maintaining their nutritional and nutraceutical quality.

ACKNOWLEDGEMENTS

To the Mexican *Consejo Nacional de Humanidades, Ciencias y Tecnologías* (CONAHCYT), Convocatoria 2019 - Ciencia de Frontera (Grupal) for the funds supporting this research (ID Number: 263,352). To *Programa de Fomento y Apoyo a Proyectos de Investigación* (PROFAPI) under the *Universidad Autónoma de Sinaloa*, for supplementary funds.

REFERENCES

Abdel-Aty AM, Elsayed AM, Salah HA, Bassuiny RI, Mohamed SA. 2021. Egyptian chia seeds (*Salvia hispanica* L.) during germination: Upgrading of phenolic profile, antioxidant, antibacterial properties and relevant enzymes activities. Food Science and Biotechnology 30 (5): 723–734. https://doi.org/10.1007/s10068-021-00902-2

Albarracín M, de Greef D, González R, Drago S. 2015. Germination and extrusion as combined processes for reducing phytates and increasing phenolics content and antioxidant capacity of *Oryza sativa* L. whole grain flours. International Journal of Food Sciences and Nutrition 66 (8): 904–911. https://doi.org/10.3109/09637486.2015.1110689

Albarracín M, Dyner L, Giacomino MS, Weisstaub A, Zuleta A, Drago SR. 2019. Modification of nutritional properties of whole rice flours (*Oryza sativa* L.) by soaking, germination, and extrusion. Journal of Food Biochemistry 43 (7): 12854. https://doi.org/10.1111/jfbc.12854

Argüelles-López OD, Reyes-Moreno C, Gutiérrez-Dorado R, Sánchez-Osuna MF, López-Cervantes J, Cuevas-Rodríguez EO, Milán-Carrillo J, Perales-Sánchez JXK. 2018. Functional beverages elaborated from amaranth and chia flours processed by germination and extrusion. Biotecnia 20 (3): 135–145.

Bermejo NF, Munné-Bosch 2023. Mixing chia seeds and sprouts at different developmental stages: A cost-effective way to improve antioxidant vitamin composition. Food Chemistry 405: 134880. https://doi.org/10.1016/j.foodchem.2022.134880

Cava R, Sangronis E, Rodríguez M, Colinas J. 2009. Calidad microbiológica de semillas germinadas de *Phaseolus vulgaris*. Interciencia 34 (11): 796–800.

DOF (Diario Oficial de la Federación). 1994a. NORMA Oficial Mexicana NOM-092-SSA1-1994. Bienes y servicios. Método para la cuenta de bacterias aerobias en placa. Gobierno de México. Secretaría de Salud. Ciudad de México, México. http://www.salud.gob.mx/unidades/cdi/nom/092ssa14.html (Retrieved: May 2024).

DOF (Diario Oficial de la Federación). 1994b. NORMA Oficial Mexicana NOM-111-SSA1-1994. Bienes y servicios. Método para la cuenta de mohos y levaduras en alimentos. Gobierno de México. Secretaría de Salud. Ciudad de México, México. http://www.salud.gob.mx/unidades/cdi/nom/092ssa14.html (Retrieved: May 2024).

DOF (Diario Oficial de la Federación). 1994c. NORMA Oficial Mexicana NOM-113-SSA1-1994. Bienes y servicios. Método para la cuenta de microorganismos coliformes totales en placa. Gobierno de México. Secretaría de Salud. Ciudad de México, México. http://www.salud.gob.mx/unidades/cdi/nom/113ssa14.html (Retrieved: May 2024).

DOF (Diario Oficial de la Federación). 1996. NORMA Oficial Mexicana NOM-147-SSA1-1996. Bienes y servicios. Cereales y sus productos. Harinas de cereales, sémolas o semolinas. Alimentos a base de cereales, de semillas comestibles, harinas, sémolas o semolinas o sus mezclas. Productos de panificación. Gobierno de México. Secretaría de Salud. Ciudad de México, México. http://www.salud.gob.mx/unidades/cdi/nom/147ssa16.html (Retrieved: May 2024).

El-Hady EAA, Habiba RA. 2003. Effect of soaking and extrusion conditions on antinutrients and protein digestibility of legume seeds. LWT - Food Science and Technology 36 (3): 285–293. https://doi.org/10.1016/S0023-6438(02)00217-7

FAO (Food and Agriculture Organization). 2013. Dietary protein quality evaluation in human nutrition: report of a FAO expert consultation. FAO Food and Nutrition Paper 92. Food and Agriculture Organization. Rome, Italy. 79 p.

Gamel TH, Mesallam AS, Damir AA. 2007. Characterization of amaranth seeds oil. Journal of Food Lipids 14 (3): 323–334. https://doi.org/10.1111/j.1745-4522.2007.00089.x

Ghafoor K, Ahmed IAM, Özcan MM, Al-Juhaimi FY, Babiker EE, Azmi IU. 2020. An evaluation of bioactive compounds, fatty acid composition and oil quality of chia (*Salvia hispanica* L.) seed roasted at different temperatures. Food Chemistry 333: 127531. https://doi.org/10.1016/j.foodchem.2020.127531

Gong K, Chen L, Li X, Sun L, Liu K. 2018. Effects of germination combined with extrusion on the nutritional composition, functional properties and polyphenol profile and related *in vitro* hypoglycemic effect of whole grain corn. Journal of Cereal Science 83: 1–8. https://doi.org/10.1016/j.jcs.2018.07.002

Gómez-Favela MA, Gutiérrez-Dorado R, Cuevas-Rodríguez EO, Canizalez-Román VA, León-Sicairos C, Milán-Carrillo J, Reyes-Moreno C. 2017. Improvement of chia seed with antioxidant activity, GABA, essential amino acids, and dietary fiber by controlled germination bioprocess. Plant Foods for Human Nutrition 72 (4): 345–352. https://doi.org/10.1007/s11130-017-0631-4

Hegazy HS, El-Fath A, El-Sayed HR, Ahmed MG. 2017. Effect of extrusion processes on nutritional, functional properties and antioxidant activity of germinated chickpea incorporated corn extrudates. American Journal of Food Science and Nutrition Research 4 (1): 59–66.

Hernández-Pérez T, Valverde-González ME, Orona-Tamayo D, Paredes-López O. 2020. Chia (*Salvia hispánica*): Nutraceutical properties and therapeutic applications. Proceedings 53 (1): 17. https://doi.org/10.3390/proceedings2020053017

Khang DT, Dung TN, Elzaawely AA, Xuan TD. 2016. Phenolic profiles and antioxidant activity of germinated legumes. Foods 5 (4): 27. https://doi.org/10.3390/foods5020027

Ohanenye IC, Ekezie FGC, Sarteshnizi RA, Boachie RT, Emenike CU, Sun X, Nwachukwu ID, Udenigwe CC. 2022. Legume seed protein digestibility as influenced by traditional and emerging physical processing technologies. Foods 11 (15): 2299. https://doi.org/10.3390/foods11152299

Paucar-Menacho LM, Schmiele M, Lavado-Cruz AA, Verona-Ruiz AL, Mollá C, Peñas E, Frias J, Simpalo-Lopez WD, Castillo-Martínez WE, Martínez-Villaluenga C. 2022. Andean sprouted pseudocereals to produce healthier extrudates: Impact in nutritional and physicochemical properties. Foods 11 (20): 3259. https://doi.org/10.3390/foods11203259

Perales-Sánchez JXK, Reyes-Moreno C, Gómez-Favela MA, Milán-Carrillo J, Cuevas-Rodríguez EO, Valdez-Ortiz A, Gutiérrez-Dorado R. 2014. Increasing the antioxidant activity, total phenolic and flavonoid contents by optimizing the germination conditions of amaranth seeds. Plant Foods for Human Nutrition 69 (3): 196–202. https://doi.org/10.1007/s11130-014-0430-0

Salas-López F, Gutiérrez-Dorado R, Milán-Carrillo J, Cuevas-Rodríguez EO, Canizalez-Román VA, León-Sicairos C del R, Reyes-Moreno C. 2018. Nutritional and antioxidant potential of a desert underutilized legume – tepary bean (*Phaseolus acutifolius*). Optimization of germination bioprocess. Food Science and Technology 38 (1): 254–262. https://doi.org/10.1590/fst.25316

Salgado V dos SCN, Zago L, Antunes AEC, Miyahira RF. 2022. Chia (*Salvia hispanica* L.) seed germination: A brief review. Plant Foods for Human Nutrition 77 (4): 485–494. https://doi.org/10.1007/s11130-022-01011-z

Sandoval-Oliveros MR, Paredes-López O. 2013. Isolation and characterization of proteins from chia seeds (*Salvia hispanica* L.). Journal of Agricultural and Food Chemistry 61 (1): 193–201. https://doi.org/10.1021/jf3034978

Servín de la Mora-López G, López-Cervantes J, Gutiérrez-Dorado R, Cuevas-Rodríguez E, Milán-Carrillo J, Sánchez-Machado D, Reyes-Moreno C. 2018. Effect of optimal germination conditions on antioxidant activity, phenolic content and fatty acids and amino acids profiles of *Moringa oleifera* seeds. Revista Mexicana de Ingeniería Química 17 (2): 547–560. https://doi.org/10.24275/10.24275/uam/izt/dcbi/revmexingquim/2018v17n2/servin

Temgire S, Borah A, Kumthekar S, Idate A. 2021. Recent trends in ready to eat/cook food products: A review. The Pharma Innovation Journal 10 (5): 211–217. https://doi.org/10.22271/tpi.2021.v10.i5c.6207

Watchararparpaiboon W, Laohakunjit N, Kerdchoechuen O. 2010. An improved process for high quality and nutrition of brown rice production. Food Science and Technology International 16 (2): 147–158. https://doi.org/10.1177/1082013209353220

Zhu L, Adedeji AA, Alavi S. 2017. Effect of germination and extrusion on physicochemical properties and nutritional qualities of extrudates and tortilla from wheat. Journal of Food Science 82 (8): 1867–1875. https://doi.org/10.1111/1750-3841.13797

Agrociencia

ROOTING OF JUVENILE CUTTINGS OF *Pinus patula* Schiede ex Schltdl. *et* Cham. HEDGES

Nohemí **Escamilla-Hernández**[1], Arnulfo **Aldrete**[1*], J. Jesús **Vargas-Hernández**[1], Ángel **Villegas-Monter**[1], Miguel Ángel **López-López**[1]

[1]Colegio de Postgraduados Campus Montecillo. Postgrado en Ciencias Forestales. Carretera Mexico-Texcoco km 36.5, Montecillo, Texcoco, State of Mexico, Mexico. C. P. 56264.
* Author for correspondence: aaldrete@colpos.mx

Citation: Escamilla-Hernández N, Aldrete A, Vargas-Hernández JJ, Villegas-Monter A, López-López MA. 2024. Rooting of juvenile cuttings of *Pinus patula* Schiede ex Schltdl. et Cham. hedges. **Agrociencia** 58(4): 474-485. https://doi.org/ 10.47163/agrociencia.v58i4.2901

Editor in Chief:
Dr. Fernando C. Gómez Merino

Received: November 13, 2022.
Approved: February 27, 2024.
Published in Agrociencia: June 07, 2024.

ABSTRACT

Pinus patula Schiede ex Schltdl. *et* Cham. is endemic to Mexico and is used in both reforestation programs and in the timber industry due to its fast growth, wood quality, and easy handling. With the advance in genetic breeding programs, there is a need to massively propagate new plants from cuttings. One of the main challenges for this purpose is to know the effect of the age of the mother plant (hedge) on the rooting of cuttings. The younger the plant, the greater the rooting is expected to be. Three ontological ages of *P. patula* mother plants were compared (7, 10, and 13 months). The experimental design was in complete random blocks, with four replications and 25 cuttings per experimental unit. The response variables were evaluated 20 weeks after the experiment was established. No significant differences were observed in the rooting of the three ages evaluated (67.3 to 81 %), nor in the quality of the root (number and length of primary roots, percentage of plants with secondary roots). The results point out an advantage for the propagation of *Pinus* cuttings since the mother plants at those ages are capable of generating juvenile cuttings that are adequate to obtain percentages of rooting of over 75 %.

Keywords: vegetative propagation, maturity, ontogeny, mother plants, juvenility.

INTRODUCTION

Pinus patula Schiede ex Schldl. *et* Cham. is a Mexican pine tree widely planted around the world, with close to one million hectares (Tadesse and Fidalgo-Fonseca, 2022), due to its fast growth, straight trunk, lack of knots, wood quality, and easy silvicultural management (Velázquez *et al*., 2004). It is intensively used in plantations with improved trees in countries in Africa and America (Kanzler *et al*., 2012), although in Mexico, wild forests are primarily used. This has led to the extinction of superior trees in the purest *P. patula* stands (Aparicio-Rentería *et al*., 2014).

Due to the genetic deterioration and the practical difficulties of supplying seeds for reforestation, isolated efforts have been made to establish seed orchards in the past 20 years (Salaya-Domínguez *et al*., 2012), which consist in the planting of genetically superior trees that are resistant to pests and diseases, able to adapt to harsh environments (such as degraded soils and extreme climates), and have a high commercial value

(Ohira *et al*., 2009). After selecting the best parents based on the progeny trials, the massive multiplication of these individuals is carried out to incorporate genetic gain into the plantations or natural stands (Bonga, 2016).

There are several cloning techniques (grafting, layering, rooting of cuttings, and *in vitro* cultivation); however, propagation via cuttings is used because it is very affordable on an economic scale (Trueman, 2006). Unfortunately, for most conifers, the ontogenic age of donor plants or mother plants is a limiting factor (Mitchell *et al*., 2004a). Wendling *et al*. (2014) define ontogenic maturity as the process of development in woody plants that implies the start of reproductive maturity, with a reduction in both the growth rate and the rooting of cuttings. Morphological (Menzies *et al*., 2000), physiological (Fraga *et al*., 2002), hormonal (Valdés *et al*., 2002; Valdés *et al*., 2004), and genetic (Alvarez *et al*., 2016) changes are involved in this phase. In a review on the effect of ontogenic age on the rooting of conifer cuttings, Mitchell *et al.* (2004a) found that the percentage of rooting ranges between 25 and 100 % in juvenile material and between 1 and 75 % in mature material. In addition, a loss in root quality has been reported for *Dalbergia melanoxylon* (Amri *et al*., 2010), *Grewia optiva* (Husen, 2012), and other species as the ontogenic age progresses.

In order to reduce the negative effect of ontogenic maturation, different methods and techniques have been implemented to obtain young sprouts from the mother plants (Mitchell and Jones, 2006; Wendling *et al*., 2014). One of them is the formation of propagation hedges in which the mother plant is kept between 15 and 20 cm tall by frequently pruning to favor the emission of new sprouts from lateral buds and delay the maturing process (Mitchell *et al*., 2004b). Despite this, in different *Pinus* species, loss of rooting capacity has been reported, varying between 35 and 64 % (Mitchell *et al*., 2004a). In the case of *P. patula*, Mitchell *et al.* (2004b) reported a reduction of 35 to 80 % in rooting, as well as in root quality (number of roots, diameter, and dry mass of the root), in hedges between one and four years of age. The reduction in the quality of the roots leads to a lower growth in the height and diameter of the plants rooted in the field.

In Mexico, there are few studies and advances regarding this topic. Aparicio-Rentería (2014) was one of the first to address the topic of the production of *P. patula* cuttings, obtaining weighted rootings of 81 % when using 21-month-old hedges without the use of auxins in forest soil and mine sand substrate (1:2). Despite obtaining satisfactory results, they do not provide any details on their methodology. On the other hand, Rivera-Rodríguez *et al.* (2016) evaluated three factors (substrate, auxins, and ontogenic age) of the ontogenic effect on rooting, and they reported a reduction of 10 to 57.5 % for the ages of 12 and 24 months, respectively, without the application of auxins. These authors proposed the establishment of cuttings in a rooting chamber created by them with controlled nebulization and a night/day thermal system under two substrates (perlite and a mixture of vermiculite and peat moss); however, they showed humidity problems, which had a negative impact on the percentage of rooting.

In order to establish more favorable conditions for the establishment of cuttings, Escamilla-Hernández *et al.* (2021) proposed an alternative design based on 220 cm^3

containers (tubes) with the recirculation of water by bagging to avoid excess humidity in the substrate, testing alternative sawdust- and bark-based mixtures, and they obtained a rooting of 77 % in cuttings from 10-month-old hedges, without the use of auxins, with a survival rate of 100 %. This was an important advance for the establishment of cuttings, which helps investigate other factors.

The ontogenic process is an important factor since the juvenile phase is very short; after the second year, the rooting of *P. patula* starts reducing significantly (Mitchell *et al.*, 2004b). Whether the ontogenic maturity process is observed before 12 months is currently unknown. If this were the case, the different physiological, biochemical, and genetic studies would have to focus on earlier ages to better explain the ontogenic maturity process; otherwise, the possibility of maximizing the stage of production of cuttings opens up. The aim of this study was to evaluate the percentage and quality of the rooting of cuttings obtained from 7-, 10-, and 13-month-old *P. patula* hedges.

MATERIALS AND METHODS

Hedge establishment and management

The investigation was conducted in a greenhouse of the forest nursery of the Colegio de Postgraduados, located in Texcoco, State of Mexico, Mexico (19° 27′ 38.25′′ N, 98° 54′ 23.91′′ O), at an altitude of 2240 m. The propagation hedges were established from a seed lot of the first-generation "Reserva Forestal Multifuncional" clonal seed orchard in Aquixtla, Puebla, Mexico. The lot included the *P. patula* seeds of the eleven best clones, according to the evaluations of the progeny trials carried out by Salaya-Domínguez *et al.* (2012).

To generate 7-, 10-, and 13-month-old plants to create hedges and ensure that the three ages were examined at the same time while constructing the experiment, they were planted in a staggered fashion with a 3-month gap. The first was planted on June 6th (E_3), the second on September 6th (E_2), and the last one on December 6th (E_1) of 2017. The plants were sown directly in 220 cm^3 containers (tubes). A total of 300 plants were sown, 100 per treatment.

The initial pruning was carried out on the main stem to remove the apical part (3 cm) when the secondary leaves emerged (Escamilla-Hernández *et al*., 2020); this criterion was consistent throughout all plant ages. The youngest plants (E_1) were pruned at an age of four and a half months with an average height of 14 cm; the medium-aged plants (E_2), after five months and with an average height of 10 cm, and the oldest plants (E_3), after seven months and with an average age of 16 cm. Differences in plant heights are due to the season of their production; the growth of the younger plants (E_1) was higher in March and April, along with their development, whereas E_2 plants were produced in less favorable environmental conditions.

Fifteen days after pruning, the mother plants were transplanted into 4 L pots in a substrate mixture formed by composted pine bark, peat moss, vermiculite, and perlite

(60:15:15:10, v/v/v/v) with 7 g L^{-1} of Osmocote® controlled release fertilizer (15-9-12, N-P-K) with a release period of eight to nine months. The mother plants (hedges) were kept under greenhouse conditions, beneath a 50 % shade cloth (Escamilla-Hernández *et al*., 2020).

All hedges were adjusted by pruning five primary branches to control the architecture of the plant. To synchronize the production of cuttings with the moment of the evaluation, several prunes were made for every ontogenic age. After forming the hedges, the E_1 plants were no longer trimmed, whereas the E_2 hedges were pruned for the second time after seven months, and the E_3 hedges were pruned another two times (at nine and 10 months). To obtain homogenous, quality sprouts, four sprouts were left on the main stem and two on each main branch (Figure 1). The criterion at the moment of harvest was determined based on the phenological characteristics and not on the chronological age of the sprout, according to Menzies *et al.* (2000). The age of the sprouts in the E_1 hedges was two and a half months, and in the E_2 and E_3 hedges, three months.

Figure 1. Management of *Pinus patula* hedges to obtain cuttings. E_3, E_2, and E_1: mother plants aged 13, 10, and 7 months, respectively.

Obtaining and managing of cuttings

To establish the experiment, 50 hedges were selected from every treatment, and the sprouts generated on the main stem and the pruned branches of each hedge were

harvested. To do this, a Felco F2 hand pruner was used. The disinfection process was carried out for every hedge. The pruner was disinfected with 96° ethyl alcohol before cutting. Next, Captan (N-trichloromethylthio-4-cyclohexene-1,2-dicarboximide) was applied at a dose of 1.5 g L^{-1} at the freshly pruned areas of the plant. The average length of the cuttings was 9 cm (Rivera-Rodríguez *et al.*, 2016), measured using a graduated ruler to the closest millimeter. The average basal diameter was between 2 and 2.5 mm, and it was measured using a digital vernier with an accuracy of 0.01 mm.

The phenological characteristics of the cuttings were described for every treatment at the moment of harvesting for their evaluation. The cuttings from the E_1 hedges presented more juvenile characteristics (flexible stem, primary leaves, and the presence of axillary buds), whereas those from E_3 displayed a greater degree of development (less flexible stem, primary and secondary leaves, without axillary buds). The cuttings from the E_2 hedges displayed intermediate characteristics (flexible stem, primary leaves, start of secondary leaves, and the presence of axillary buds), as described by Menzies *et al*. (2000). The needles were removed from the buds harvested in the first 3 cm from the base, and they were disinfected using Captan in doses of 1.5 g L^{-1} for 15 min (Figure 2).

Figure 2. Characteristics of *Pinus patula* sprouts for the rooting of cuttings from mother plants E_3 (13 months), E_2 (10 months), and E_1 (7 months).

Treatments and experimental design

The experiment was conducted in mid-July 2018. The three hedge ages (E1, E2, and E3) were assessed using a complete random block design with four replications. One hundred cuttings were used per treatment and 25 per experimental unit. The cuttings were transplanted in individual 220 cm^3 containers that were placed in trays with 25 cells at 3 cm of depth into the substrate, and they were sprayed with fungicide solution (thiabendazole 1.5 g L^{-1}) and insecticide (Imidacloprid 1.5 g L^{-1}). To maintain the relative humidity at saturation, each tray was covered in a 90 cm wide by 120 cm tall plastic bag and placed in a rustic greenhouse. The rooting substrate used in the containers was a mixture of fresh pine sawdust and composted pine bark (90:10 v/v). The bark was sieved through a 0.5 cm mesh. The substrates were disinfected using Tecto ® fungicide in a dose of 1.5 g L^{-1} of water.

Air and substrate temperatures were taken with a HOBO sensor at 15-minute intervals. The mean monthly temperature varied between 18 and 20.7 °C during the rooting period (July–November, 2018). However, the daytime temperature in that period varied between 10.8 °C (average minimum) and 36.3 °C (average maximum). The monthly mean temperature of the substrate varied between 17.5 and 20.8 °C during the same period, with average minimum and maximum values of 11.5 °C and 31 °C, respectively.

Variables evaluated

Twenty weeks after the experiment was established, the cuttings were removed from the substrate, and the following characteristics were evaluated: survival, rooting, the presence of callus, the number and length of primary roots, and the presence of secondary roots. Live cuttings were considered to be those that displayed no necrotized tissue anywhere. The cuttings with at least one root of 1 mm in length were considered rooted (Rivera-Rodríguez *et al.*, 2016). The presence of callus was identified as the bulking of meristematic tissue at the base of the stem, resulting from cell division (Rasmussen *et al.*, 2009). Primary roots are those that originate at the base or lateral part of the stem, and secondary roots are those that form from the primary roots, with a minimum length of 0.5 cm (Hartmann *et al.,* 2014). The primary roots were measured using a ruler graduated in centimeters to the nearest millimeter. From the characteristics evaluated in every cutting, the percentage of live cuttings with callus and root was obtained for each experimental unit. Considering only rooted cuttings, the average number and length of primary roots per cutting were obtained, as well as the percentage of cuttings with secondary roots.

Statistical analysis

A one-way analysis of variance was carried out using the Mixed procedure of the SAS program, version 9.4 (SAS Institute, 2004). In cases where a significant effect of the age of the mother plant was found, Tukey's mean comparison test with $p = 0.05$ was carried out. The model used in the analysis of variance was as follows:

$$Y_{ij} = \mu + B_i + T_j + \varepsilon_{ij}$$

where Y_{ij} is the observed value of the variable in the i-th experimental unit of the j-th treatment, μ is the effect of the general mean, B_i is the random effect of the i-th block, T_j is the fixed effect of the j-th treatment, and ε_{ij} is the experimental error. All the response variables, except for the root number and length, were transformed with the arcsine function before the analysis of variance, and the average values were then transformed to their original scale.

RESULTS AND DISCUSSION

There were significant differences between treatments in the survival of the cuttings (p = 0.029). However, in the rooting variables, presence of callus, number of primary roots, root length, and presence of secondary roots, no significant effect was found ($p \geq 0.05$) of the age of the mother plant (Table 1).

Table 1. Results of the analysis of variance of the characteristics evaluated in the trial for the rooting of *Pinus patula* cuttings obtained from hedges aged 7, 10, and 13 months.

Variable	Mean	GL	F	P
Survival (%)	98.3	2	6.76	0.029
Rooted cuttings (%)	75.6	2	3.35	0.082
Cuttings with calluses (%)	22.1	2	1.42	0.291
Primary roots (number)	1.8	2	0.15	0.865
Root length (cm)	7.1	2	0.06	0.943
Rooted cuttings with secondary roots (%)	84.9	2	1.49	0.298

The survival rate of the cuttings was 100 % in the treatments of younger plants (E_1 and E_2) (Figure 3A), while the cuttings from the more aged plants (E_3) displayed a survival rate of 95 %. The death rate in the cuttings from E_3 was due mainly to management aspects and/or specific conditions of the trial, since the lower percentage of survival in them was found in one of the replications, with 84 %.

Rooting efficiency

The rooting percentage in the whole trial was 75.6 % (Table 1). Although this value varied between 67.3 and 81 % in the treatments, the differences were not significant between them (Figure 3B). These results are comparable to the values obtained by Mitchell *et al.* (2004b) in *P. patula* (80 %) with one-year-old mother plants and Majada *et al*. (2011) in *P. pinaster* (84.7 %) with 11-month-old plants. The weighted percentage of rooting reached (75.6 %) indicates an achievement for the establishment of *P. patula* cuttings in Mexico, since it approximates the percentages reported in countries with production systems by cuttings in *Pinus* (Trueman, 2006).

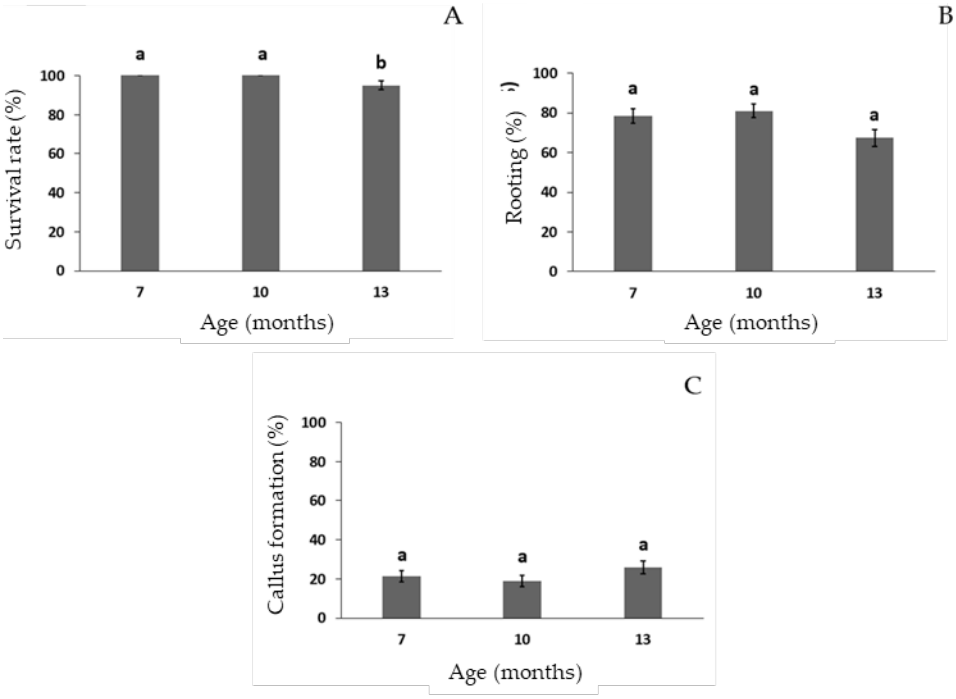

Figure 3. Effect of the ontogenic age (7, 10, and 13 months) of the mother plant. A: survival; B: rooting; C: presence of callus**.**

In the ages evaluated (7, 10, and 13 months), no effect of the ontogenic age was observed, as reported by Wendling *et al.* (2014) in conifers, who mention that the older the plant, the less rooting it will have. These results are encouraging, since most production systems by cuttings begin at 12 months with a rooting percentage of 80 % for *P. patula* and decrease after the third year with a rooting percentage of 70 % until they reach 35 % after four years (Mitchell *et al.,* 2004b). As mentioned earlier, the production system for cuttings is short. With these results, it is possible to broaden the cutting production cycle, starting at 7 months.

On the other hand, in the three evaluated ages of the plant, cuttings displayed morphological characteristics such as stem, leaf, and axillary bud types (Figure 2), considered juvenile traits by Menzies *et al.* (2000). This fact contributes towards the identification of juvenile characteristics as a practical and inexpensive tool, unlike others such as physiological, hormonal, or genetic ones (Fraga *et al.*, 2002; Valdés *et al.*, 2004; Alvarez *et al*., 2016). It is worth mentioning that in the same hedge, buds with different degrees of maturity can be found due to the position of the buds in the hedge (apical or basal) or due to their management in the nursery (water stress, excess or insufficient nutrients, and extreme temperature changes) (Wendling *et al.,* 2014).

A high weighted rooting percentage (75.6 %) without the use of rooting hormones indicates that the cuttings have adequate levels of endogenous auxins (Osterc *et al*.,

2009). Despite this, a 14 % reduction was observed in the rooting ability between E_2 (81 %) and E_3 (67 %) (Figure 3B), probably due to a slight effect of the maturity of the mother plant, which may be related to a decrease in auxins (Wendling *et al*., 2014). For these cases, the use of external stimulants on the base of the cutting could increase the percentage of rooting (Rosier *et al*., 2004).

On average for the entire trial, 22.1 % of the cuttings formed a callus on the base, with a variation between 19 and 26 % in the three ages (Figure 3C); the lower values were displayed in E_1 and E_2 (22 and 19 %) and the highest in E_3 (26 %). This variable is complementary to the percentage of rooting; that is, as the percentage of calluses decreases, the percentage of rooting increases, and vice versa (Hartmann *et al*., 2014). Rivera-Rodríguez *et al.* (2016) reported 42.5 % of calluses in mother plants aged 12 months, in complement with 57.5 % of rooting.

Rooting quality

The hedge's ontogenic age had no effect on rooting quality; the number of primary roots per cutting remained between 1.8 and 1.9; root length was between 7 and 7.3 cm; and between 82 and 88 % of the rooted cuttings presented secondary roots (Table 2). These values are similar to those recorded by Escamilla-Hernández *et al.* (2020) in 10-month-old *P. patula* hedges, where they reported values of 2.1 for the number of roots, 6.7 cm in length, and 76.1 % rooted cuttings with secondary roots. Majada *et al.* (2011), in a four-month evaluation, reported an average of 2.9 primary roots and 3.3 cm for root length in *P. pinaster* cuttings obtained from 11-month-old hedges without the application of auxins. In another study, when *P. patula* cuttings were analyzed after three and a half months, an average of 1.4 primary roots were found per cutting, with a length of 3.8 cm and 36.7 % of cuttings with secondary roots (Rivera-Rodríguez *et al*., 2016).

Table 2. Average values (± standard error), by age of the mother plant, of the characteristics of the roots evaluated in the trial for the rooting of *Pinus patula* cuttings.

Age of mother plant (months)	Primary roots		Cuttings with secondary roots (%)
	Number	Length (cm)	
7	1.9 ± 0.16 a	7.0 ± 0.60 a	84.9 ± 3.1 a
10	1.8 ± 0.16 a	7.0 ± 0.60 a	87.7 ± 2.8 a
13	1.8 ± 0.16 a	7.3 ± 0.60 a	82.1 ± 3.3 a

Average values followed by the same letter do not differ significantly (Tukey, $p = 0.05$).

Although these studies evaluated the quality of the rooting in less time, the data are similar to those obtained in a sample of 30 cuttings per treatment evaluated after four months in this study. This indicates that the roots from the cuttings aged 7, 10, and 13 months display favorable attributes for greater rooting efficiency and quality (Figure

4). These mother plants help obtain a better distribution in the root architecture to make water and nutrient absorption more efficient and give adequate mechanical support in the field (Davis and Jacobs, 2005; Mitchell *et al.*, 2005).

Figure 4. Rooting of *Pinus patula* cuttings with three ontogenic ages (7, 10, and 13 months, E1, E2, and E3, respectively).

CONCLUSIONS

No important ontogenic effects were observed in the capacity of the rootings or on the quality of the roots in the cuttings from 7-, 10-, and 13-month-old mother plants. This indicates that, in less than a year, the hedge produces sprouts with distinctive juvenile characteristics that can be used as a practical and inexpensive tool to identify juvenile material for *Pinus patula* cuttings propagation.

REFERENCES

Alvarez C, Valledor L, Sáez P, Hasbún R, Sánchez-Olate M, Cañal MJ, Ríos D. 2016. Changes in gene expression in needles and stems of *Pinus radiata* rootstock plants of different ontogenic age. American Journal of Plant Sciences 7 (8): 1205–1216. https://doi.org/10.4236/ajps.2016.78116

Amri E, Lyaruu HVM, Nyomora AS, Kanyeka ZL. 2010. Vegetative propagation of African Blackwood (*Dalbergia melanoxylon* Guill. & Perr.): Effects of age of donor plant, IBA treatment and cutting position on rooting ability of stem cuttings. New Forests 39 (2): 183–194. https://doi.org/10.1007/s11056-009-9163-6

Aparicio-Rentería A, Juárez-Cerrillo SF, Sánchez-Velásquez LR. 2014. Propagación por enraizamiento de estacas y conservación de árboles plus extintos de *Pinus patula* procedentes del norte de Veracruz, México. Madera y Bosques 20 (1): 85–96.

Bonga JM. 2016. Conifer clonal propagation in tree improvement programs. *In* Park YS, Bonga JM, Moon HK. (eds.), Vegetative Propagation of Forest Trees. National Institute of Forest Science: Seoul, Korea, pp: 3-31.

Davis AS, Jacobs DF. 2005. Quantifying root system quality of nursery seedlings and relationship to outplanting performance. New Forests 30 (2–3): 295–311. https://doi.org/10.1007/s11056-005-7480-y

Escamilla-Hernández N, Aldrete A, Vargas-Hernández JJ, Villegas-Monter A, López-López MA. 2020. Propagación vegetativa de *Pinus patula* Schiede ex Schltdl. *et* Cham. en diferentes sustratos. Revista Fitotecnia Mexicana 43 (2): 215–221. https://doi.org/10.35196/rfm.2020.2.215

Fraga MF, Cañal M, Rodríguez R. 2002. Phase-change related epigenetic and physiological changes in *Pinus radiata* D. Don. Planta 215 (4): 672–678. https://doi.org/10.1007/s00425-002-0795-4

Hartmann HT, Kester DE, Davies FT, Geneve RL. 2014. Plant propagation: Principles and practices (Eighth edition). Pearson: London, UK. 922 p.

Husen A. 2012. Changes of soluble sugars and enzymatic activities during adventitious rooting in cuttings of *Grewia optiva* as affected by age of donor plants and auxin treatments. American Journal of Plant Physiology 7 (1): 1–16. https://doi.org/10.3923/ajpp.2012.1.16

Kanzler A, Payn K, Nel A. 2012. Performance of two *Pinus patula* hybrids in southern Africa. Southern Forests: A Journal of Forest Science 74 (1): 19–25. https://doi.org/10.2989/20702620.2012.683639

Majada J, Martínez-Alonso C, Feito I, Kidelman A, Aranda I, Alía R. 2011. Mini-cuttings: An effective technique for the propagation of *Pinus pinaster* Ait. New Forests 41 (3): 399–412. https://doi.org/10.1007/s11056-010-9232-x

Menzies MI, Dibley MJ, Faulds T, Aimers-Halliday J, Holden DG. 2000. Morphological markers of physiological age for *Pinus radiata*. New Zealand Journal of Forestry Science 30 (3): 359–364.

Mitchell RG, Zwolinski J, Jones NB. 2004a. A review on the effects of donor maturation on rooting and field performance of conifer cuttings. Southern African Forestry Journal 201 (1): 53–63. https://doi.org/10.1080/20702620.2004.10431774

Mitchell RG, Zwolinski J, Jones NB. 2004b. The effects of ontogenetic maturation in *Pinus patula*—Part 1: Nursery performance. Southern African Forestry Journal 202 (1): 29–36. https://doi.org/10.1080/20702620.2004.10431787

Mitchell RG, Zwolinski J, Jones NB, Bayley AD. 2005. Root volume and raising period affect field performance of *Pinus patula* cuttings in South Africa. Southern African Forestry Journal 204 (1): 15–21. https://doi.org/10.2989/10295920509505223

Mitchell RG, Jones NB. 2006. The effects of ontogenetic maturation in *Pinus patula*—Part II: Hedge cycling and field performance. Southern African Forestry Journal 207 (1): 3–6. https://doi.org/10.2989/10295920609505246

Ohira M, Kuramoto N, Fujisawa Y, Shiraishi S. 2009. Usefulness of the closed cutting system for the vegetative propagation of *Pinus thunbergii* resistant to pine wilt disease. Journal of the Japanese Forest Society 91 (4): 266–276. https://doi.org/10.4005/jjfs.91.266

Osterc G, Štefančič M, Štampar F. 2009. Juvenile stockplant material enhances root development through higher endogenous auxin level. Acta Physiologiae Plantarum 31 (5): 899–903. https://doi.org/10.1007/s11738-009-0303-6

Rasmussen A, Smith TE, Hunt MA. 2009. Cellular stages of root formation, root system quality and survival of *Pinus elliottii* var. *elliottii* x *P. caribaea* var. *hondurensis* cuttings in different temperature environments. New Forests 38 (3): 285–294. https://doi.org/10.1007/s11056-009-9147-6

Rivera-Rodríguez MO, Vargas-Hernández JJ, López-Upton J, Villegas-Monter A, Jiménez-Casas M. 2016. Enraizamiento de estacas de *Pinus patula*. Revista Fitotecnia Mexicana 39 (4): 385–392.

Rosier CL, Frampton J, Goldfarb B, Blazich FA, Wise FC. 2004. Growth stage, auxin type, and concentration influence rooting of stem cuttings of Fraser fir. HortScience 39 (6): 1397–1402. https:// doi.org/10.21273/hortsci.39.6.1397

Salaya-Domínguez JM, López-Upton J, Vargas-Hernández JJ. 2012. Variación genética y ambiental en dos ensayos de progenies de *Pinus patula*. Agrociencia 46(5): 519-534.

SAS Institute Inc. 2004. The SAS system for windows. Release 9.4. SAS Institute. Cary, NC. USA.

Tadesse W, Fidalgo-Fonseca T. 2022. *Pinus patula* plantations in Africa: An overview of its silvicultural traits and use under SDG. *In* Gonçalves AC, Fidalgo-Fonseca T. (eds.), IntechOpen: London, UK, pp: 1–13. https://doi.org/10.5772/intechopen.104889

Trueman SJ. 2006. Clonal propagation and storage of subtropical pines in Queensland, Australia. Southern African Forestry Journal 208 (1): 49–52. https://doi.org/10.2989/10295920609505261

Valdés AE, Centeno ML, Espinel S, Fernández B. 2002. Could plant hormones be the basis of maturation indices in *Pinus radiata*? Plant Physiology and Biochemistry 40 (3): 211–216. https://doi.org/10.1016/S0981-9428(02)01371-2

Valdés AE, Fernández B, Centeno ML. 2004. Hormonal changes throughout maturation and ageing in *Pinus pinea*. Plant Physiology and Biochemistry 42 (4): 335–340. https://doi.org/10.1016/j.plaphy.2004.02.004

Velázquez MA, Ángeles G, Llanderal T, Román AR, Reyes V. 2004. Monografía de *Pinus patula*. Secretaría de Medio Ambiente y Recursos Naturales. Comisión Nacional Forestal. Colegio de Postgraduados. Zapopan, México. 124 p.

Wendling I, Trueman SJ, Xavier A. 2014. Maturation and related aspects in clonal forestry—Part I: Concepts, regulation and consequences of phase change. New Forests 45: 449–471. https://doi.org/10.1007/s11056-014-9421-0

Agrociencia

PRODUCTION OF *Pinus durangensis* Mart. UNDER DIFFERENT SUBSTRATE AND MYCORRHIZAL INOCULATION CONDITIONS IN NURSERY

Ricardo **Martínez-Casas**[1], José Leonardo **García-Rodríguez**[2], Silvia **Salcido-Ruiz**[1], José Rodolfo **Goche-Télles**[1], José Ángel **Prieto-Ruíz**[1*]

[1]Universidad Juárez del Estado de Durango. Facultad de Ciencias Forestales y Ambientales. Avenida Papalopan y Boulevard Durango s/n, Durango, Durango, Mexico. C. P. 34120.
[2]Instituto Nacional de Investigaciones Forestales, Agrícolas y Pecuarias. Campo Experimental Valle del Guadiana. Carretera Durango-El Mezquital km 4.5, Durango, Durango, Mexico. C. P. 43000.
* Author for correspondence: jprieto@ujed.mx

Citation: Martínez-Casas R, García-Rodríguez JL, Salcido-Ruiz S, Goche-Télles JR, Prieto-Ruíz JA. 2024. Production of *Pinus durangensis* Mart. under different substrate and mycorrhizal inoculation conditions in nursery. **Agrociencia** 58(4): 486-499. https://doi.org/ 10.47163/agrociencia.v58i4.2960

Editor in Chief:
Dr. Fernando C. Gómez Merino

Received: February 02, 2023.
Approved: January 31, 2024.
Published in Agrociencia: June 18, 2024.

ABSTRACT

Substrate and mycorrhization are important aspects when producing plants. The objective of the study was to determine the effect of three substrates inoculated with ectomycorrhizal fungal spores on the morphological characteristics of nursery-grown *Pinus durangensis* as well as the inherent costs of the substrate. A randomized block experimental design with a 3 x 3 factorial arrangement was used. The substrates evaluated were: 1) peat, vermiculite, and perlite (50:25:25) [PVP]; 2) peat, composted bark, and raw sawdust (50:25:25) [PBS]; and 3) peat and bark (50:50) [PB]. The mycorrhizal inoculants were: 1) *Pisolithus tinctorius*; 2) *Laccaria laccata*; and 3) control. The plant was produced in black polyethylene tubes (160 mL) and evaluated at 13 months. The substrate factor presented statistical differences ($p \leq 0.05$) in the variables evaluated, with higher values in PVP, followed by PBS and PB, the latter being similar to each other. The mycorrhizal inoculation factor showed differences ($p \leq 0.05$) in root and total biomass, Dickson's quality index, and mycorrhizal colonization, obtaining higher values when *P. tinctorius* was inoculated, except in the last variable, where the application of *L. laccata* stood out. In the substrate-mycorrhizal inoculation interaction, the most favorable combination was PVP and *P. tinctorius*. The PVP substrate was 28.4 and 34.6 % more expensive than PB and PBS, respectively. The combined effect of PVP and *P. tinctorius* produced the best growth, although the substrate was more expensive.

Keywords: growth media, controlled mycorrhization, plant quality, morphological characteristics, reforestation.

INTRODUCTION

Deforestation is directly related to the loss of biodiversity and the decrease in the efficiency of environmental services provided by forests and jungles, which has contributed to global warming. These ecosystems, in addition to being reservoirs of

biodiversity, are a source of consumer goods such as timber, fuelwood, and other non-timber forest products (FAO, 2018). In Mexico, due to the deterioration and decrease of forest resources, with an average annual rate of gross deforestation of 212 834 ha between 2001 and 2019, there is a need to implement strategies that favor the restoration of forest ecosystems (CONAFOR, 2021).

Using nursery-produced plants allows the generation of new forest stands, which in the future will contribute to re-establish forests and obtain economic gains in a sustainable way (Buamscha *et al*., 2012; Scholz and Morera, 2016); however, the propagation material must have quality, which is fundamental in reforestation programs (Grossnickle and MacDonald, 2018). Plant quality is the result of nursery production practices and the management of propagated material until planting (Villar-Salvador *et al*., 2021). After the nursery culture process, the initial survival and growth potential of individuals is related to their morphological and physiological attributes, as well as their eco-physiological response to site environmental conditions (Grossnickle, 2018).

The main cultural procedures that plants receive in nursery include irrigation, fertilizer, mycorrhization, pest and disease control, and environmental management (Sanchún and Obando, 2016; Grossnickle, 2018). Other important aspects include the correct selection of substrates and the proportions for mixing them, as well as the type of container. These factors are related to the formation of the root ball and the growing space for the root system of the plants (Landis, 1990). The importance of the substrate lies in the functions it performs in anchoring the root system to support the plants as a temporary store and diffuser of water and nutrient solutions that are absorbed by the root hairs. The physical and chemical characteristics of substrates are directly related to the morphology and functional performance of plants and, therefore, influence their growth and survival in the field (Villar-Salvador *et al*., 2021).

There is a search for materials to replace the substrate based on peat (50–60 %), perlite (20–25 %), and vermiculite (20–25 %), known as a base mix, whose main disadvantages are its high cost and immediate unavailability. These reasons limit their use for most nurserymen (Aguilera-Rodríguez *et al*., 2016). Therefore, it is necessary to look for alternative materials with an ecological approach (Mateo-Sánchez *et al*., 2011; Gayosso-Rodríguez *et al*., 2016). Pine bark and sawdust have favorable physical and chemical characteristics for the development of seedlings of the genus *Pinus* (Hernández-Zárate *et al*., 2014); in addition, they are by-products of forestry activity with relative abundance (Fregoso-Madueño *et al*., 2017), and it is desirable to find a potential use for them.

An important component in plant production is mycorrhizal inoculation through the application of spores of wild ectomycorrhizal fungi (HSECM) (Escobar-Alonso and Rodríguez-Trejo, 2019), which promotes plant-fungus symbiosis. This condition is desirable in species of the genus *Pinus* in nursery and field to favor plant survival and growth (García-Rodríguez *et al*., 2017).

The objective of this study was to determine the effect of three substrates and inoculation with spores of two species of ectomycorrhizal fungi and a control on the morphological characteristics of nursery-grown *Pinus durangensis* Mart. Similarly, it was sought to determine the costs inherent to the type of substrate. It was hypothesized that at least a combination of substrate and ectomycorrhizal fungus favors the survival, growth, and mycorrhizal colonization of the plant in a nursery at the lowest cost due to the components of the substrate.

MATERIALS AND METHODS

Location

The experiment was carried out in the forest nursery of the Experimental Field Valle del Guadiana, of the National Institute of Forestry, Agriculture, and Livestock Research (INIFAP), located at Carretera Durango-El Mezquital km 4.5, Durango, Durango, Mexico (24° 01′ N and 104° 44′ W), with an altitude of 1860 m and average annual rainfall of 504 mm.

Plant production

The plant was produced under three environmental conditions, with the following sequence: a) from October 17, 2019 (sowing) until seven months later, a saw-type greenhouse was used, 50 m long and 30 m wide, with plastic film cover caliber 720 μm, milky white color, treated against UV rays, and 50 % black color shade mesh, with an average temperature of 22 °C, maximum of 46 °C, and minimum of -2 °C; b) from May 8, 2020, for four months, using 50 % shade mesh, with an average temperature of 23 °C, maximum of 39 °C and minimum of 9 °C; and c) from September 3, 2020, for two months, under outdoor conditions, without sun protection, with an average temperature of 20 °C, maximum of 42 °C, and minimum of 2 °C. The production cycle lasted 13 months. Temperature was monitored with an Elitech data logger (Elitech Technology, San Jose, CA, USA).

The plants were produced in black rigid containers mounted on 98-cavity racks. Each tube was 3.8 cm in top diameter, 19 cm long, 160 mL in capacity, and had internal root guides. Prior to sowing, the seed was soaked in water for 24 hours to activate germination; subsequently, it was dried. To avoid possible damage by pathogenic damping-off fungi, it was impregnated with Tecto 60® fungicide (thiabendazole, 2-(4-thiazolyl) benzimidazole).

Experimental design and treatments

Nine treatments were evaluated, considering three substrate mixtures based on peat, composted pine bark, raw pine sawdust, vermiculite, and perlite, and two spore inocula from wild ectomycorrhizal fungi (HSECM): a) *Laccaria laccata* (Scop.) Cooke, native inoculum made from HSECM fruiting bodies collected in mid-2019

from cold temperate forest stands in the Iztaccíhuatl-Popocatépetl National Park and surroundings in Central Mexico, dehydrated fruiting bodies were ground in a Willye type mill, sieved through a 1 mm mesh, and stored at 5 °C until inoculation; b) *Pisolithus tinctorius* (Pers.) Coker et Couch, commercial spore inoculum Ecto-Rhyza®; and c) control (no inoculum) (Table 1). A randomized, complete block experimental design with a 3 x 3 factorial arrangement was used. Each treatment consisted of four replicates and 49 plants per experimental unit.

Table 1. Substrate composition and inoculum of ectomycorrhizal fungi in *Pinus durangensis* Mart. plant production in nursery conditions.

Treatment	Substrate	Mycorrhizal inoculant
1	Peat + vermiculite + perlite (50:25:25) [PVP].	No inoculum [NI].
2	Peat + bark + sawdust (50:25:25) [PBS].	No inoculum [NI].
3	Peat + bark (50:50) [PB]	No inoculum [NI].
4	Peat + vermiculite + perlite (50:25:25) [PVP].	*Laccaria laccata* [Ll]
5	Peat + bark + sawdust (50:25:25) [PBS].	*Laccaria laccata* [Ll]
6	Peat + bark (50:50) [PB]	*Laccaria laccata* [Ll]
7	Peat + vermiculite + perlite (50:25:25) [PVP].	*Pisolithus tinctorius* [Pt]
8	Peat + bark + sawdust (50:25:25) [PBS].	*Pisolithus tinctorius* [Pt]
9	Peat + bark (50:50) [PB]	*Pisolithus tinctorius* [Pt]

After preparing the substrate mixtures for disinfection, they were impregnated with Anibac® PLUS bactericide at a dose of 6.3 mL L^{-1} of water and covered for 15 d with black rubber. During mixing, eight-month-old Multicote® (12N-25P_5O-12K_2O) controlled-release fertilizer was added to each substrate at a rate of 3 g L^{-1}. Seven months after sowing, a second application of fertilizer of the same brand was made, but with a 17N-17P_5O-17K_2O ratio and with four months of release, at a dose of 2 g L^{-1}. The second application was made in each tube, burying the fertilizer 1 cm deep.

To complement the nutrition, fertilization was carried out through irrigation: a) one month after germination and up to seven months after sowing, the soluble fertilizer Master® Finalizer (4N-25P_5O_5-35K_2O) was added at a dose of 1 g L^{-1} of water (except in the period from 3 to 5.5 months of plant age, due to inoculation) (40-109-290 ppm of N-P-K); and b) after seven months of age, Master® Development (20N-7P_2O_5-19K_2O) was used at a dose of 0.5 g L^{-1} of water (100-15-79 ppm of N-P-K). During the fall and winter, water-soluble fertilizers were applied twice a week, and in the spring and summer, fertilizer was applied three times a week.

For each substrate mixture, total porosity, aeration porosity, and moisture holding capacity were estimated (Table 2) based on the methodology developed by Landis (1990). For mycorrhizal inoculants, the spore concentration of each inoculum was determined in a Neubauer chamber. On each plant, 5 mL of spore suspension were applied, equivalent to 1 643 750 spores on average. Two inoculations were performed,

the first at 3.5 months, and 30 days later (4.5 months), the second application was performed using the same dose.

Table 2. Total porosity, aeration porosity, and moisture holding capacity of the substrate mixtures used in the production of *Pinus durangensis* Mart. plants in nursery conditions.

Substrate mixture	Total porosity (%)	Aeration porosity (%)	Humidity retention capacity (%)
PVP	58.3	31.7	26.6
PBS	57.2	28.9	28.3
PB	63.4	31.4	32.0
Recommended value[+]	60 a 80	25 a 35	25 a 55

[+]Landis (1990). PVP: peat + vermiculite + perlite (50:25:25); PBS: peat + bark + sawdust (50:25:25); PB: peat + bark (50:50).

Variable evaluation and statistical analysis

The percentage of survival was evaluated thirteen months after sowing. To analyze morphological growth, 10 plants per experimental unit were randomly taken, and the height (measured using a PILOT® model graduated ruler in millimeters), root collar diameter (using a CALDI-6MP model digital vernier; Truper, Mexico), and wet and dry biomass of the aerial part and the root were recorded. Dry biomass was obtained by placing the plants at 70 °C in a forced ventilation oven (model FE-291D; Felisa, Mexico) for 72 hours. The samples were weighed on an analytical balance (model PA1502, accurate to 0.001 g; Ohaus, NJ, USA). Similarly, the dry biomass ratio of the aerial part, the dry biomass of the root, and the lignification index (Equation 1) were calculated (Villalón-Mendoza *et al*., 2016), as well as the Dickson quality index (DQI) (Equation 2) (Dickson *et al*., 1960).

$$\text{Lignification index} = \left(\frac{\text{Total dry biomass (g)}}{\text{Total wet biomass (g)}} \right) \times 100 \quad (1)$$

$$\text{DQI} = \frac{\text{Total dry biomass (g)}}{\frac{\text{Height (cm)}}{\text{Diameter (mm)}} + \frac{\text{Aerial dry biomass (g)}}{\text{Root dry biomass (g)}}} \quad (2)$$

To determine mycorrhizal colonization (MC) (Equation 3), the methodology described by Salcido-Ruiz *et al*. (2020) was used by randomly selecting three plants per experimental unit and extracting 100 cm of secondary roots, which were preserved in FAA fixative (formaldehyde, glacial acetic acid, 96° alcohol, and distilled water) in a 10:5:50:35 ratio, respectively. In each sample, direct observations were made on the

roots with an optical stereoscope (Leica S9i, Switzerland), recording the number of apices with and without mycorrhizae.

$$MC = \left(\frac{\text{Mycorrhizal apices}}{\text{Mycorrhizal apices} + \text{Non-mycorrhizal apices}} \right) \times 100 \quad (3)$$

The percentage results of MC and survival, being binomial variables, were transformed with the arcsine and square root functions. Furthermore, for the variables evaluated, analyses of variance with Tukey's multiple comparison of means tests ($p \leq 0.05$) were performed using SAS software (SAS Institute, 2009). To calculate the costs per plant, a volume of 160 mL per cavity was considered, according to the inputs used per substrate mix. The evaluation was carried out based on three quotations for the products in Durango, Durango, Mexico, and the proportions used per mixture.

RESULTS AND DISCUSSION

Substrate factor

The substrate factor showed differences ($p \leq 0.05$) in the variables evaluated; in all cases, the PVP-based treatment stood out, except in nursery survival, where PBS and PB were superiors. Likewise, there was a similarity of results between PBS and PB. For the aerial/root ratio (< 2.5) and robustness index (< 6), the values are in agreement with those suggested by Ritchie *et al*. (2010) (Tables 3 and 4).

Regarding total porosity, aeration porosity, and moisture holding capacity, the percentages are in the ranges suggested by Landis (1990) (Table 2), except for total porosity, where only the mixture composed of peat and bark was in the recommended range, which may have influenced the plants to reach the morphological characteristics stipulated by the Mexican Standard for the Certification of Forest Nursery Operation NMX-AA-170-SCFI-2016 (DOF, 2016).

Mycorrhizal inoculum factor

In the mycorrhizal inoculum factor, only the variables root and total biomass production, Dickson's quality index, and percentage of mycorrhizal colonization presented statistical differences ($p \leq 0.05$); the best results were obtained when Pt or Ll was applied for mycorrhizal colonization, but there were no differences between Ll and T for Dickson's quality index. Regarding the hardiness index (< 6) and aerial/root ratio (≤ 2.5), all treatments presented values in the range recommended by Ritchie *et al*. (2010) (Tables 3 and 4).

Vicente-Arbona *et al*. (2019) reported a similar trend when growing *Pinus greggii* Engelm. ex Parl. on five substrates, generated from combinations with sawdust as the main component (60 to 80 % in each substrate), mixed with bark, peat, compost, vermiculite,

Table 3. Morphological characteristics in nursery-grown *Pinus durangensis* Mart. plants 13 months after sowing.

T	I	S	Survival (%)	Height (cm)	Diameter (mm)	Dry biomass (g)		
						Aerial	Root	Total
	All	PVP	93.9 b	15.7 a	5.6 a	2.5 a	1.7 a	4.2 a
S	All	PBS	98.7 a	14.3 b	5.0 b	1.9 b	1.2 b	3.1 b
	All	PB	96.9 ab	13.5 b	5.0 b	1.9 b	1.3 b	3.2 b
	NI	All	95.8 a	15.1a	5.2 a	2.0 a	1.3 b	3.4 b
I	Ll	All	96.5 a	14.1a	5.2 a	2.0 a	1.4 ab	3.5 ab
	Pt	All	96.6 a	14.3 a	5.3 a	2.2 a	1.5 a	3.7 a
1	NI	PVP	94.3 ab	17.6 a	5.6 ab	2.5 ab	1.6 ab	4.1 ab
2	NI	PBS	99.5 a	14.5 b	5.0 bc	1.8 d	1.2 c	3.0 d
3	NI	PB	93.8 ab	13.3 b	5.0 bc	1.9 d	1.2 c	3.1 d
4	Ll	PVP	92.7 b	14.8 ab	5.5 abc	2.4 abc	1.6 ab	4.0 abc
5	Ll	PBS	98.4 ab	14.2 b	5.1 bc	1.9 cd	1.3 c	3.2 cd
6	Ll	PB	98.4 ab	13.4 b	5.0 bc	2.0 cd	1.3 bc	3.3 cd
7	Pt	PVP	94.8 ab	14.7 b	5.8 a	2.8 a	1.8 a	4.6 a
8	Pt	PBS	98.4 ab	14.5 b	5.1 bc	2.0 cd	1.3 bc	3.3 cd
9	Pt	PB	97.9 ab	13.7 b	5.1 bc	2.0 bcd	1.4 bc	3.4 bcd

Different letters in the same column indicate statistical differences (Tukey, $p \leq 0.05$); T: treatment; I: mycorrhizal inoculum; S: substrate; NI: no inoculum; Ll: *Laccaria laccata*; Pt: *Pisolithus tinctorius*; PVP: peat-vermiculite-perlite; PBS: peat-bark-sawdust; PB: peat-bark.

Table 4. Quality indices in nursery-grown *Pinus durangensis* Mart. plants 13 months after sowing.

T	I	S	Aerial/ root ratio	Robustness index	Lignification index (%)	DQI	MC (%)
	All	PVP	1.5 a	2.8 a	30.1 a	1.0 a	27.1 a
S	All	PBS	1.6 a	2.9 a	28.1 b	0.7 b	21.6 b
	All	PB	1.5 a	2.7 a	28.7 ab	0.8 b	21.7 b
	NI	All	1.5 a	2.9 a	28.0 a	0.7 b	15.4 b
I	Ll	All	1.4 a	2.7 a	29.4 a	0.8 ab	28.4 a
	Pt	All	1.5 a	2.7 a	29.5 a	0.9 a	26.6 a
1	NI	PVP	1.6 a	3.1 a	28.8 a	0.9 abc	16.9 bc
2	NI	PBS	1.6 a	2.9 a	27.4 a	0.7 c	14.3 c
3	NI	PB	1.6 a	2.7 a	28.0 a	0.8 bc	15.0 c
4	Ll	PVP	1.5 a	2.7 a	30.1 a	1.0 ab	33.1 a
5	Ll	PBS	1.5 a	2.8 a	29.0 a	0.8 bc	25.9 ab
6	Ll	PB	1.5 a	2.7 a	29.4 a	0.8 bc	26.1 ab
7	Pt	PVP	1.6 a	2.5 a	31.7 a	1.2 a	31.4 a
8	Pt	PBS	1.5 a	2.8 a	28.1 a	0.8 bc	24.6 ab
9	Pt	PB	1.4 a	2.7 a	29.0 a	0.9 bc	23.9 abc

Different letters in the same column indicate statistical differences (Tukey, $p \leq 0.05$). T: treatment; I: mycorrhizal inoculant; S: substrate; DQI: Dickson quality index; MC: mycorrhizal colonization; NI: no inoculum; Ll: *Laccaria laccata*; Pt: *Pisolithus tinctorius*; PVP: peat-vermiculite-perlite; PBS: peat-bark-sawdust; PB: peat-bark.

and perlite, in different proportions, with and without inoculation of *L. laccata* (1.5 g per plant). These authors observed that plant growth due to mycorrhization was not very evident, although the inoculated treatments had 44 to 64 % mycorrhization and the uninoculated individuals had between 14 and 40 % mycorrhization. The same happened with Baltasar-Martínez *et al*. (2007) when inoculating spores of *Rhizopogon roseolus* Corda on *Pinus ponderosa* Dougl. ex C. Laws. plants subjected to three fertilization levels, two inoculation times, and two nursery harvest dates, finding no differences in plant growth or mycorrhizal colonization, with values lower than 39 % in all cases.

Substrate-mycorrhizal inoculum interaction

The interaction of substrate-mycorrhizal inoculum factors was significant in the variables evaluated ($p \leq 0.05$), with the exception of the of the aerial part/root ratio, robustness index, and lignification index. Survival only showed differences between treatments 2 (PBS-SI) (99.5 %) and 4 (PVP-Ll) (92.7 %) (Table 3). Salcido-Ruiz *et al*. (2020) obtained similar results, with 80 to 96 % survival in *Pinus engelmannii* Carr. plants grown in a substrate based on peat, vermiculite, and perlite (57:23:20) eight months after being inoculated with ectomycorrhizal fungi (HECM). Plant survival in the forest nursery at INIFAP's Guadiana Valley Experimental Field was satisfactory (> 90 %) due to relatively controlled environmental conditions.

In the present study, differences ($p \leq 0.05$) were found in morphological variables. Height ranged from 13.3 to 17.6 cm, with treatments 1 (PVP-SI) and 4 (PVP-Ll) in the top statistical group (although there were no differences between the two, nor between the latter and the rest of the treatments) ($p > 0.05$). Diameter ranged from 5 to 5.8 mm, with the highest value in treatment 7 (PVP-Pt), with no differences with treatments 1 and 4; the rest of the treatments had average data from 5 to 5.1 mm (Table 3). The height variable is important because it is associated with the number of needles produced in the plants, which in turn is related to photosynthetic capacity and transpiration area; meanwhile, the diameter of the collar is related to the robustness of the plants (Ritchie *et al*., 2010).

The values of the morphological parameters evaluated comply with the ranges recommended in NMX-AA-170-SCFI-2016 (DOF, 2016), which establishes a height of 15 to 20 cm and neck diameter greater than 4 mm; both parameters are met in treatment 1 (PVP-SI), while the second variable is met in all treatments evaluated. The most prominent substrate (PVP) is the most widely used in Mexico; however, its cost is higher than the other two evaluated (PBS and PB), which is why the latter are beginning to be widely used in nurseries located in central and northern Mexico (Aguilera-Rodríguez *et al*., 2016).

The production of dry biomass of the aerial part fluctuated from 1.8 to 2.8 g, with the formation of diverse statistical groups, where treatment 7 (PVP-Pt) stood out without statistical differences with treatments 1 (PVP-SI) and 4 (PVP-Ll) and values of 2.8, 2.5, and 2.4 g, respectively; the other treatments produced from 1.8 to 2 g. For root dry

biomass, the averages ranged from 1.2 to 1.8 g, with the same behavior as the aerial biomass variable (treatments 7, 1, and 4); total biomass varied from 3 to 4.6 g, and the best results were obtained in the same treatments as for aerial and root biomass (Table 3).

For the aerial/root ratio, the index ranged from 1.4 to 1.6 (Table 4), while the robustness index ranged from 2.5 to 3.1. This implies a robust and balanced plant between root biomass and the aerial part, which favors its quality (Ritchie *et al*., 2010). As for the lignification index, the percentages ranged from 27.4 to 31.7 %, with no differences ($p > 0.05$) between treatments. For the Dickson quality index, values from 0.7 to 1.2 were found, with differences ($p > 0.05$) between treatments. Treatment 7 (PVP-Pt) showed better results, with no significant differences with treatments 4 (PVP-Ll) and 1 (PVP-SI). In general, the PVP substrate stood out (Table 4).

When evaluating *Pinus cooperi* Blanco, produced on four substrates based on S1: peat and bark (54:46); S2: raw sawdust, composted bark, and peat (50:20:30); S3: sawdust, bark, and peat (50:20:30); and S4: sawdust, bark, and peat (50:25:25), González-Orozco *et al*. (2018) reported satisfactory results in S1 in the variables height (15.1 cm), root collar diameter (4 mm), and total biomass (2.8), although S2 and S3 produced plants with acceptable morphological characteristics in height (16.4 and 16.2 cm), diameter (3.8 and 3.7 mm), and total biomass (2.5 and 2.4 g). Castro-Garibay *et al*. (2018) found similar results in plant quality due to the use of sawdust when producing *Pinus greggii* plants on sawdust, bark, and peat-based substrates (60:20:20).

Mycorrhizal colonization (MC) (14.3 to 33.1 %) showed differences ($p \leq 0.05$), forming several statistical groups where treatments 4 to 9 (inoculated with ectomycorrhizal fungi, regardless of the substrate used, and MC from 23.9 to 33.1 %) stood out, although in several cases without differences with the rest of the treatments, which had colonization percentages from 14.3 to 16.9 % (Table 4). Inoculation with spore suspensions with *P. tinctorius* and *L. laccata* allowed mycorrhization in the root systems of *P. durangensis* 13 months after sowing and eight months after inoculation. However, the values were less than 34 %, considered medium to low, including the percentage of undesirable mycorrhization observed in the control treatment (uninoculated). This effect is difficult to avoid in experiments of this nature, since the inoculum can arrive through the air, from the mycorrhizal treatments, or even from outside the experiment; however, it was always significantly lower compared to the inoculated treatments.

The mycorrhizal colonization resulting from this trial is lower than that recorded by Salcido-Ruiz *et al*. (2020), who inoculated *Pinus engelmannii* plants with two mixtures of HECM spores, one composed of *Amanita rubescens* (Pers. ex Fr.) Gray, *Amanita* sp., *Lactarius indigo* (Schwein.), *Ramaria* sp., and *Boletus* sp., and another by a mixture of *P. tinctorius* and *Scleroderma citrinum* Pers; in addition, they added controlled release fertilizer (3 and 6 g L-1 of substrate), obtaining from 15 to 71 % mycorrhization, with an inverse trend in plant quality as a function of the fertilization dose applied. Proper substrate selection is a key element because it favors the production of aerial and root biomass compared to uninoculated plants (Rentería-Chávez *et al*., 2017).

In general, mycorrhizal fungi are aerobic. Saif (1981) indicates that oxygen concentrations between 12 and 16 % are ideal for both mycorrhization and the beneficial expression of this symbiosis in plant growth. In the present study, the lowest MC percentages coincide with the substrates with the highest percentage of moisture retention (PBS and PB) and the highest with the one with the highest aeration porosity (PVP).

This study's mycorrhization percentages were modest, and the mycorrhizal component had little effect on the morphological growth of *Pinus durangensis*. This was similar to Vicente-Arbona *et al.* (2019) on *Pinus greggii* with *L. laccata* and Baltasar-Martínez *et al*. (2007) with *Pinus ponderosa* and *Rhizopogon roseolus*, who found slight differences in plant growth and mycorrhizal colonization due to mycorrhizal inoculum application. Both studies agree that this issue should be further studied in nurseries and plantations. At the latter site, positive effects of mycorrhizal inoculation on initial growth are more likely to be found. This situation was corroborated by Barroetaveña *et al*. (2016), who found that after five years of inoculating *P. ponderosa* plants in nursery conditions with *Suillus luteus* (L) Roussel, *Rhizopogon roseolus*, *Hebeloma mesophaeum* (Louis), and leaf litter, the first two species significantly favored the growth of the plants under study during the period after planting in the field, despite the prevailing conditions of water stress.

The factor with the greatest influence on the results was the substrate, where the PVP combination stood out, but with close values in the other two substrates (PBS and PB). This was largely because the three substrates evaluated, in general, meet the criteria for total porosity, aeration porosity, and moisture holding capacity recommended by Landis (1990). In relation to mycorrhization, although it was not a determining factor in the quality of the plants evaluated, the plant material inoculated with *P. tinctorius* stood out.

Based on the results obtained, treatment 7 (PVP-Pt) stands out with the best values in the variables evaluated, and above all, it complies with the recommendations of NMX-AA-170-SCFI-2016 (DOF, 2016), which establishes the minimum morphological parameters to consider that the plant produced in nursery conditions will have the necessary attributes for adequate survival and initial growth after planting. In the case of the other two substrates evaluated (PB and PBS in interaction with Pt and Ll), they also comply with the minimum values suggested by the standard.

Substrate costs

Based on the price of each component used to prepare the substrates evaluated, the cost per cubic meter was determined (Table 5), with the PVP combination being the highest, followed by PB and PBS (Figure 1). Of the three substrates evaluated, the first was 28.4 % more expensive than PB and 34.6 % higher than PBS, which proved to be the most economical. The difference between the two most economical substrates (PB and PBS) was 8.6 %, with PBS being the least expensive of all.

Table 5. Costs of the materials used in the substrate mixtures evaluated in the production of *Pinus durangensis* in nursery.

Component	Volume presentation (L)	Cost per bulk (USD)¶	Bulks per cubic meter	Cost per cubic meter ($USD)
Peat	160⁺	45.26	6.25	282.9
Vermiculite	114	35.14	8.77	308.2
Agrolite	100	10.65	10	106.5
Bark	1000	69.22	1	69.2
Sawdust	1000	10.64	1	10.6

⁺Volume of the bulk once the peat has been decompacted. ¶Dollar costs as of January 31, 2023, based on three quotes in Durango, Durango, Mexico ($18.78 MXN per $1 USD).

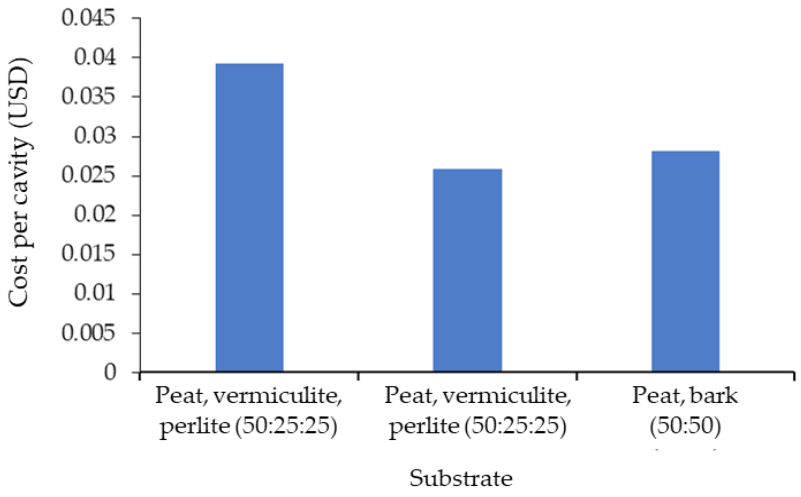

Figure 1. Cost of the evaluated substrates per 160 mL cavity.

Madrid-Aispuro *et al*. (2020) evaluated four substrates based on composted pine bark, raw pine sawdust, and peat, mixed in different proportions, and found that the substrate based on raw sawdust, composted pine bark, and peat is an alternative to produce quality forest plants at a lower production cost, as long as sawdust is incorporated up to a maximum of 50 % in the mixture.

Aguilera-Rodríguez *et al.* (2016) compared in *Pinus montezumae* Lamb. the quality of the plant produced and production costs due to the use of two substrates: composted pine sawdust, composted pine bark, and vermiculite (70:15:15), and peat, perlite, and vermiculite (60:20:20); in both substrates, plant quality was favorable. However, they recommend the former because it is 45.8 % cheaper. González-Orozco *et al*. (2018) compared costs on four substrates: S1: peat and composted pine bark (46:54); S2:

peat, composted bark, and raw pine sawdust (30:20:50); S3: peat, bark, and sawdust (25:25:50); and S4: peat, bark, and sawdust (20:30:50). Although in the first substrate they obtained favorable results in plant quality, S2 and S3 also produced acceptable growth, with lower production costs by 39.8 and 43.1 % in relation to S1.

CONCLUSIONS

The combination of the substrate composed of peat, vermiculite, and perlite (50:25:25) and the inoculation with spores of *Pisolithus tinctorius* had superior values in the morphological characteristics of *Pinus durangensis* plants produced in nursery conditions. The substrate based on peat, vermiculite, and perlite (50:25:25) gave the best results in plant growth; however, the addition to peat of alternative substrates, such as composted bark and raw sawdust (50:25:25), and peat plus composted bark (50:50), also generated good-quality plants, reducing costs by 28. 4 % when using the mixture of peat and bark, and by 34.6 % with the combination of peat, bark, and sawdust. Mycorrhization of *Pinus durangensis* with *Pisolithus tinctorius* produced under nursery conditions generated better quality plants, followed using *Laccaria laccata*.

ACKNOWLEDGMENTS

To the Universidad Juárez del Estado de Durango, for its support to the author of the correspondence "in the exercise of the sabbatical year during the period August 2022-July 2023".

REFERENCES

Aguilera-Rodríguez M, Aldrete A, Martínez-Trinidad T, Ordáz-Chaparro VM. 2016. Producción de *Pinus montezumae* Lamb. con diferentes sustratos y fertilizantes de liberación controlada. Agrociencia 50 (1): 107–118.

Baltasar-Martínez D, Barroetaveña C, Rajchenberg M. 2007. Influencia del régimen de fertilización y del momento de inoculación en la micorrización de *Pinus ponderosa* en la etapa de vivero. Bosque 28 (3): 226–233.

Barroetaveña C, Bassani VN, Monges JI, Rajchenberg M. 2016. Field performance of *Pinus ponderosa* seedlings inoculated with ectomycorrhizal fungi planted in steppe-grasslands of Andean Patagonia, Argentina. Bosque 37 (2): 307–316.

Buamscha MG, Contardi LT, Kasten DR, Enricci JA, Escobar RR, Gonda HE, Jacobs DF, Landis TD, Luna T, Mexal JG, Wilkinson KM. 2012. Colección Nexos. Producción de plantas en viveros forestales. Consejo Federal de Inversiones: Buenos Aires. Argentina. 188 p.

Castro-Garibay SL, Aldrete A, López-Upton J, Ordáz-Chaparro VM. 2018. Efecto del envase, sustrato y fertilización en el crecimiento de *Pinus greggii* var. *australis* en vivero. Agrociencia 52 (1): 115–127.

CONAFOR (Comisión Nacional Forestal). 2021. Estado que guarda el sector forestal en México. Comisión Nacional Forestal: Zapopan, México, 454 p.

Dickson A, Leaf AL, Hosner JF. 1960. Quality appraisal of white spruce and white pine seedling stock in nurseries. The Forestry Chronicle 36 (1): 10–13. https://doi.org/10.5558/tfc36010-1

DOF (Diario Oficial de la Federación). 2016. Declaratoria de vigencia de la Norma Mexicana NMX-AA-170-SCFI-2016, Certificación de operación de viveros forestales. Gobierno de México. Secretaría de Economía. Ciudad de México, México. https://www.dof.gob.mx/nota_detalle.php?codigo=5464460&fecha=07/12/2016#gsc.tab=0 (Retrieved: June 2023).

Escobar-Alonso S, Rodríguez-Trejo DA. 2019. Estado del arte en la investigación sobre calidad de planta del género *Pinus* en México. Revista Mexicana de Ciencias Forestales 10 (55): 4–38. https://doi.org/10.29298/rmcf.v10i55.558

FAO (Food and Agriculture Organization of the United Nations). 2018. The state of the world's forests 2018. Rome, Italy. 27 p. https://www.fao.org/3/CA0188EN/ca0188en.pdf (Retrieved: September 2022).

Fregoso-Madueño JN, Goche-Télles JR, Rutiaga-Quiñones JG, González-Laredo RF, Bocanegra-Salazar M, Chávez-Simental JA. 2017. Alternative uses of sawmill industry waste. Revista Chapingo Serie Ciencias Forestales y del Ambiente 23 (2): 243–260. https://doi.org/10.5154/r.rchscfa.2016.06.040

García-Rodríguez JL, Pérez-Moreno J, Ríos-Leal D, Saez-Delgado P, Atala-Bianchi C, Sánchez-Olate M, Pereira-Cancino G. 2017. *In vitro* growth of ectomycorrhizal fungi associated with *Pinus radiata* plantations in Chile. Revista Fitotecnia Mexicana 40 (4): 413–431.

Gayosso-Rodríguez S, Borges-Gómez L, Villanueva-Couoh E, Estrada-Botello MA, Garruña-Hernández R. 2016. Sustratos para producción de flores. Agrociencia 50 (5): 617–631.

González-Orozco MM, Prieto-Ruíz JÁ, Aldrete A, Hernández-Díaz JC, Chávez-Simental JA, Rodríguez-Laguna R. 2018. Sustratos a base de aserrín crudo con fertilización y la calidad de planta de *Pinus cooperi* Blanco en vivero. Revista Mexicana de Ciencias Forestales 9 (48): 203–225. https://doi.org/10.29298/rmcf.v8i48.125

Grossnickle SC. 2018. Seedling establishment on a forest restoration site. Reforesta 6: 110–139. https://doi.org/10.21750/refor.6.09.62

Grossnickle SC, MacDonald JE. 2018. Seedling quality: History, application, and plant attributes. Forests 9 (5): 283–139. https://doi.org/10.3390/f9050283

Hernández-Zarate L, Aldrete A, Ordaz-Chaparro VM, López-Upton J, López-López MÁ. 2014. Crecimiento de *Pinus montezumae* Lamb. en vivero influenciado por diferentes mezclas de sustratos. Agrociencia 48 (6): 627–637.

Landis TD. 1990. Containers and growing media. *In* Landis TD, Tinus RW, McDonald SE, Barnett JP. (eds.), The container tree nursery manual Vol II, Agriculture Handbook 674. USDA Forest Service: Wahington, DC, USA, pp: 41–85.

Madrid-Aispuro RE, Prieto-Ruíz JÁ, Aldrete A, Hernández-Díaz JC, Wehenkel C, Chávez-Simental, JA. 2020. Crecimiento de *Pinus cembroides* Zucc. en vivero en diversos sustratos y fertilizantes. Agrociencia 54 (4): 539–554. https://doi.org/10.47163/agrociencia.v54i4.2051

Mateo-Sánchez JJ, Bonifacio-Vázquez R, Pérez-Ríos SR, Mohedano-Caballero L, Capulín-Grande J. 2011. Producción de *Cedrela odorata* L. en sustrato a base de aserrín crudo en sistema tecnificado en Tecpan de Galeana, Guerrero, México. Ra Ximhai 7 (1): 123–132.

Rentería-Chávez MC, Pérez-Moreno J, Cetina-Alcalá VM, Ferrera-Cerrato R, Xoconostle-Cázares B. 2017. Transferencia de nutrientes y crecimiento de *Pinus greggii* Engelm. inoculado con hongos comestibles ectomicorrícicos en dos sustratos. Revista Argentina de Microbiología 49 (1): 93–104. https://doi.org/10.1016/j.ram.2016.06.004

Ritchie GA, Landis TD, Dumroese RK, Hasse D. 2010. Assessing Plant Quality. *In*: Landis TD, Dumroese RK, Hasse DL. (eds.) The container tree nursery manual: Volume 7, Seedling processing, storage, and outplanting. Agriculture Handbook 674. USDA Forest Service: Wahington, DC, USA, pp: 17–81.

Saif SR. 1981. The influence of soil aeration on the efficiency of vesicular-arbuscular mycorrhizae. I. Effect of soil oxygen on the growth and mineral uptake of *Eupatorium odoratum* L. inoculated with *Glomus macrocarpus*. New Phytologist 88 (4): 649–659. https://doi.org/10.1111/j.1469-8137.1981.tb01741.x

Salcido-Ruiz S, Prieto-Ruíz JÁ, García-Rodríguez JL, Santana-Aispuro E, Chávez-Simental JA. 2020. Mycorrhiza and fertilization: effect on the production of *Pinus engelmannii* Carr. in nursery. Revista Chapingo Serie Ciencias Forestales y del Ambiente 26 (3): 327–342. https://doi.org/10.5154/r.rchscfa.2019.11.080

Sanchún A, Obando G. 2016. El papel de los viveros forestales en la restauración. *In* Sanchún A, Botero R, Morera A, Obando G, Russo RO, Scholz C, Spinola M. (eds.), Restauración funcional del paisaje rural: manual de técnicas. Unión Internacional para la Conservación de la Naturaleza: San José, Costa Rica, pp: 349–371.

SAS Institute. 2009. SAS/STAT® 9.2. User´s Guide. SAS Institute Inc. Cary, NC, USA. http://support.sas.com/documentation/cdl/en/statugmcmc/63125/PDF/default/statugmcmc.pdf (Retrieved: July 2022).

Scholz C, Morera A. 2016. Restauración de pasajes forestales. *In* Sanchún A, Botero R, Morera A, Obando G, Russo RO, Scholz C, Spinola M. (eds.). Restauración funcional del paisaje rural: manual de técnicas. Unión Internacional para la Conservación de la Naturaleza: San José, Costa Rica, pp: 13–24.

Vicente-Arbona JC, Carrasco-Hernández V, Rodríguez-Trejo DA, Villanueva-Morales A. 2019. Calidad de planta de *Pinus greggii* producida en sustratos a base de aserrín. Madera y Bosques 25 (2): e2521784. https://doi.org/10.21829/myb.2019.2521784

Villalón-Mendoza H, Ramos-Reyes JC, Vega-López JA, Marino B, Muños-Palomino MA, Garza-Ocañas F. 2016. Indicadores de calidad de la planta de *Quercus canby* Trel. (encino) en vivero forestal. Revista Latinoamericana de Recursos Naturales 12 (1): 46–52.

Villar-Salvador P, Peñuelas-Rubira JL, Nicolás-Peragón JL. 2021. La calidad de los materiales de reproducción. *In* Pemán García J, Navarro Cerrillo RM, Prada Sáez MA, Serrada Hierro R. (coords.), Bases Técnicas y Ecológicas del Proyecto de Repoblación Forestal. Ministerio para la Transición Ecológica: Madrid, España, pp: 781–822.

Agrociencia

BIODIESEL CONSUMPTION OUTLOOK IN MEXICO

Laura Elena **Cantú-Nieves**[1*], Oscar Antonio **Arana-Coronado**[1], Graciela Margarita **Bueno-Aguilar**[1], José Jaime **Arana-Coronado**[1], José de Jesús **Brambila-Paz**[1], Erik Oswaldo **Camacho-Villán**[2]

[1]Colegio de Postgraduados Campus Montecillo. Postgrado en Socioeconomía, Estadística e Informática. Carretera Mexico-Texcoco km 36.5, Montecillo, Texcoco, State of Mexico, Mexico. C.P. 56230.
[2]Universidad Nacional Autónoma de México. Facultad de Ingeniería. Escolar 04360, Ciudad Universitaria, Coyoacán, Mexico City, Mexico. C.P. 04510.
* Author for correspondence: laura_cantu2016@hotmail.com

Citation: Cantú-Nieves LE, Arana-Coronado OA, Bueno-Aguilar GM, Arana-Coronado JJ, Brambila-Paz J de J, Camacho-Villán EO. 2024. Biodiesel consumption outlook in Mexico. **Agrociencia** 58(4): 500-513. https://doi.org/ 10.47163/agrociencia.v58i4.2818

Editor in Chief:
Dr. Fernando C. Gómez Merino

Received: May 31, 2022.
Approved: January 30, 2024.
Published in Agrociencia: May 30, 2024.

ABSTRACT

Mexico has a developing biodiesel market. Although the international trend of production and consumption has increased over the last decade, the quantities produced in the country are still minimal compared to those of petrodiesel. To understand the reasons why Mexico has an under-exploited and under-utilized market, this work describes the current demand situation with a theoretical proposal of a model that responds to seven explanatory variables of its behavior: price of biodiesel, price of petrodiesel as a substitute good, price of petrodiesel as a complementary good, income of the population, number of transports with a functional diesel engine, certifications, and the availability of the product in the supply chain. The lack of regulation regarding the norms for the production, handling, transport, and disposal of this type of biofuel means that there is still no defined biodiesel market in Mexico, which means that most biodiesel production is destined for self-consumption or informal retail sales, which means that the product does not have a defined supply chain in the country.

Keywords: certifications, demand, petrodiesel.

INTRODUCTION

Mexico is considered one of the 10 largest oil producers and exporters in the world (PEMEX, 2020). The country's budget revenue from oil in 2019 was 3.9 %, and by 2020 it was 3.5 % of total GDP (SHCP, 2020), representing an important part of the nation's income. However, the National Hydrocarbons Commission mentions that the country has 8.8 years of proven reserves with minimal risk for extraction according to the relationship between reserves and crude oil production, considering 1.6 million barrels per day under current technological conditions. These types of reserves, from a financial perspective, are the most important because they underpin investment projects, as they have a probability of extraction of at least 90 % (CNH, 2021).

Various organizations worldwide have examined the sustainability of the current energy system and hold a general view: "The energy system as we know it is

unsustainable." The energy model is conditioned by three factors: 1) the availability of resources to meet the demand for energy; 2) the environmental impact caused by the means used for its supply and consumption; and 3) the lack of equity in access to this essential element for human development (Castro-Martínez *et al*., 2012). These factors call for the use of bioenergy and renewable energies that have a low environmental impact, contribute to climate change mitigation, and reduce dependence on fossil fuels (Montero-Alpírez *et al*., 2016).

Bioenergy use falls into two main categories: traditional and modern. Traditional use refers to the combustion of biomass in forms such as wood for fuelwood, animal waste, and traditional charcoal. Modern bioenergy technologies include liquid biofuels produced from different plant species and oils, biorefineries, biogas produced by anaerobic digestion of waste, and heating systems using wood pellets, among other technologies. At present, two types of liquid biofuels can be distinguished: bioethanol and biodiesel. Modern bioenergy accounted for approximately 5.1 % of total global energy demand in 2018 (REN21, 2020).

Biofuels are an attractive source of energy because they are produced from renewable feedstock sources. They are also biodegradable, non-toxic, and generate fewer undesirable emissions (CO, aromatic hydrocarbons, soot particles, metals, sulfur, and nitrogen oxides). They are produced in liquid form and are mainly used for the transport sector as substitutes for gasoline and diesel, either in full or in blends (OECD, 2018). The production and use of renewable energy have led to an increase in the use of labor, generating a total of 12 018 041 jobs worldwide in 2020, of which 2 410 862 were created by production activities related to liquid biofuels (IRENA, 2022).

This essay takes a critical approach to analyzing the current state of the biodiesel market in Mexico, which was found to be incipient compared to the fossil diesel market. A theoretical model of biodiesel demand was proposed, documented by the behavior of the components that could explain the consumption of this biofuel, with the aim of determining the variables that have an impact on the consumer and thus encouraging the development of this market and understanding the challenges and opportunities of optimizing its use and consumption.

BIODIESEL AS A PRODUCT

Over the past decade, according to data from the International Renewable Energy Agency, there has been an increasing trend in energy capacity from bioenergy (Table 1). This can be classified into four categories: solid biofuels, comprising solid organic non-fossil material of biological origin (also known as biomass) such as charcoal, wood, wood residues and by-products, black liquor, bagasse, animal waste, vegetable waste, and the renewable fraction of industrial waste; biogas, consisting mainly of methane and carbon dioxide, produced by anaerobic digestion of biomass or by thermal processes from biomass, including that contained in waste; municipal waste; and liquid biofuels such as ethanol or biodiesel (IRENA, 2022).

Table 1. Global comparison of bioenergy categories produced (MW).

Year	2010	2020
Solid biofuels	47 788	89 042
Biogas	9519	20 108
Municipal renewable waste	6677	15 414
Liquid biofuels	1869	2637
TOTAL	65 853	127 201

The American Society for Testing and Materials defines biodiesel as a mixture of mono-alkyl esters of long-chain fatty acids obtained from vegetable oils or animal fats used in compression ignition engines (ASTM, 2021). This fuel is an alternative to petroleum diesel and is obtained from biomass, making it renewable. Depending on the raw material source, it is classified as first, second, or third generation. First generation biodiesel is defined as biodiesel produced from the processing of oils extracted from food crops, such as soybean, sunflower, and canola oils. Second-generation feedstocks come from non-food-competing crops or from animal and plant residues such as *Jatropha curcas* L., *Ricinus communis* L., yellow fats, animal tallow, and waste vegetable oils. Lastly, third-generation microalgae are produced from microalgae (Montero-Alpírez *et al*., 2016).

In Mexico, the Ministry of Agriculture and Rural Development (SADER) is in charge of granting prior permits for the production of first-generation biodiesel from maize grain in its various forms, which are granted only when there are surplus inventories of domestic maize production to satisfy national consumption. The production of second-generation bioenergy does not require a prior permit (DOF, 2008).

Biodiesel is commercially produced by transesterifying vegetable oils with alcohol. The most commonly used alcohols are methanol and ethanol, which can be produced from renewable energy sources. In this reaction, vegetable oils or animal fats react with an alcohol in the presence of a catalyst (acidic, basic, or enzymatic), producing the corresponding alkyl esters of alcohol and glycerol (Castellar-Ortega *et al*., 2014). As a liquid biofuel, biodiesel is part of a cleaner transition to a mobility paradigm based on internal combustion. While providing environmentally more sustainable mobility alternatives to fossil fuels, biodiesel enables cleaner mobility without major technical changes (Torroba, 2020).

Regarding the energy efficiency of pure biodiesel (100 %), which is known as B100, Balan-Chan (2018) reported a reduction of 9 mg kg kg^{-1} sulfur over fossil diesel fuel, a reduction of 0.02 kg MJ^{-1} carbon dioxide (CO_2), 0 % m/m paraffin content, and 11 % m/m oxygen content, which makes it have a cleaner combustion process. However, it should also be noted that their combustion can lead to an increase in nitrogen oxides (NO_x) by 10 % compared to fossil diesel.

BIODIESEL PRODUCTION IN MEXICO AND THE WORLD

Biodiesel production and consumption are relatively recent. For example, for the United States, the second largest biodiesel producer in 2020 and the main foreign supplier of biodiesel to Mexico, its production in 2000 was zero (EIA, 2021); however, at the international level, there has been an increasing production trend in recent years (Table 2).

Table 2. Global biofuel production (thousands of barrels per day).

	2015	2016	2017	2018	2019
Production	2218	2324	2393	2612	2690
Bioethanol	1685	1703	1731	1850	1886
Biodiesel	533	621	662	762	805

Globally, in 2019, bioethanol accounted for around 59 % of biofuel production (in terms of energy). Fatty acid methyl ester (FAME) biodiesel accounted for 35 % and hydro-biodiesel (HVO hydrotreated vegetable oil) for 6 % (REN21, 2020).

Biodiesel production is geographically diverse. In 2021, in order of production importance, are the European Union, Indonesia, Brazil, the USA, Argentina, China, Thailand, Malaysia, Colombia, and Canada (Table 3) (Statista, 2023).

Table 3. Main biodiesel producing countries in 2021.

Location	Country	Biodiesel (Mg)
1	European Union	9.92
2	Indonesia	8.2
3	Brazil	5.95
4	United States	5.46
5	Argentina	1.72
6	China	1.5
7	Thailand	1.46
8	Malaysia	1
9	Colombia	0.58
10	Canada	0.32

In Mexico, there are no reliable statistics on biodiesel production (Sosa-Rodríguez and Vázquez-Arenas, 2021), despite the fact that the country has a high potential for biodiesel production from non-food crops and plant and animal waste. Riegelhaupt *et al.* (2016) estimated that, in Mexico, the production of oilseeds (palm, coconut, soybean, sunflower, higuerilla, and jatropha) specifically for the production of oils for biodiesel could evolve from 295 019 oil-equivalent m^3 in 2014 to 607 223 oil-equivalent m^3 in 2030.

However, production is still incipient (Montero-Alpírez *et al*., 2016), and the quantities produced and marketed are not comparable to those of fossil fuels (Paredes-Cervantes *et al*., 2020). This is reflected in the energy consumption of petroleum diesel, which in 2020 in Mexico was 627 880 PJ, while the total energy consumption of all renewable energies for the same year in the country was 387 170 PJ (SENER, 2021). In 2020, Mexico bought 2240 Mg of biodiesel from the United States, its main supplier. These imports contribute to the product being marketed in the country (Table 4).

Table 4. US biodiesel exports to Mexico.

Year	Mg	Participation (%)
2017	20440	6.96
2018	12180	3.9
2019	3920	1.13
2020	2240	0.59

As for the legal framework underpinning the production of biodiesel in the country as a bioenergy, we find the Law for the Promotion and Development of Bioenergy (LPDB), which regulates articles 27 and 27 Section XX of the Political Constitution of the United Mexican States, with the purpose of planning the development of activities in this area.

BIODIESEL DEMAND

In order to understand the consumption behavior of a product, it is necessary to study how its demand behaves, which refers to the complete relationship between the price of a good and the quantity demanded of it. Many factors influence purchasing plans for biodiesel or any satisfactory biodiesel. For example, the quantity of a satisfier that a person wants to buy in a given period is a function of the price of the satisfier, or the person's monetary income, the price of other satisfiers, and the person's tastes (Salvatore, 1977).

The behavior of biodiesel demand could be explained by a theoretical model composed of the following variables:

QBD as a function of (*PBD*, *PPDS*, *PPDC*, *IP*, *QTR*, *CER*, *DIS*)

where *QBD* is the quantity demand for biodiesel (product), *PBD* is the price of biodiesel (good price), *PPDS* is the price of petrodiesel (substitute good price), *PPDC* is the price of petrodiesel (complementary good price), *IP* is the income of the population (income received by the population), *QTR* is the number of transports that have a functional diesel engine (population), *CER* is the certifications (market variable), and *DIS* is the availability in the supply chain (market variable).

Biodiesel price

The first determining factor is the relationship between the quantity of biodiesel demanded and its price. Biodiesel prices depend mainly on the costs of the raw materials used for its production, with this price being approximately 76 % of the biodiesel production costs (Almeida-Naranjo *et al*., 2022). This cost is attributed to a feedstock with a different environmental profile, which makes decision-making at the operational level crucial to reducing production costs and managing the environmental performance of biodiesel while maintaining the quality and parameters set by regulatory institutions. In this regard, Sandar *et al*. (2019) mentioned that the low probability of a successful introduction of liquid biofuels is due to high production costs, which would lead to high prices, and therefore biofuel would not be consumed in high quantities according to the law of demand.

Bioenergy competes in an open market field against traditional fossil fuels that are still abundant and cheap, as their environmental costs are not internalized. This means that bioenergy prices are often not competitive with fossil fuel prices (Sosa-Rodríguez and Vázquez-Arenas, 2021). The cost of biodiesel is 10 to 50 % higher than that of petroleum diesel. Although biodiesel has many advantages over petrodiesel, high production prices are a barrier to its commercialization. Opportunities for biodiesel are small, mainly due to insufficient feedstock production that requires a fiscal incentive policy to keep producers in the market (Paredes-Cervantes *et al*., 2020). Improving production processes and lowering processing costs may represent an area of opportunity.

In Mexico, there are two sources for producing biodiesel: a) crude vegetable oils; and b) used oils and fats. Of the former, 38 % of biodiesel was produced in 2016 from seeds such as Mexican piñón (*Jatrophacurcas*) and higuerilla (*Ricinus communis*) (Riegelhaupt *et al*., 2016). Mexico has potential areas for the production of crops that will supply biorefineries or biofuel production centers. However, it requires the establishment of legislation to maintain the price of inputs, as well as production guidelines to consolidate supply chains that allow for sustainable and economically viable development (Rosas-Barajas *et al*., 2017).

The second method, using low-cost, non-edible oils, could be an option to enhance the competitiveness of biodiesel production and commercial production on an industrial scale (Salvi and Panwar, 2012). Biodiesel will be a sustainable alternative when the challenge of a cost-effective source of supply is overcome (Rosas-Barajas *et al*., 2017). The use of low-cost feedstocks, such as used cooking oils, has gained importance in biodiesel production due to its potential economic and environmental advantages (Caldeira *et al*., 2014). The use of waste oils as feedstock can consider two options that exist in practice in Mexico: 1) the company pays a set price for used oil through independent collectors; and 2) the company collects the used oil and pays a price at source (Riegelhaupt *et al*., 2016).

In Mexico, it was reported that a liter of used oil at the factory gate is paid between 7 and 8 MXN L^{-1} and that the conversion ratio of oil to biodiesel is 1:1 (by volume). Oil is

the largest component (55 %) of the production cost of biodiesel from waste oils, which is estimated at 13.72 MXN L^{-1}, and the price of biodiesel ranges between 14.22 and 18.22 MXN L^{-1} (Riegelhaupt *et al*., 2016). However, it is difficult to define an average price for biodiesel due to the structure of the market, which is mostly informal or self-consumption. Sosa-Rodríguez and Vázquez-Arenas (2021) indicated a biodiesel price in the range of 0.53 to 0.87 USD L^{-1}, which in national currency is equivalent to 9.13 to 14.99 MXN L^{-1}. However, Mexico does not have sufficient infrastructure to transform the amount of waste oil required to supply the national demand for biofuels (Rosas-Barajas *et al*., 2017).

In Mexico City, the Ministry of the Environment (SEDEMA) is in charge of promoting the proper management of the final disposal of cooking oil. In 2015, the environmental standard NADF-012-AMBT-2015 was created to establish the technical specifications for the integrated management of waste animal and/or vegetable fats and oils in the city and thus facilitate their use and recovery in order to reincorporate them into production processes such as obtaining biodiesel. According to SEDEMA (2017), there are only 10 registered companies dedicated to the collection and storage of cooking oil. According to Riegelhaupt *et al.* (2016), the companies involved in collecting cooking oil for biodiesel production in various parts of the country are: Reoil Mexico, Moreco, Biofuels of Mexico, and Solben (two of them with activities in Mexico City).

Likewise, documentation is needed on pre-treatment methods by type of oil or fat to optimize their use, as their cost varies depending on the raw material and the technology used without being able to contribute to an overall cost that is attractive to bidders, in addition to not including logistics and operating costs, which are also a barrier for those who want to participate in the supply of biodiesel, as they are high.

On the other hand, some private sector companies recycle the oil used in their production processes to produce biodiesel, as it is cheaper than final disposal and is considered wasteful in Mexico. The biodiesel generated by these companies is used for self-consumption as an additive to the fuel used in their transport fleet, seeking recognition as socially responsible companies. For this reason, one of the main challenges for biodiesel production in Mexico is related to its input and transport costs, restricting its pre-production and consumption locally (Sosa-Rodríguez and Vázquez-Arenas, 2021).

Price of the substitute good

Biodiesel obtained from vegetable oils is an alternative to replace part of the oil demanded, proving to be a good fuel when blended in any proportion with diesel from fossil fuels (Mofijur *et al*., 2016). In this scenario, it was considered that the best substitute for biodiesel is fossil diesel, and vice versa. The most obvious benefits of using biodiesel as a complement or substitute for fossil diesel is that it is a biodegradable, non-explosive, non-flammable, renewable, and non-toxic substance whose combustion generates low levels of greenhouse gas emissions such as CO_2, NO_x, SO_x, and particulate matter (Mofijur *et al*., 2016). For biodiesel to become a real energy

alternative, it is necessary that this product not only has equivalent characteristics to fossil diesel, but also that positive greenhouse gas emission balances are achieved throughout the production process and that it reaches the market at a lower or similar price to petroleum diesel (Medina-Ramírez *et al*., 2012).

The fossil energy balance represents the ratio between the energy contained in the biofuel and the fossil energy used in its production. A fossil energy balance of 1.0 means that it takes as much energy to produce one liter of biofuel as there is energy in the biofuel; in other words, the biofuel in question is neither a net energy gain nor a net energy loss. An energy balance of 2.0 means that one liter of biofuel contains twice the energy needed to produce it (FAO, 2008). For biodiesel produced from waste vegetable oil, the energy balance is between 4.8 and 5.8 energy units, and for diesel, it is slightly less than 1 energy unit (FAO, 2008).

Price of the complementary good

Normally, biodiesel is blended with fossil diesel, with the B20 blend (20 % biodiesel and 80 % fossil diesel) being the most common in Mexico. Some countries have used blends with higher proportions, such as B30 (30 % biodiesel and 70 % fossil diesel) and the pure form B100, because the percentage of biodiesel that can be used varies by engine year and manufacture (IMP, 2017). In this case, diesel can also be considered a complementary good. The benefits inside combustion engines are notable, as they can extend engine life, aid fuel efficiency, and reduce greenhouse gas emissions (Ogunkunle and Ahmed, 2019).

In Mexico, in order to use biofuels within the national territory in the automotive and aeronautical sectors, they must be blended with fossil fuels in terms of NOM-016-CRE. However, when the standard was studied, it was found that there is no technical specification for the blending of biodiesel, and those mentioned for biofuels refer specifically to bioethanol. High production costs restrict the profitability of this fuel, as the selling price of biodiesel depends on the price of fossil fuels. Therefore, in order to create a market, it is essential that the price of biodiesel becomes independent of non-renewable fuels (Sosa-Rodríguez and Vázquez-Arenas, 2021).

Income of the population

Consumer income also influences demand. Although an increase in income leads to an increase in demand for most goods, this demand does not extend to all goods. A normal good is one for which demand increases as income rises; an inferior good is one for which demand falls as income rises (Salvatore, 1977). In this work, biodiesel was considered to belong to the classification of an inferior good because of the hypothesis that suggests that, if the income of the population increases, they will no longer be forced to use the diesel substitute, so they will be indifferent to purchasing one or the other depending on their prices. For practicality, the consumer will be inclined to use petroleum diesel as biodiesel does not have a defined supply chain within the national territory (Rosas-Barajas *et al*., 2017).

Number of transports with a functional diesel engine

In recent years, biodiesel production in the international context has increased as a result of efforts to mitigate climate change and promote sustainable development (Montero-Alpírez *et al*., 2016). The global adoption of biodiesel in the transport sector has brought with it a reliable fuel supply that can be used in diesel-type engines without modification (Ogunkunle and Ahmed, 2019).

By 2020, 1 411 242 trucks and cargo vans were registered in circulation in the State of Mexico and 57 046 passenger trucks were using diesel, figures that increased compared to those registered in 2010, which were 560 346 trucks and cargo vans and 10 909 passenger trucks (INEGI, 2020), with these types of transport being the main potential consumers of biodiesel. By increasing its presence, biodiesel consumption could also increase its demand.

Certifications

The properties of biodiesel are highly dependent on the type of feedstock used for its production (Zhang and Jiang, 2017). Therefore, fuel specifications are necessary to confine fuel properties to an acceptable range, control fuel quality, and ensure reliable performance in engine use, as the rational consumer will always be looking for the best possible quality. One of the main technical challenges involved in biodiesel production in Mexico is the fact that low-quality feedstocks are used, mainly waste and used oils, which have a high percentage of free fatty acids that hinder the alkaline transesterification process (Sosa-Rodríguez and Vázquez-Arenas, 2021).

Quality assurance of biodiesel through technical specifications is not only functional to ensure the physico-chemical characteristics of the biofuel but also influences consumer confidence and, in turn, the successful marketing of the product, so its implementation is essential to stimulate the market. Sandar *et al*. (2019) noted that global quality standardization would enhance the potential of this product by making it a commodity.

Among the existing worldwide specifications for biodiesel, those of the American Society for Testing and Materials (ASTM) and the European Committee for Standardization (CEN) stand out, particularly ASTM D6751 and UNE EN14214, which define the quality of pure biodiesel, while ASTM D7467 and EN590 explain biodiesel blends. The properties listed in these specifications include calorific value, cetane number, density, viscosity, ash content, copper corrosion, water content, sulfur, and glycerin, among others (ASTM, 2021). In the United States and Canada, the National Biodiesel Accreditation Commission, through the BQ-9000 standard, regulates the characteristics of biodiesel.

Mexico is recognized as an oil-producing and exporting country, so little attention has been paid to energy policy to develop alternative sources, including biofuels. Thus, the Mexican government lacks mandates for specific biodiesel production targets (blending obligations), unlike countries such as Brazil and the European Union (Sosa-Rodríguez and Vázquez-Arenas, 2021). There is a need to create a standardized

method to determine the quality parameters included in the Mexican standards for the production and marketing of biofuels, as there is currently no such regulation, which prevents the production of quality biodiesel and continues to encourage the self-consumption market (SENER, 2017).

Supply chain availability

In Mexico, there is little information for the identification of biofuel supply chains, which is insufficient to build indicators of the links of a real supply chain and to initiate a standardization and optimization of production processes (Rosas-Barajas *et al*., 2018). Yue *et al.* (2014) proposed five key components of the biofuel value chain, which are: biomass production system, biomass logistics system, biofuel production system, distribution system, and biofuel end use.

The biodiesel industry in Mexico is incipient and slow-growing, as it is mostly composed of small-scale production for self-consumption (Riegelhaupt *et al*., 2016). Most of the distribution is done using demijohns or containers (Sosa-Rodríguez y Vázquez-Arenas, 2021). Currently, there are 29 Mexican companies that are part of the supply chain and received permits in a period between December 2009 and April 2018 to carry out activities authorized by the Ministry of Energy for the marketing and transportation of biodiesel. In that period, only one permit was issued for its production (SENER, 2018).

Cabrera-Munguia *et al*. (2022) mention that there are seven companies leading the biodiesel production chain (production, collection, and technology generation), which together generate around 5277 m^3 per year. These companies are: 1) Probioram S. de R.L. de M. I, located in the state of Puebla, which started operations in 2013 and uses animal fat as raw material for the production of biodiesel; 2) RicinoMex, inaugurated in 2017 in the state of Oaxaca as an initiative to build a bio-refinery, managing the link with farmers in the region for the planting of fig trees and the production of biodiesel and castor oil; 3) Cooperativa Agrícola Luz Michell S.C. de R.L. de C.V., located in the state of Durango, is one of the largest biodiesel producers in Mexico, which started operations in 2015 and uses animal fats and cottonseed oil as feedstock; 4) CEDA, which started operations in 2020 in the Central de Abastos in the Iztapalapa mayoralty of Mexico City, with support from the city government through the Ministry of Education, Science, Technology, and Innovation (SECTEI) and the National Polytechnic Institute (IPN), and has a large production capacity plant that converts waste edible oil into biodiesel; 5) Enrimex, located in the north of the state of Baja California, has been producing biodiesel since 2014, using fig seed oil as a raw material; 6) Grima Biodiésel, a company that started operating in 2010 in the state of Puebla that also offers advice, technical support, training, consultancy, and certified equipment for bioenergy projects focused on the use of biofuels; and 7) Biorecen, established in 2011 in the state of Mexico, produces biodiesel and is dedicated to the collection, management, and final disposal of all types of waste.

In terms of research, the Ministry of Energy, together with the National Council of Humanities, Sciences and Technologies (CONAHCYT), established the Sectoral Fund for Energy Sustainability (FSE), whose purpose is to finance initiatives and programs to promote the design and implementation of projects for the sustainable use of various renewable energy sources. The ESF was created in 2008 and financed the Mexican Energy Innovation Centres (CEMIEs), which are groupings of public or private research centers, higher education institutions, companies and governmental entities that aim to work together on projects dedicated to developing technologies, products and services that allow the country to take advantage of its potential in the main renewable energies. Within CEMIEs, research is considered for solid biofuels, bio-alcohols, biodiesel, biogas and bioturbosine (CONAHCYT, 2016). The "advanced biodiesel cluster", located in the city of Guadalajara, is intended for the scientific and technological development of biodiesel. Currently, it is not operating due to the cancellation of the government budget in 2021 (Advanced Biodiesel Cluster, 2016).

In general, information on marketing channels, customers, and prices is scarce and unreliable, making it difficult to describe a formal biodiesel market (Riegelhaupt *et al*., 2016). Sosa-Rodríguez and Vázquez-Arenas (2021) found that there are currently no service stations or infrastructure for the distribution of biodiesel, as is the case for hydrocarbons (pipelines), nor security for transport guidelines. This makes it difficult for consumers to access the product, and the way in which it is distributed, without a regulatory framework, as it is marketed in cylinders, leads to a lack of confidence in biodiesel purchases. Therefore, there is a need for rules that not only regulate production standards, but also take care of the technical requirements for the distribution of biofuel.

CONCLUSIONS

International demand for biodiesel has increased; however, in countries such as Mexico, the market is still incipient compared to that of petrodiesel, as its low production is destined for self-consumption or informal sales. According to the structure of biodiesel demand analyzed, petroleum diesel is its main substitute and, at the same time, its main complementary good, as both are used simultaneously, with the B20 blend being the most common for Mexico. It was determined that for there to be an increase in the amount of biodiesel consumed, its price needs to be lower than that of petrodiesel, with the use of recycled feedstock from used cooking oil being an option to reduce its production cMexico lacks official figures on biodiesel consumption. Several studies pointed out that tastes and preferences for their use are growing for reasons of contributing to climate change mitigation. Furthermore, the consumption of this biofuel is growing with the increasing presence of functional biodiesel engines. Likewise, it was detected that the necessary certifications to regulate the consumption of biodiesel and thus ensure consumer confidence through quality standards do not exist. Finally, this essay analyzed the need for standards to regulate the biodiesel market production chain, from raw material collection and handling to

control at points of sale to facilitate its distribution and supply in the national territory. Despite Mexico's potential for the production of alternative fuels and the benefits they represent, there is no clarity regarding their future development. To achieve this, the intervention of federal agencies is necessary to promote biofuel production based on a well-defined national development plan.

REFERENCES

Almeida-Naranjo CE, Jacome E, Soria R. 2022. Biodiesel market share in Ecuador: Current situation and perspectives. Materials Today: Proceedings 49: 202–209. https://doi.org/10.1016/j.matpr.2021.09.050

ASTM (American Society of Testing and Materials). 2021. Standard specification for biodiesel fuel Blendstock (B100) for middle distillate fuels. West Conshohocken, PA, USA. https://www.astm.org/d6751-23a.html (Retrieved: December 2021).

Balan-Chan RM, Elizalde-Martínez I. 2018. Algunos aspectos de producción de diésel verde a partir de materias primas de segunda generación y la tecnología del hidrotratamiento. Revista Internacional de Investigación e Innovación Tecnológica 6 (31).

Cabrera-Munguia DA, Romero-Galarza A, López-Montes RA, Ríos-González LJ, Leyva-Inzunza ZC. 2022. Producción de biodiésel en México: estado actual y perspectivas. CienciAcierta 72.

Caldeira C, Gülsen E, Olivetti EA, Kirchain R, Dias L, Freire FA. 2014. A multiobjective model for biodiesel blends minimizing cost and greenhouse gas emissions. *In* Murgante B. (ed.), Computational Science and its Applications – ICCSA 2014. Springer: Cham, Switzerland, pp: 653–666. https://doi.org/10.1007/978-3-319-09150-1_48

Castellar-Ortega GC, Angulo-Mercado ER, Cardozo-Arrieta BM. 2014. Transesterificación de aceites vegetales empleando catalizadores heterogéneos. Prospectiva 12 (2): 90–104. https://doi.org/10.15665/rp.v12i2.293

Castro-Martínez C, Beltrán-Arredondo LI, Ortiz-Ojeda JC. 2012. Producción de biodiesel y bioetanol: ¿una alternativa sustentable a la crisis energética? Ra Ximhai 8 (3): 93–100. https://doi.org/10.35197/rx.08.03.e2.2012.09.cc

CONAHCYT (Consejo Nacional de Humanidades, Ciencias y Tecnologías). 2016. Convocatorias Abiertas SENER-CONACYT/ Sustentabilidad energética. Gobierno de México. Consejo Nacional de Humanidades, Ciencias y Tecnologías. Ciudad de México, México. https://conahcyt.mx/ (Retrieved: September 2023).

CNH (Comisión Nacional de Hidrocarburos). 2021. Proceso de cuantificación y certificación de reservas de hidrocarburos al 1 de enero de 2021. Dirección general de reservas. Gobierno de México. Comisión Nacional de Hidrocarburos. Ciudad de México, México. 22 p.

EIA (U.S. Energy Information Administration). 2021. February 2022 monthly energy review. U.S. Department of Energy. U.S. Energy Information Administration. Washington, DC, USA. https://www.eia.gov/totalenergy/data/monthly/pdf/mer.pdf (Retrieved: January 2022).

Yue D, You F, Snyder SW. 2014. Biomass-to-bioenergy and biofuel supply chain optimization: Overview, key issues and challenges. Computers and Chemical Engineering 6 (5): 36–56. https://doi.org/10.1016/j.compchemeng.2013.11.016

DOF (Diario Oficial de la Federación). 2008. Ley de desarrollo y promoción de los bioenergéticos. Gobierno de México. Secretaría de Energía. Ciudad de México, México. http://www.diputados.gob.mx/LeyesBiblio/pdf/LPDB.pdf (Retrieved: September 2023).

FAO (Organización de las Naciones Unidas para la Alimentación y la Agricultura). 2008. El estado mundial de la agricultura y la alimentación, 2008. Biocombustibles: perspectivas, riesgos y oportunidades. Roma, Italia. https://www.fao.org/documents/card/en?details=5e4052d8-1130-5756-9da6-f6e52a3995cb%2f (Retrieved: September 2023).

Torroba A. 2020. Atlas de los biocombustibles líquidos 2019-2020. Instituto Interamericano de Cooperación para la Agricultura: San José, Costa Rica. 42 p.

INEGI (Instituto Nacional de Estadística, Geografía e Informática). 2020. Vehículos de motor registrados en circulación. Instituto Nacional de Estadística, Geografía e Informática. Ciudad de México, México. https://www.inegi.org.mx/ (Retrieved: March 2022).

IMP (Instituto Mexicano del Petróleo). 2017. Reporte de inteligencia tecnológica biodiesel. Secretaría de Energía, Fondo de Sustentabilidad Energética, Instituto Mexicano del Petróleo. Ciudad de México, México. 100 p.

IRENA (International Renewable Energy Agency). 2022. Bioenergy. Masdar City, United Arab Emirates. https://www.irena.org/bioenergy (Retrieved: January 2022).

Medina-Ramírez IE, Chávez-Vela NA, Jáuregui-Rincón J. 2012. Biodiesel, un combustible renovable. Investigación y Ciencia 20 (55): 62–70.

Mofijur M, Rasul MG, Hyde J, Azad AK, Mamat R, Bhuiya MMK. 2016. Role of biofuel and their binary (diesel–biodiesel) and ternary (ethanol–biodiesel–diesel) blends on internal combustion engines emission reduction. Renewable and Sustainable Energy Reviews 53: 265–278. https://doi.org/10.1016/j.rser.2015.08.046

Montero-Alpírez G, Jaramillo-Colorado BE, Vázquez-Espinoza AM, Coronado-Ortega MA, García-González C, Toscano-Palomar L. 2016. Experiencias de aprovechamiento de residuos para la generación de biodiesel en Colombia y México. Revista Internacional de Contaminación Ambiental 32 (2): 77–90. https://doi.org/10.20937/rica.2016.32.05.06

OECD (Organisation for Economic Co-operation and Development). 2018. OCDE-FAO Perspectivas agrícolas 2017-2026. Paris, Francia. https://doi.org/10.1787/agr_outlook-2017-es

Ogunkunle O, Ahmed NA. 2019. A review of global current scenario of biodiesel adoption and combustion in vehicular diesel engines. Energy Reports 5: 1560–1579. https://doi.org/10.1016/j.egyr.2019.10.028

Paredes-Cervantes SA, Barahona-Pérez LF, Barroso-Tanoira FG, Ponce-Marbán DV. 2020. Biocombustibles y su potencial en el mercado energético mexicano. Revista de Economía 37 (94): 36–57. https://doi.org/10.33937/reveco.2020.128

PEMEX (Petróleos Mexicanos). 2020. Valor del comercio exterior de Pemex-Petroquímica. Gobierno de México. Petróleos Mexicanos. Ciudad de México, México. https://datos.gob.mx/busca/dataset/valor-del-comercio-exterior-de-pemex-petroquimica (Retrieved: December 2021).

REN21 (Renewable Energy Policy Network for the 21st Century). 2020. Renewables 2020 Global Status Report. Paris, France. https://www.ren21.net/gsr-2020/ (Retrieved: December 2021).

Riegelhaupt E, Odenthal J, Janeiro L. 2016. Diagnóstico de la situación actual del biodiésel en México y escenarios para su aprovechamiento. Red Mexicana de Bioenergía, Ecofys: Utrecht, Países Bajos. 129 p.

Rosas-Barajas JA, Aguilar-Ortega A, Cornejo-Corona I, Rizo-Fernández Z, Córdova-de la Cruz SE, Ramos-Frausto LG, Esparza-Claudio J de J. 2018. Análisis de las cadenas de suministro de bioetanol y biodiésel en México: estudios de caso. Nova Scientia 10 (20): 13–29. https://doi.org/10.21640/ns.v10i20.1145

Sandar S, Tibebu DT, Shromova OA, Kuittinen S, Turunen O, Pappinen A. 2019. Lake bottom biomass as a potential source for the biorefining industry. Bioresource Technology Reports 7: 100282. https://doi.org/10.1016/j.biteb.2019.100282

Salvatore D. 1977. Teoría y problemas de microeconomía. McGraw-Hill: Ciudad de México, México. 279 p.

Salvi BL, Panwar NL. 2012. Biodiesel resources and production technologies - a review. Renewable And Sustainable Energy Reviews 16 (6): 3680–3689. https://doi.org/10.1016/j.rser.2012.03.050

SEDEMA (Secretaría del Medio Ambiente). 2017. Directorio de centros de acopio de residuos urbanos en la CDMX. Gobierno de la Ciudad de México. Secretaría del Medio Ambiente. Ciudad de México, México. http://data.sedema.cdmx.gob.mx/nadf24/images/infografias/planes_de_manejo_autorizados.pdf (Retrieved: September 2023).

SENER (Secretaría de Energía). 2017. Cartera de necesidades de innovación y desarrollo tecnológico, biocombustibles sólidos. Gobierno de México, Fondo de Sustentabilidad Energética, Instituto Mexicano del Petróleo, Secretaría de Energía. Ciudad de México, México. 43 p.

SENER (Secretaría de Energía). 2018. Permisos otorgados por SENER para la producción, comercialización, y transporte de bioenergéticos. Gobierno de México, Secretaría de Energía. Ciudad de México, México. https://www.gob.mx/sener/documentos/permisos-otorgados-por-sener-para-la-produccion-comercializacion-y-transporte-de-bioenergeticos (Retrieved: March 2022).

SENER (Secretaría de Energía). 2021. Balance nacional de energía: consumo final energético total por combustible. Dirección general de planeación e información energéticas. Gobierno de México. Secretaría de Energía. Sistema de Información Energética. Ciudad de México, México. https://sie.energia.gob.mx/ (Retrieved: March 2022).

SHCP (Secretaría de Hacienda y Crédito Público). 2020. Exposición de motivos. Proyecto de presupuesto de egresos de la Federación. Gobierno de México. Secretaría de Hacienda y Crédito Público. Ciudad de México, México. https://www.ppef.hacienda.gob.mx/work/models/PPEF2020/docs/exposicion/EM_Documento_Completo.pdf (Retrieved: November 2021).

Sosa-Rodríguez FS, Vázquez-Arenas J.2021. The biodiesel market in Mexico: Challenges and perspectives to overcome in Latin-American countries. Energy Conversion and Management 10 (12): 100149. https://doi.org/10.1016/j.ecmx.2021.100149

Statista. 2023. La Unión Europea e Indonesia lideres en producción de biodiesel. 10 agosto 2023. https://es.statista.com/grafico/30574/paises-y-region-con-la-mayor-produccion-de-biodiesel-en-el-mundo/ (Retrieved: December 2023).

Zhang Y, Jiang Y. 2017. Robust optimization on sustainable biodiesel supply chain produced from waste cooking oil under price uncertainty. Waste Management 60: 329–339. https://doi.org/10.1016/j.wasman.2016.11.004

Agrociencia

SPATIAL-TEMPORAL SURFACE WATER AVAILABILITY IN THE TULANCINGO RIVER BASIN, HIDALGO, MEXICO

Sandra Luz **Torres-Suárez**[1], Martín Alejandro **Bolaños-González**[1*], Laura Alicia **Ibáñez-Castillo**[2], Abel **Quevedo-Nolasco**[1], Ramón **Arteaga-Ramírez**[2], Axel Eduardo **Rico-Sánchez**[1], Humberto **Vaquera-Huerta**[1]

[1]Colegio de Postgraduados Campus Montecillo. Posgrado en Hidrociencias. Carretera México-Texcoco km 36.5, Montecillo, Texcoco, State of Mexico, Mexico. C. P. 56264.
[2]Universidad Autónoma Chapingo. Departamento de Irrigación, Posgrado en Ingeniería Agrícola y Uso Integral del Agua. Carretera México-Texcoco km 38.5, Chapingo, Texcoco, State of Mexico, Mexico. C. P. 56227.
* Author for correspondence: bolanos@colpos.mx

Citation: Torres-Suárez SL, Bolaños-González MA, Ibáñez-Castillo L, Quevedo-Nolasco A, Arteaga-Ramírez R, Rico-Sánchez A, Vaquera-Huerta H. 2024. Spatial-temporal surface water availability in the Tulancingo River basin, Hidalgo, Mexico. **Agrociencia** 58(4): 514-532. https://doi.org/ 10.47163/agrociencia.v58i4.2904

Editor in Chief:
Dr. Fernando C. Gómez Merino

Received: November 10, 2022.
Approved: January 03, 2024.
Published in Agrociencia: May 29, 2024.

ABSTRACT

The Tulancingo River basin is part of the upper Metztitlán River basin and has an aquifer deficiency that covers 87 % of its surface area; however, floods have occurred in the valley region. This disparity encouraged the current work, the goal of which was to estimate the spatio-temporal availability of water in the soil within the basin from the modeling of surface water balance elements. Sensitivity analysis of the model fit parameters was performed with the SWATCUP program and the SUFI2 algorithm. The runoff values were estimated with the SWAT program and were compared with the records of the Venados Hydrometric Station, obtaining values of the statistical indicators R^2 = 0.89 and Nash Sutcliffe (NS) = 0.86 for the calibration period (1982–2002); and R^2 = 0.77 and NS = 0.62 for the validation period (2003–2013). Of the nine sub-basins that make up the Tulancingo basin, the upper sub-basins of the Río Chico (11), Ventoquipa stream (12), and San Lorenzo River (13) showed values 2.2 times higher than the rainfall depth of the lower sub-basins (5, 6, 7, 8, 9, and 10). Surface runoff and infiltration reported maximum values from July to October and minimum values from April to May. The maximum final water availability in the soil occurred in September. Regarding the analysis by periods, the Generalized Additive Model provided a good fit for most of the variables ($0.6 < R^2 < 0.94$); during the last period, higher values were observed than in the previous periods ($p < 0.001$), identifying a change in the hydrological state of the basin. This was mainly associated with a significant change in rainfall, which was reflected in the trend of surface runoff.

Keywords: water balance, calibration, SWAT, Generalized Additive Model.

INTRODUCTION

The surface area of the Tulancingo River basin is subject to 87 % of the "Decree establishing a ban on the abstraction of groundwater," as it is located within aquifer 1317, "Valle de Tulancingo." This aquifer tripled its average annual water availability deficit in just seven years, from -6.84 to -20.93 hm^3 $year^{-1}$ (DOF, 2020). This situation,

while reflecting the scarcity of groundwater resources within the same region, contrasts with the presence of extreme hydrometeorological events.

Herrera *et al*. (2018) mention that these phenomena are related to the interaction of easterly waves with westerly flow and tropical cyclones from the Gulf of Mexico, mainly from August to October, and have motivated two-dimensional hydraulic modeling to obtain flood risk maps in the city of Tulancingo, such as the one carried out by Bonasia *et al*. (2017). Similarly, Valdez-Lazalde *et al.* (2011), Ortíz-Gómez *et al*. (2015), and Mendoza-Cariño *et al*. (2018) developed basin-wide studies of land use change, water allocation by type of use, and hydrological analysis, down to the Metztitlán River.

These studies present the general conditions of the basin to which the Tulancingo River belongs; however, as they have been oriented towards the analysis of a particular element, runoff or land use and vegetation, without considering the relationship that exists between them or with other elements of the balance (infiltration, base flow, etc.), they do not explain the deficit-excess phenomenon that occurs locally. In this sense, the integration of the elements that constitute the water balance, analyzed geospatially and temporally, can help in the assimilation of the problem of origin, zoning the availability, and planning the management of water resources in a sustainable manner.

In a water balance, the spatio-temporal distribution of precipitation determines the amount of water reaching the land surface; temperature, humidity, and vegetation cover influence the proportion of water evapotranspired; slope and soil characteristics and conditions influence infiltration and runoff (Siad *et al*., 2019). Thus, soil water storage and availability at the catchment level are influenced by each element, given their interaction and influence.

A large number of hydrological models have been developed to quantify the elements that make up the hydrological cycle at the catchment level. Lopes *et al.* (2021) mention that it is necessary to take into account model factors such as purpose, level of complexity, and availability of information for the selection of the most appropriate model in a study. The Soil and Water Assessment Tool (SWAT) hydrological model has been used and tested in a number of areas, including water balances (Shawul *et al*., 2019). The evaluation and critical review by Keller *et al.* (2023) of the 21 most widely used hydrological models gave SWAT an "H" (high) rating, highlighting it in terms of functionality, catchment applicability, and scales, among other aspects.

The results provided by such a program have proven to be favorable if sufficient climate data are available to establish a validation and calibration time period (Marín *et al*., 2020). Given the above, the objective of this study is to quantify spatially and temporally the availability of water in the soil from the water balance in the Tulancingo River basin, identify the areas with availability and deficit, and observe its historical behavior in sub-periods. It was considered that the SWAT model has sufficient capacity and accuracy for this purpose, so that the results obtained can serve as a basis for the implementation of specific measures for the conservation and proper management of water resources at the basin level.

MATERIALS AND METHODS

The Tulancingo River rises at the border of the states of Hidalgo and Puebla, crosses the valley and the city of the same name in a north-westerly direction, continues its course as the Alcholoya River, and finally receives the name of Metztitlán within Hydrological Region 26 "Río Pánuco." The modeling of the basin, which was carried out with the help of the SWAT program, covers the basin from its origin to the hydrometric station 26024 "Venados" on the Metztitlán River, at coordinates 20° 28′ 2.38″ N and 98° 40′ 15.52″ W. Information for calibration and validation is available at this site. The Tulancingo basin (Figure 1) is indicated as having its outlet at coordinates 20° 10′ 36.3″ N and 98° 22′ 28.19″ W.

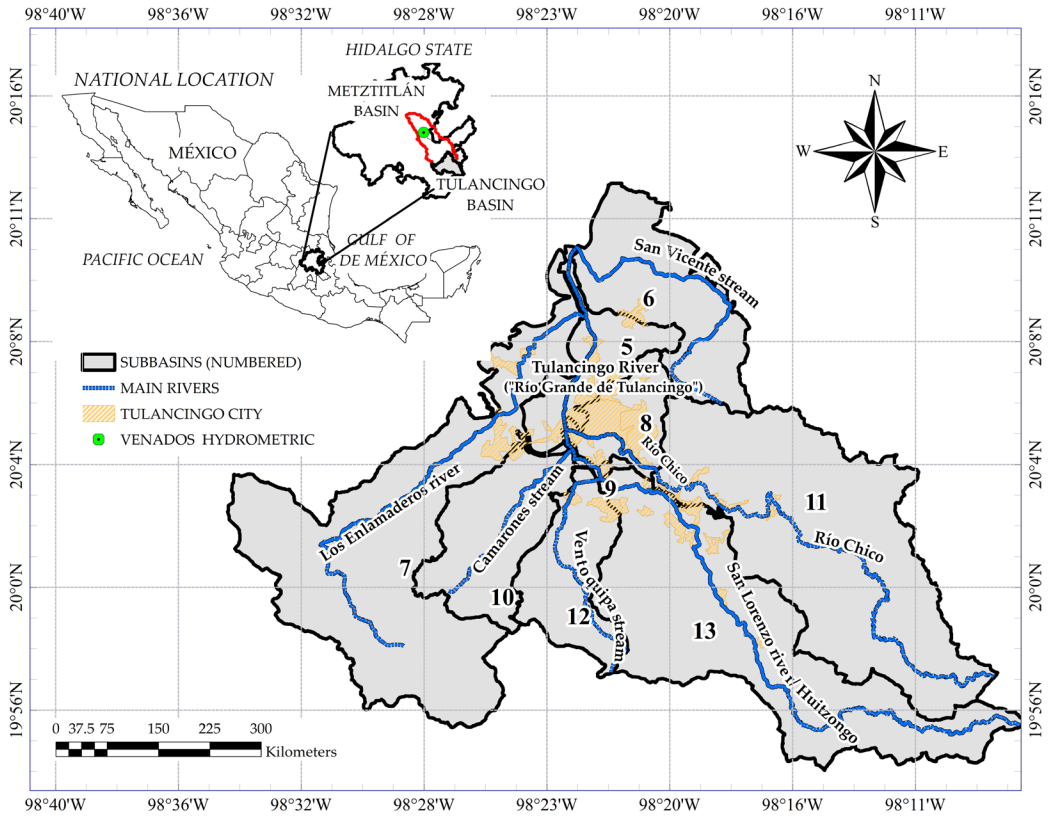

Figure 1. Geographic coordinates for the Tulancingo basin's sub-basins and main streams (INEGI, 2014).

After calibrating using hydrometric data 83 km downstream, the considerations made to the model described below in the input data were applied to the Venados catchment, with output at the hydrometric station. The representation, quantification of hydrological balance elements, and analysis carried out for the Tulancingo basin

reflect the most realistic condition possible for its surface area, which covers almost 40 % of the total area (733 out of 1953 km^2).

Model input data

Weather information

Daily precipitation and temperature data from nine meteorological stations within the watershed were included, covering a 38-year period (1980–2017). Missing data estimation was performed using the U.S. National Weather Service method (Ramírez-Cruz *et al*., 2015), which is an average obtained with the inverse of the squared distance as the weighting factor. Solar radiation, dew point temperature, and wind speed values were obtained with the help of the Climate Forecast System Reanalysis (CFSR) (Table 1).

Land use and vegetation (USV)

Seven USV coverages were analyzed in vector type format, denominated: Series II, 2001 edition; Series 2.5, 2002 edition; Series III, 2005 edition; Series IV, 2009 edition; Series V, 2013 edition; Series VI, 2016 edition; and Series 6.5, 2017 edition. These series are published by the National Institute of Statistics and Geography (INEGI) and the Mexican Carbon Program and are freely available for download (INEGI, 2019). When plotting the areas covered by the USV types associated with the year of their image, the most noticeable change was observed in 2002 (Series III), with a 22 % reduction in the area of forest (oak plus oak-pine) and a 168 % increase in shrub secondary vegetation (Table 1). For this reason, the distribution and surface areas of Series II were assigned to the period 1980–2001, and, by means of percentage changes by USV in each sub-basin, the differences identified in Series III were incorporated for the period 2002–2017.

Soil type

The spatial distribution by soil type was taken from Series II (INEGI, 2014), serving as a complement to the laboratory analysis of 32 soil samples taken at the following depths: 0–40, 40–80, 80–120, and < 120 cm, in eight sites distributed within the basin (two in each of the four soil types that dominate 92 % of its surface: Phaeozem, Luvisol, Vertisol, and Umbrisol). Hydraulic conductivity values associated with the main streams, with variations ranging from 13.74 to 48.1 mm h^{-1}, were measured with infiltration tests using a Guelph model 2800K1 permeameter (ICT International, Australia).

Losses due to water demand for different uses

The volumes concessioned by type of use, currently in the Public Registry of Water Rights (REPDA, 2018), were taken. Once located and differentiated by sub-basin, they were separated by type of source (surface and groundwater). For the estimation of the

Table 1. Characteristics of the SWAT model's information and input data.

Type	Information	Format	Source	Image
Climatological	Precipitation and temperature	csv/txt	Climate Computing Project (CLICOM)	 Thiessen polygons
	Solar radiation, dew point temperature and wind speed		Climate Forecast System Reanalysis (CFSR)	
Land Use and Vegetation (USV)	Series II (1993)* Series 2.5 (1999) Series III (2002)* Series IV (2007) Series V (2011) Series VI (2014) Series 6.5 (2016)	Vector (polygon)	USV INEGI scale 1:250 000	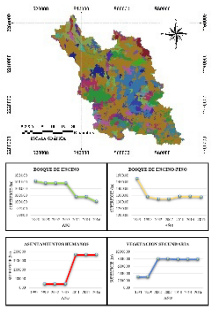
Soil	Edaphological	Vector (polygon)	Edaphology Series II, INEGI, scale 1:250000	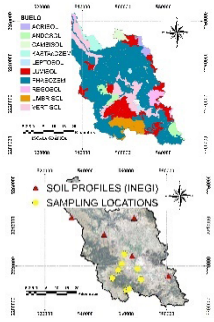
	pH, electrical conductivity, organic matter, texture, bulk density, and moisture content at saturation	txt	Laboratory analysis of soil samples	
		Vector (points with information)	Soil profiles, series II, INEGI, scale 1:250,000.	
Slopes and elevations	Elevation	Raster	Mexican Elevation Continuum (CEM 3.0)	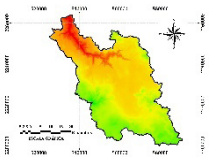

*USV series used directly within the program, year to which the image corresponds in parentheses. INEGI: National Institute of Statistic and Geography (Mexico).

volume of returns, the Official Mexican Standard NOM-011-CONAGUA-2015 (DOF, 2015) was used as a basis. Both the average daily water removal from the riverbed and the average daily water removal from the shallow aquifer, both in $m^3\ d^{-1}$, were assigned on a monthly basis as appropriate in each sub-basin after subtracting the volume of returns.

Special considerations

The proportion of surface area covered by the aquifers within the Venados basin is: 1317 Valle de Tulancingo 60 %, 1315 Huasca-Zoquital 25 %, and 1314 Metztitlán 15 %, the three of the free type and with availability of -20.93, 9.5, and 9.9 hm^3, respectively. The method selected for the calculation of evapotranspiration was Penman-Monteith (Allen, 2005), and for surface runoff, the USDA Soil Conservation Service (SCS) numerical curve method (Mishra and Singh, 2003).

Calibration and validation

Sensitivity analysis of the parameters was performed with the SWATCUP program. The Sequential Uncertainty Fitting algorithm was selected to find the best-fit parameters, so SUFI-2, of Bayesian structure, was chosen (Ma *et al*., 2022). The Nash Sutcliffe performance indicator (NS) and the coefficient of determination (R^2) were the target functions in the calibration and validation processes for 1982–2002 and 2003–2013, respectively. The equilibrium period, warming, or number of years omitted, was 1980 and 1981.

Hydrological balance

The elements that constitute the soil-water balance equation were determined, which is expressed by an adaptation of the equation of Neitsch *et al*. (2011) that uses daily values, considering monthly values through two proposals. In the first, the water stored in the soil profile (SW) is assumed to be the initial water content, deriving the following equation:

$$SW1_{mi} = SW_{mi} + \Sigma(PREC_{mi} - SURQ_{mi} - ET_{mi} - PERC_{mi} - GW_{mi}) \quad (1)$$

where $SW1_{mi}$ is the final water availability in soil number one, the mean value of month *i* (mm), and the amount of water in the soil profile at the end of the period (month); SW_{mi} is the initial water content in the soil profile, mean value of month i (mm); $PREC_{mi}$ is the amount of precipitation (rainfall in this case), mean value of month i (mm); $SURQ_{mi}$ is the amount of surface runoff, mean value of month i (mm); ET_{mi} is the amount of evapotranspiration, mean value of month i (mm); $PERC_{mi}$ is the amount of water infiltrating into the soil profile, mean value of month i (mm); and GW_{mi} is the contribution of groundwater or baseflow entering the mainstream, mean value of month i (mm).

For the construction of the present surface approach model, limited subway hydrological information was available, where aquifer 1317 presents a deficit of -20.93 $hm^3\ yr^{-1}$ (DOF, 2020). In the second proposal, the nullity of water stored in the soil profile was assumed in the balance equation:

$$SW2_{mi} = SW1_{mi} - SW_{mi} + \Sigma(PREC_{mi} - SURQ_{mi} - ET_{mi} - PERC_{mi} - GW_{mi}) \quad (2)$$

where $SW2_{mi}$, is the final water availability in soil profile number two, the mean value of month i (mm).

Temporal analysis

Temporal variation in water balance elements and water availability was analyzed. After 36 years of modeling (38 years of data minus two years of warming), 12-year subperiods were chosen for each subbasin, for which the final monthly mean soil water availability ($SW1_{mi}$) was estimated in three subperiods: A) from 1982 to 1993, B) from 1994 to 2005, and C) from 2006 to 2017. The Generalized Additive Model (GAM) was used to compare their behavior at the level of monthly mean values. This is a smoothed, non-parametric regression model, which is considered an extension of the Generalized Linear Models (GLM) (Dubos *et al*., 2022), choosing the Gaussian family for the response variable. The plots and statistical parameters derived from the GAM application were obtained with the help of the ggplot2 and mgcv libraries within the RStudio software (R Core Team, 2022).

RESULTS AND DISCUSSION

Calibration

In the sensitivity analysis to the model fit parameters, it was found that the variables moisture condition curve number 2 (CN2), initial depth in the shallow aquifer (SHALLST), groundwater lag time (GW_DELAY), and depth of water in the shallow aquifer required for return flow (GWQMN) had a significant effect on the results ($p < 0.05$), so their incorporation into the final model resulted in the hydrographs with monthly mean flows estimated in SWAT (Figure 2). When comparing these hydrographs with those observed at the Venados Hydrometric Station, three periods stand out in which the model underestimated the flow during the calibration period, occurring in September 1984, October 1998, and October 1999, whose progressive order in the graph corresponds to numbers 33, 202, and 214, respectively.

The overall performance of the model was adequate according to the statistical indicators, the coefficient of determination (R^2), and the Nash-Sutcliffe index (NS). Both calibration ($R^2 = 0.89$ and NS = 0.86) and validation ($R^2 = 0.77$ and NS = 0.62) were favorable (Molnar, 2011). Higher calibration and validation parameters were identified than those obtained by Mengistu *et al.* (2019) in arid and semi-arid areas of Southern Africa, which reached R^2 and NS > 0.71 for both periods.

Elements of the Balance

The percentage distribution at the sub-basin level of land use and vegetation, as well as soil type (Table 2), is useful for understanding and analyzing the results of the balance elements, highlighting that the predominant land use is agricultural (46.85 %) and the soil type is Phaeozem (45.31 %). The most significant changes during

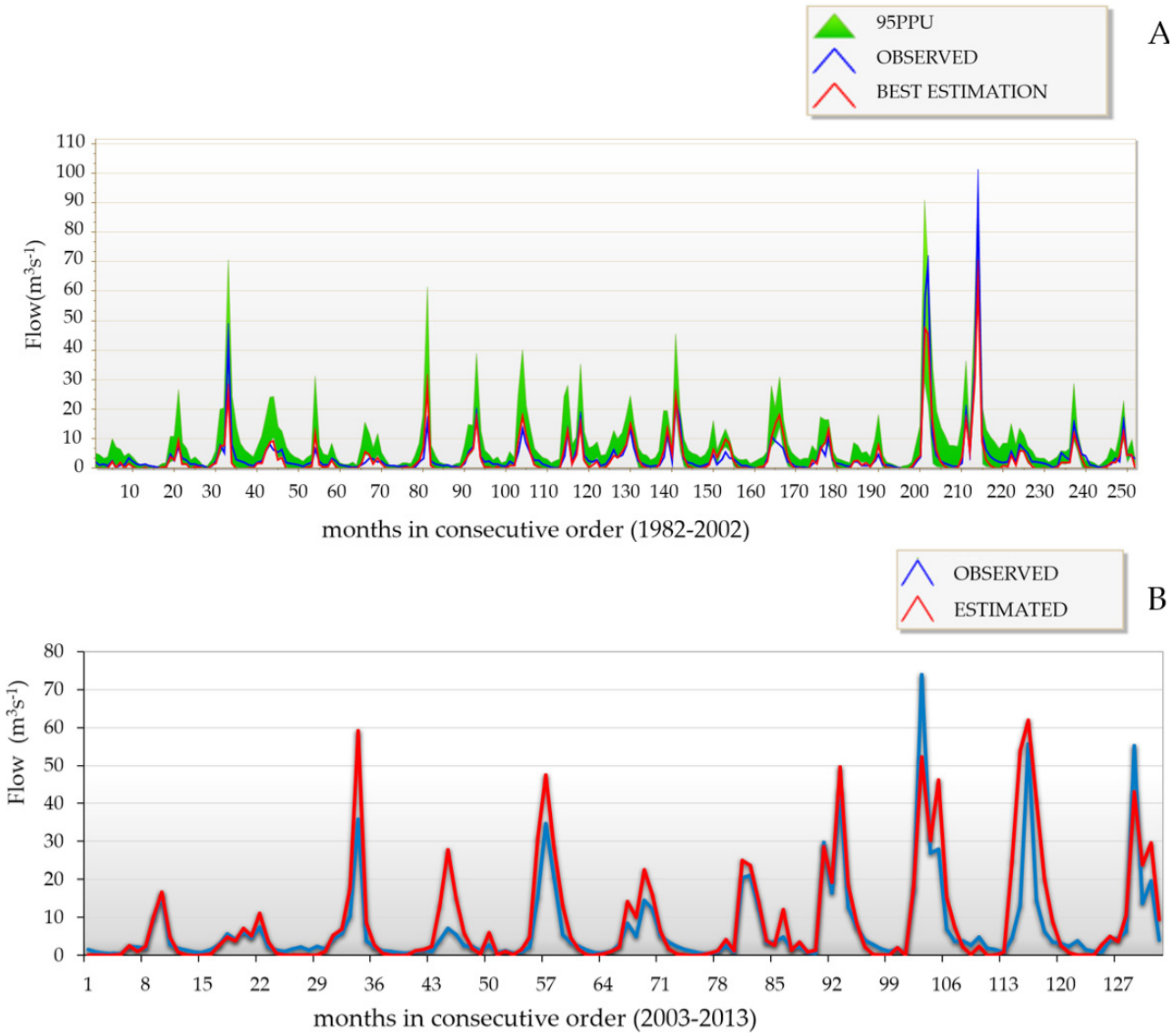

Figure 2. Hydrographs with mean monthly flow values observed at the Venados Hydrometric Station (20° 28′ 2.38″ N, 98° 40′ 15.52″ W), estimated with SWAT, in $m^3 s^{-1}$. 95PPU: 95 % uncertainty in the prediction. A: calibration period (1982–2002); B: validation period (2003–2013).

the period analyzed (1982–2017) were the 168 % increase in secondary vegetation and the 22 % reduction of the different forest types, as indicated in the model as of 2002. This condition was not considered to have a great impact on the water balance since its changes represent low percentages of the basin's total, 6 and 4 %, respectively. However, the reduction in forest types can potentially impact annual discharge, as suggested by Sharma *et al*. (2022) in a study conducted in the Sabarmati River basin in western India.

Table 2. Land use and vegetation distribution (INEGI Series II,1993), and soil type by sub-basin (in percentage) in the Tulancingo River basin, Mexico (INEGI, 2019).

Land Use and Vegetation	Sub-basin									Total
	5	6	7	8	9	10	11	12	13	
Vsa / Pine-oak B			2.70							0.66
B oak-pine		9.72	5.56			11.03	0.40	8.66	2.84	4.29
Vsa / B for tasteless						1.67		5.25	0.23	0.48
Rainfed and irrigated agriculture	**68.20**	**71.41**	**73.29**	29.03	**73.72**	**51.41**	**66.98**	**43.45**	**65.95**	**64.85**
B oak		2.12	0.89			10.16		2.32		1.31
Vsa / B oak	6.17	3.39	5.11	0.78		3.79	1.47	0.74		2.55
B pine		3.51	5.30	0.71		20.73	21.14	35.14	18.36	14.08
Vsa / B pine									0.85	0.18
Crassicaule scrub	3.32									0.15
Vsa		1.19								0.11
Induced pasture	3.88	5.80	3.72	21.12			8.78	0.25	7.63	6.06
Urban area	18.43	2.86	3.34	**47.77**	26.28	1.22	1.21	4.18	4.14	5.23
Water body			0.09	0.58			0.02			0.05
Soil type										
Andosol							15.98		0.98	3.98
Leptosol			0.86	10.40	39.44		0.46		1.30	1.10
Luvisol	1.42	0.03	26.44			**51.11**	20.08	17.40	19.39	20.11
Phaeozem	32.41	**64.88**	**48.45**	**55.52**		0.41	**46.47**	14.34	**58.25**	**45.31**
Regosol		16.75					7.89			3.43
Umbrisol			13.03			40.93		**59.63**	14.84	12.85
Vertisol	61.45	16.88	11.22	11.94	60.56	7.54	8.97	5.83	4.49	11.71
Urban soil	4.73	1.46		**22.13**			0.14	2.79	0.75	1.51

Vsa: shrub secondary vegetation; B: forest. Underlined values indicate maximum percentages per sub-basin.

When comparing the elements of the water balance at the sub-basin level, it was consistently identified that the highest estimates were associated with the upper sub-basins (11, 12, and 13), whose main streams are the Río Chico (upstream), Ventoquipa Stream, and San Lorenzo River, respectively. On the contrary, the lower values were related to the lower sub-basins (5, 6, 7, 8, 9, and 10), where their main streams are the Tulancingo River (downstream), San Vicente stream, Los Enlamaderos River, Río Chico (downstream), Tulancingo River (upstream), and Camarones stream, in that order (Figure 3). As an example, the element water stored in the soil profile (SW) presented, on average, values of depth 2.8 times higher in the upper sub-basins than those obtained in the lower sub-basins.

The second element of the balance, rainfall (PREC), showed a similar behavior in which the upper sub-basins obtained 220 % more depth height than the lower sub-basins, with a maximum period from May to October and a minimum from November to April. This condition in the rainfall of the present study coincides with what was

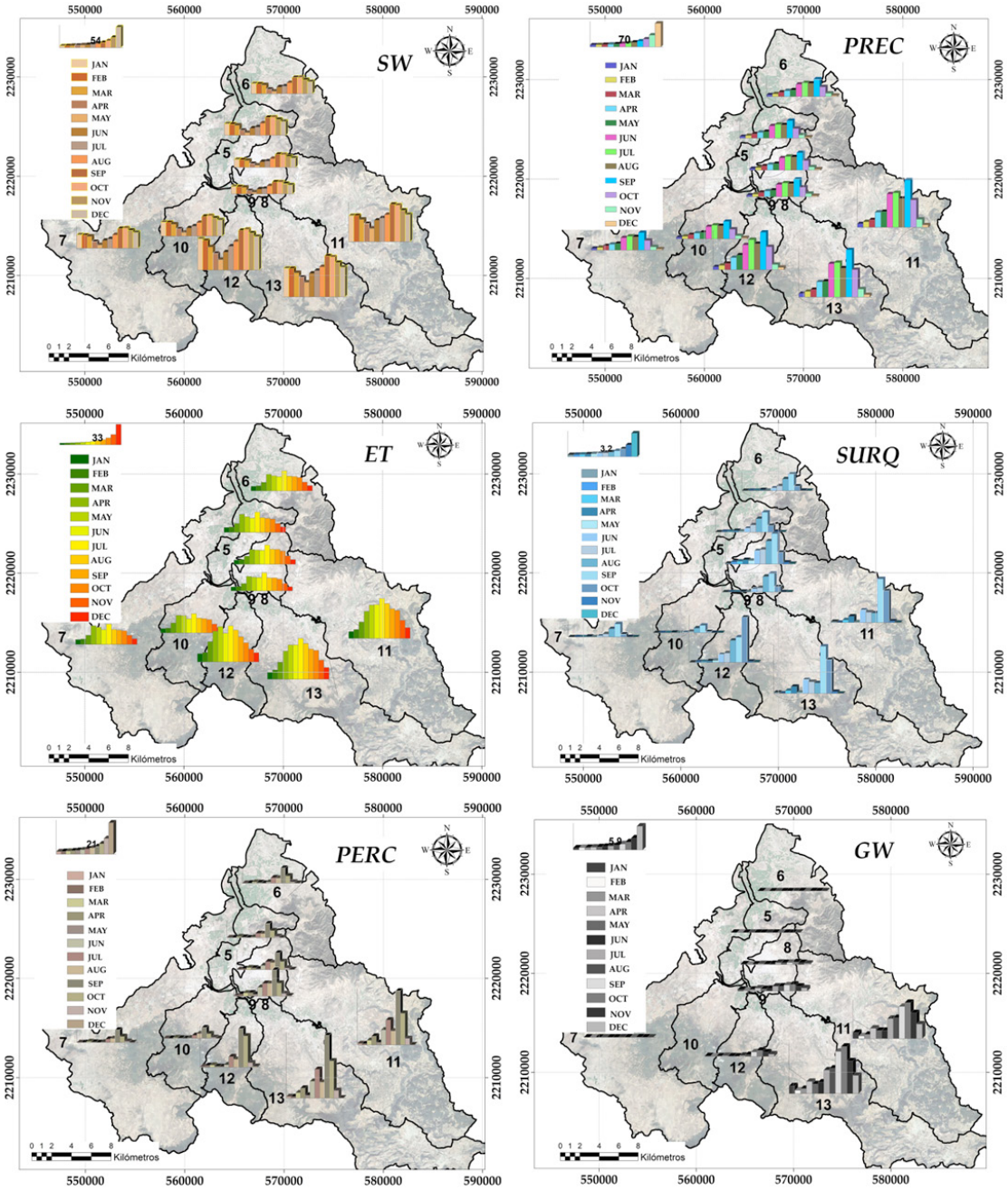

Figure 3. Mean monthly distribution of water balance elements by sub-basin for the 1982–2017 period in the Tulancingo River basin, Mexico. SW: initial soil water content; PREC: precipitation; ET: evapotranspiration; SURQ: surface runoff; PERC: infiltration; GW: baseflow, water depth in millimeters.

previously reported by Herrera *et al.* (2018), where when analyzing the Tulancingo basin, they grouped the rainy months (May–October) into two periods: May–July and August–October, warning of a high probability of an extreme event in the second one. In relation to the average monthly behavior of the third element, evapotranspiration (ET), it was observed that the maximum levels occur during the summer (July to September), when crop production in Mexico is highest (Monterroso-Rivas and Gómez-Díaz, 2021). This could be associated with evapotranspiration in the agricultural zone, which dominates 64 % of the basin. However, the forest zone in the upper watersheds, which covers 18 to 35 % of its surface, also has an impact on this condition. In fact, both uses in basins 10, 11, and 12 occupy more than 80 % of their surface area, and their average annual average evapotranspiration level is 38.4 mm, 202 % higher than the average evapotranspiration level of the rest of the sub-basins (18.9 mm).

The maximum surface runoff (SURQ) occurred in September, which coincides with the wettest month in all sub-basins. Sub-basins 7 and 10 stand out in this case for their lower runoff. In these areas, the dominance of rainfed and irrigated agriculture, combined with the good porosity of their soils (Phaeozen and Umbrisol), explain the increase in evapotranspiration and, in this case, the reduction of surface runoff (Qiu *et al*., 2011).

According to Bernal-Santana *et al*. (2022), the characteristics that influence a lower infiltration rate determine the higher runoff rate in a watershed, such as soil permeability or slope. In the Tulancingo watershed, the dominant soil type is Phaeozem (45.3 %), which is characterized by good fertility and porosity (IUSS, 2015) and contributes to the period of maximum infiltration (PERC). However, the period of maximum infiltration coincides with the period of maximum runoff, so it is assumed that it is due to the magnitude of rainfall, so this assertion does not apply in this case.

Of the elements analyzed in the balance, sub-basins 11, 12, and 13 showed higher values of rainfall depth, evapotranspiration, and infiltration, reflecting their contribution to baseflow (GW) and highlighting their influence in sub-basins 11 and 13, where the sum of their monthly average values was 250 % higher than the sum in sub-basins 5, 6, 7, 8, 9, 10, and 12. It is in these same sub-basins (5 to 12) that, when the maximum surface runoff occurs, the lowest baseflow depth is generated, similar to what happened in the Awash River in Ethiopia (Shawul *et al*., 2019).

Surface Balance

The mean monthly final water availability in soil number one ($SW1_{mi}$) showed temporal and spatial variation, accentuated in some months (Figure 4). The time of highest availability was observed in September in sub-basins 11, 12, and 13, in which the estimated rainfall depth was 139.6, 143.9, and 139.5 mm, respectively, exceeding sub-basin 5 (63.8 mm), where the outlet of the Tulancingo basin is located, by a little more than 200 %. The difference is greater (over 300 %) in the sub-basins where the settlements of the city of Tulancingo are located (sub-basins 8 and 9), with depths of 45.6 and 40.6 mm, respectively. This result is attributable to the difference in the

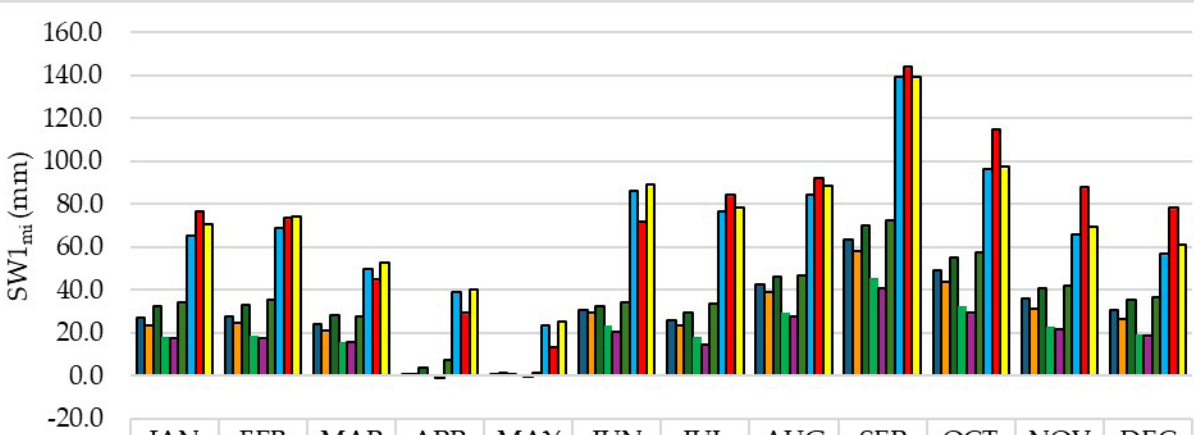

	JAN	FEB	MAR	APR	MAY	JUN	JUL	AUG	SEP	OCT	NOV	DEC
5	27.2	27.7	23.9	0.4	1.0	30.8	25.9	42.8	63.8	49.0	36.1	30.5
6	23.8	24.6	21.3	0.9	1.3	29.7	23.8	39.2	58.4	43.6	31.2	26.3
7	32.2	33.2	28.5	3.8	0.5	32.5	29.6	46.3	70.0	55.1	41.0	35.3
8	18.3	18.7	15.7	1.1	0.7	23.6	18.1	29.6	45.6	32.6	22.9	19.7
9	17.3	17.6	15.8	-1.0	0.0	20.4	14.4	27.7	40.6	29.7	22.1	19.0
10	34.2	35.5	27.6	7.3	1.4	34.3	33.9	47.1	72.4	57.5	42.3	36.9
11	65.6	69.2	49.6	39.3	23.7	86.5	76.4	84.7	139.6	96.7	65.9	57.1
12	76.8	73.6	45.2	29.6	13.2	71.9	84.6	92.1	143.9	115.1	88.2	78.8
13	70.8	74.1	52.9	40.3	25.2	89.0	78.2	88.7	139.5	97.7	69.7	61.3

Figure 4. Mean monthly final water availability in soil number one ($SW1_{mi}$) by sub-basin, in millimeters, in the Tulancingo River basin, Mexico.

proportion of vegetation present in both groups of watersheds, since the upper watersheds have a greater area of forest and shrub secondary vegetation, while the lower watersheds have a greater proportion of induced grassland and settlements. This condition is similar to that of the Luanhe River basin in northern China, where it was identified that the forested area not only increased infiltration and soil water storage but also reduced surface runoff by 11 % (Yang *et al*., 2019).

The trend when comparing the availability of high basins with low basins was analogous for most of the seasons; however, in April and May, the difference was accentuated. For example, in April, the basin with the highest availability was number 13 with 40.3 mm, while sub-basin 9 presented a deficit (negative value) of -1 mm. The decrease in soil moisture content in the lower basins is associated with the increase in evapotranspirative demand and scarcity of rainfall in that season, in addition to the impermeability that characterizes the soil in the urban area established in basins 8 and 9. According to Puskás and Farsang (2009), these urban land modifications frequently

cause changes in fluvial dynamics, highlighting the modification in soil moisture regimes, so it is expected that phenomena associated with these modifications will be reflected in watersheds 8 and 9.

In the mean monthly final water availability in soil number two ($SW2_{mi}$), which was calculated under the assumption of no initial availability, a deficit (negative values) was observed from November to May, which ranged from -20.81 mm of depth (in December for watershed 13) to -0.31 mm (in February for watershed 10) (Table 3). On the contrary, availability (positive values) was observed from June to September. October showed a mixed performance. This scenario, although unlikely, provides evidence of the importance of initial soil moisture content and warns about the continuation of overexploitation of the 1317 Valle de Tulancingo aquifer. Thus, with rainfall being the only source of supply for the requirements within the basin, it will only be enough to cover four of the eight months. Except for the construction of hydraulic infrastructure for water retention and catchment, the deficit trend could be on the rise.

Table 3. Mean monthly final water availability in soil number two (SW2mi) by sub-basin, in millimeters, in the Tulancingo River basin, Mexico.

Month	Sub-basin								
	5	6	7	8	9	10	11	12	13
Jan	-3.09	-2.62	-2.86	-2.46	-2.45	-2.24	-3.03	-5.55	-4.18
Feb	-1.22	-0.81	-0.93	-1.28	-1.14	-0.31	0.62	-4.02	-0.42
Mar	-2.42	-1.88	-2.75	-2.50	-1.64	-3.83	-8.81	-15.74	-10.69
Apr	-12.86	-10.96	-13.64	-8.89	-9.55	-11.72	-8.42	-14.90	-11.66
May	-5.99	-5.11	-8.38	-5.00	-4.57	-8.50	-11.19	-14.65	-13.44
Jun	12.24	12.20	12.12	8.80	7.70	13.01	30.18	24.19	26.94
Jul	4.08	3.93	5.09	1.59	0.36	7.45	14.01	21.55	8.93
Aug	10.90	10.36	11.33	6.46	6.28	11.45	13.44	16.97	9.40
Sep	16.75	15.99	18.39	11.48	9.02	20.38	41.48	39.41	31.53
Oct	1.32	1.19	2.19	-0.97	-1.70	3.72	1.03	7.96	-7.27
Nov	-5.66	-5.50	-5.91	-5.71	-5.23	-5.46	-16.63	-9.50	-20.81
Dec	-5.61	-5.19	-5.83	-4.87	-4.52	-5.40	-14.26	-9.57	-16.69

Temporal analysis

The Generalized Additive Model (GAM) was applied to each set of monthly mean values of the balance depth variables (Equation 1): PREC, SURQ, ET, PERC, GW, SW, and SW1, in addition to potential evapotranspiration (PET) and water productivity (WYLD), in three time periods (A: 1982–1993, B: 1994–2005, and C: 2006–2017). Such a model provided smoothed trend lines for each analysis period, flexible in the form of the relationships between the explanatory variable (months) and its response (balance depth item under study) (Ouarda *et al*., 2018). The level of adjustment was considered

positive based on the extent to which its variance is explained by more than 60 % (Table 4), according to the calculated coefficient of determination R^2.

The model best represented the behavior of monthly mean potential evapotranspiration (PET) by presenting a value of $R^2 > 0.9$ in all sub-basins, followed by ET $0.79 < R^2 < 0.95$, SW $0.83 < R^2 < 0.3$, SW1 $0.66 < R^2 < 0.84$, PREC $0.64 < R^2 < 0.81$, GW $0.65 < R^2 < 0.75$, and WYLD $0.61 < R^2 < 0.64$. The presence of empty spaces in the table of coefficients of determination is due to R^2 values lower than 0.6, a condition that was assumed to be an insufficient adjustment of the model to the monthly mean behavior of the variable. The absence of surface runoff observed in each sub-basin (SURQ) and water infiltrating into the soil profile (PERC) is due to the same reason.

Table 4. Coefficients of determination (R^2), obtained from the application of the Generalized Additive Model (GAM) model, for each variable by sub-basin.

Sub-basin		PREC	ET	GW	WYLD	PET	SW	SW1
5	R^2	0.64	0.79	-	-	0.94	0.83	0.71
		C***	AC***			B*	C***	C***
6	R^2	0.64	0.81	0.72	-	0.94	0.84	0.71
		C***	A C***	C***		B*	C***	C***
7	R^2	0.64	0.81	0.72	-	0.94	0.84	0.73
		C***	AC***	C***		B*	C***	C***
8	R^2	0.64	0.84	0.68	-	0.94	0.85	0.71
		C***	AC***	C***		B*	C***	C***
9	R^2	0.64	0.81	0.75	0.61	0.94	-	0.68
		C***	AC***	C***	C***	B*		C***
10	R^2	0.77	0.93	-	0.63	0.94	0.84	0.75
		A*** C**	BC*		C***		C***	C***
11	R^2	0.77	0.93	-	0.63	0.94	0.84	0.67
		A*** C**	BC*		C***		C***	A***
12	R^2	0.81	0.95	-	-	0.94	0.93	0.84
		A***	C*				B*C***	AC***
13	R^2	0.77	0.93	0.65	0.64	0.93	0.84	0.66
		A*** C**	BC*	C***	C***		C***	A***

A: 1982–1993; B: 1994–2005; C: 2006-2017; *$p < 0.05$, **$p < 0.01$, ***$p < 0.001$; PREC: rainfall; ET: evapotranspiration; GW: baseflow; WYLD: water productivity: PET: potential evapotranspiration; SW: initial soil water content; SW1: final soil water availability.

Additional to that proven by Dubos *et al*. (2022), who demonstrated the effectiveness of applying the GAM model to climate data, the significance level obtained in this study for the fit function in the period 2006–2017 (C), mostly $p < 0.001$, indicates that the line describes very well the monthly mean behavior for the variables ET, GW, WYLD, PET, SW, and SW1. It is evident that their increase separates them from the previous periods A and B (Figure 5).

The results obtained show that the response of runoff in relation to rainfall during the three periods analyzed is consistent with studies focused on the analysis of the effects of climate change, such as those of Swain *et al*. (2021) and Xuan *et al*. (2021), where the temporal variation patterns of flow are complementary to those of rainfall. Thus, the lower sub-basins, from 5 to 10, show a significant increase in groundwater availability in the last period of analysis (2006–2017), as a result of the increase in rainfall depth. This situation is congruent with the separation that the last period of available information presents both the Venados Hydrometric Station (2006–2013) and the runoff of sub-basin 1 (2006–2017).

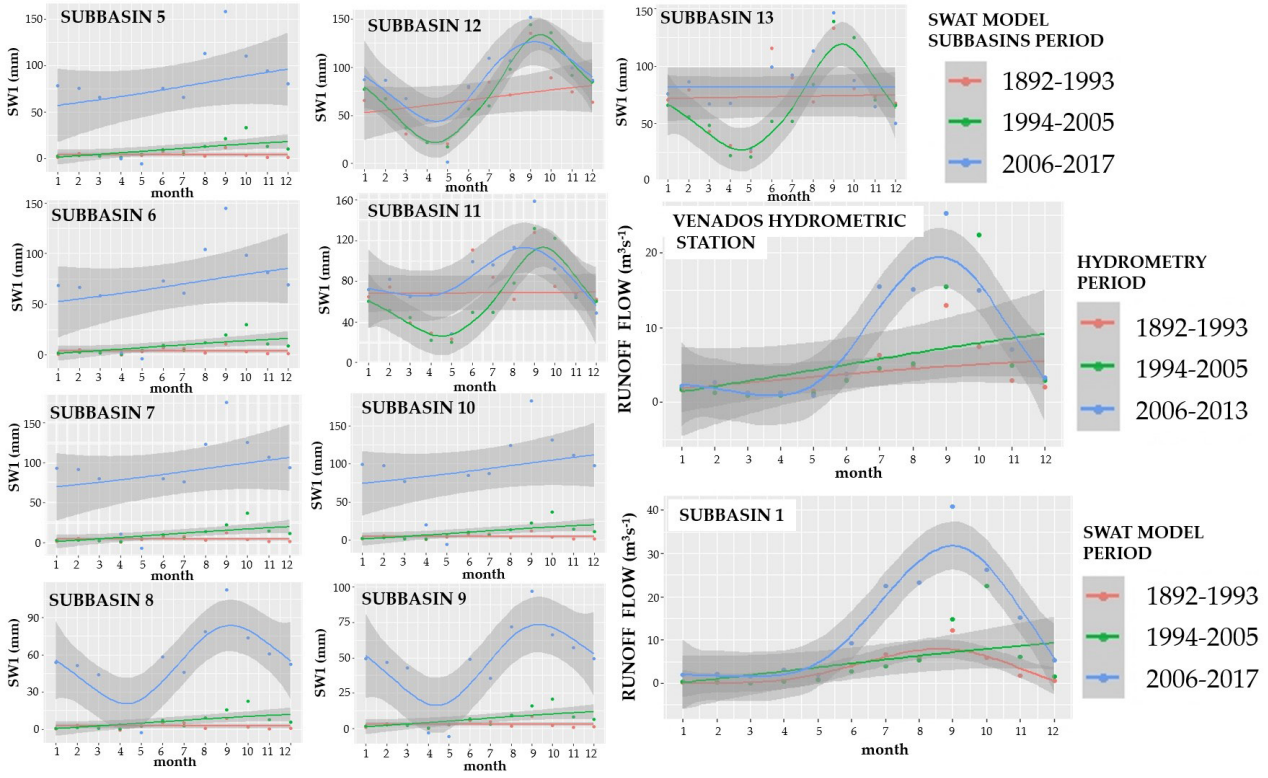

Figure 5. Smoothed trend functions with the Generalized Additive Model (GAM) for mean monthly mean final soil water availability by sub-basin (SW1) (mm); mean monthly runoff flow measured at the Venados Hydrometric Station; and SWAT-estimated flows to the outlet basin (sub-basin 1) (m^3 s^{-1}). The gray area indicates a 95 % confidence interval.

CONCLUSIONS

The Generalized Additive Model presented a good statistical fit for most of the hydrologic balance variables ($0.6 < R^2 < 0.94$), so its performance was adequate. In the 2006–2017 period, values notoriously higher than the two previous periods of analysis were observed, identifying a change in the hydrological state of the basin associated

with rainfall in this last period of analysis. Consequently, an analogous change in the surface runoff trend was identified, both in the values modeled with SWAT and those measured at the Venados Hydrometric Station.

Final soil water availability showed a marked spatial and temporal variation. The upper sub-basins had a higher water supply than those located in the lower zone; however, it is in the latter where the largest population is concentrated, as well as the economic activities with the highest demand, mainly agricultural, and therefore, where greater volumes of water are required. In relation to temporal availability, under the scenario of no initial water available in the soil, a water deficit was estimated for most of the year (from October to May) and availability only in the period from June to September. Surface runoff, which is greater in the upper sub-basins during the months of August to October, represents a flood risk in the lower areas, especially considering that in the last period of analysis these differences were accentuated.

The marked differences in water availability, both spatially and temporally, call for the implementation of management actions in the highlands, primarily focused on the conservation and restoration of native vegetation forests to slow runoff, increase aquifer recharge, and reduce peak flows. It is important to manage this resource more efficiently in low-lying areas, mainly those related to agricultural activities, and which correspond to the highest land use in the study basin, in order to prevent a more adverse scenario, similar to that of zero initial soil water availability (SW2).

REFERENCES

Allen R. 2005. Penman-Monteith equation. *In* Encyclopedia of Soils in the Environment. Academic Press: New York, NY, USA, pp: 180–188. https://doi.org/10.1016/b0-12-348530-4/00399-4

Bernal-Santana N, Cruz-Cárdenas G, Silva JT, Martínez-Trinidad S, Moncayo-Estrada R, Estrada-Godoy F, Ochoa-Estrada S, Álvarez-Bernal D. 2022. Variación de la escorrentía superficial por el cambio de uso de suelo en la cuenca del río Duero. Tecnología y Ciencias del Agua 13 (1): 427–469. https://doi.org/10.24850/j-tyca-2022-01-10

Bonasia R, Areu-Rangel OS, Tolentino D, Mendoza-Sanchez I, González-Cao J, Klapp J. 2017. Flooding hazard assessment at Tulancingo (Hidalgo, Mexico). Journal of Flood Risk Management 11 (S2): 1116–1124. https://doi.org/10.1111/jfr3.12312

Dubos V, Hani I, Ouarda TBMJ, St-Hilaire A. 2022. Short-term forecasting of spring freshet peak flow with the Generalized Additive model. Journal of Hydrology 612: 5–11. https://doi.org/10.1016/j.jhydrol.2022.128089

DOF (Diario Oficial de la Federación). 2015. NORMA Oficial Mexicana NOM-011-CONAGUA-2015, que establece las especificaciones y el método para determinar la disponibilidad media anual de las aguas nacionales. Gobierno de México, Secretaría del Medio Ambiente y Recursos Naturales. Ciudad de México, México. https://www.dof.gob.mx/nota_detalle.php?codigo=5387027&fecha=27/03/2015#gsc.tab=0 (Retrieved: January 2023).

DOF (Diario Oficial de la Federación). 2020. ACUERDO por el que se actualiza la disponibilidad media anual de agua subterránea de los 653 acuíferos de los Estados Unidos Mexicanos,

mismos que forman parte de las regiones hidrológico-administrativas que se indican. Gobierno de México, Secretaría del Medio Ambiente y Recursos Naturales. Ciudad de México, México. https://www.dof.gob.mx/nota_detalle.php?codigo=5600593&fecha=17/09/2020#gsc.tab=0 (Retrieved: February 2022).

Herrera E, Magaña V, Morett S. 2018. Relación entre eventos extremos de precipitación con inundaciones. Estudio de caso: Tulancingo, Hidalgo. Nova Scientia 10 (21): 1–19. https://doi.org/10.21640/ns.v10i21.1527

INEGI (Instituto Nacional de Estadística y Geografía). 2014. Mapas edafológicos a escala 1: 250 000, Serie II. México. Instituto Nacional de Estadística y Geografía. Ciudad de México, México. https://www.inegi.org.mx/temas/edafologia/#Descargas (Retrieved: March 2019).

INEGI (Instituto Nacional de Estadística y Geografía). 2019. Mapas de uso de suelo y vegetación a escala 1: 250 000, Series: II, 2.5, III, IV, V, VI y 6.5. Ciudad de México, México. https://www.inegi.org.mx/temas/usosuelo/#Descargas (Retrieved: March 2019).

IUSS (International Union of Soil Sciences). 2015. Base referencial mundial del recurso suelo 2014, Actualización 2015. Sistema internacional de clasificación de suelos para la nomenclatura de suelos y la creación de leyendas de mapas de suelos. Informes sobre recursos mundiales de suelos 106. International Union of Soil Sciences. Roma, Italia. 218 p.

Keller AA, Garner K, Rao N, Knipping E, Thomas J. 2023. Hydrological models for climate-based assessments at the watershed scale: A critical review of existing hydrologic and water quality models. Science of the Total Environment 867: 161209. https://doi.org/10.1016/j.scitotenv.2022.161209

Lopes TR, Zolin CA, Mingoti R, Vendrusculo LG, de Almeida FT, de Souza AP, de Oliveira RF, Paulino J, Uliana EM. 2021. Hydrological regime, water availability and land use/land cover change impact on the water balance in a large agriculture basin in the Southern Brazilian Amazon. Journal of South American Earth Sciences 108: 103224. https://doi.org/10.1016/j.jsames.2021.103224

Ma J, Rao K, Li R, Yang Y, Li W, Zheng H. 2022. Improved Hadoop-based cloud for complex model simulation optimization: Calibration of SWAT as an example. Environmental Modelling and Software 149: 105330. https://doi.org/10.1016/j.envsoft.2022.105330

Marín M, Clinciu I, Tudose NC, Ungurean C, Adorjani A, Mihalache AL, Davidescu AA, Davidescu Șerban O, Dinca L, Cacovean H. 2020. Assessing the vulnerability of water resources in the context of climate changes in a small forested watershed using SWAT: A review. Environmental Research 184: 109330. https://doi.org/10.1016/j.envres.2020.109330

Mendoza-Cariño M, Bautista-Olivas AL, Quevedo-Nolasco A, Mendoza-Cariño D. 2018. Análisis hidrológico de largo plazo en la cuenca del río Metztitlán Hidalgo, México, y su relación con el cambio climático. Hidrobiológica 28 (1): 17–30.

Mengistu AG, van Rensburg LD, Woyessa YE. 2019. Techniques for calibration and validation of SWAT model in data scarce arid and semi-arid catchments in South Africa. Journal of Hydrology: Regional Studies 25: 100621. https://doi.org/10.1016/j.ejrh.2019.100621

Mishra SK, Singh VP. 2003. SCS-CN method. *In* Soil Conservation Service Curve Number (SCS-CN) Methodology. Water Science and Technology Library, vol 42. Springer: Dordrecht, Netherlands, pp: 84–146. https://doi.org/10.1007/978-94-017-0147-1_2

Molnar P. 2011. Calibration. Watershed modelling, SS 2011. Institute of Environmental Engineering, Chair of Hydrology and Water Resources Management. ETH Zurich: Zurich, Switzerland.

Monterroso-Rivas AI, Gómez-Díaz JD. 2021. Impacto del cambio climático en la evapotranspiración potencial y periodo de crecimiento en México. Terra Latinoamericana 39: 1–19. https://doi.org/10.28940/terra.v39i0.774

Neitsch SL, Arnold JG, Kiniri JR, Williams JR. 2011. Soil and water assessment tool, theoretical documentation version 2009. Texas Water Resources Institute: College Station, TX, USA. 618 p.

Ouarda TBMJ, Charron C, Hundecha Y, St-Hilaire A, Chebana F. 2018. Introduction of the GAM model for regional low-flow frequency analysis at ungauged basins and comparison with commonly used approaches. Environmental Modelling and Software 109: 256–271. https://doi.org/10.1016/j.envsoft.2018.08.031

Ortíz-Gómez R, González-Camacho JM, Chávez-Morales J. 2015. Modelo de asignación de agua considerando un caudal ambiental mínimo en la cuenca del río Metztitlán en Hidalgo, México. Agrociencia 49 (7): 703–721.

Puskás I, Farsang A. 2009. Diagnostic indicators for characterizing urban soils of Szeged, Hungary. Geoderma 148 (3): 267–281. https://doi.org/10.1016/j.geoderma.2008.10.014

Qiu GY, Yin J, Tian F, Geng S. 2011. Effects of the «Conversion of Cropland to Forest and Grassland Program» on the water budget of the Jinghe River catchment in China. Journal of environmental quality 40 (6): 1745–1755. https://doi.org/10.2134/jeq2010.0263

R Core Team. 2022. R: A language and environment for statistical computing. R Foundation for Statistical Computing. Vienna, Austria. https://www.R-project.org/ (Retrieved: May 2022).

Ramírez-Cruz H, López-Velasco O, Ibáñez-Castillo LA. 2015. Estimación mensual de intensidad de la lluvia en 30 minutos a partir de datos pluviométricos. Terra Latinoamericana 33 (2): 151–159.

REPDA (Registro Público de Derechos de Agua). 2018. Base de datos de los registros inscritos publicados. Con fecha de corte al 31 de diciembre de 2018. Gobierno de México. Registro Público de Derechos de Agua. Comisión Nacional del Agua. https://app.conagua.gob.mx/consultarepda.aspx (Retrieved: June 2019).

Sharma A, Patel PL, Sharma PJ. 2022. Influence of climate and land-use changes on the sensitivity of SWAT model parameters and water availability in a semi-arid river basin. CATENA 215: 106298. https://doi.org/10.1016/j.catena.2022.106298

Shawul AA, Chakma S, Melesse AM. 2019. The response of water balance components to land cover change based on hydrologic modeling and partial least squares regression (PLSR) analysis in the Upper Awash Basin. Journal of Hydrology: Regional Studies 26: 100640. https://doi.org/10.1016/j.ejrh.2019.100640

Siad SM, Iacobellis V, Zdruli P, Gioia A, Stavi I, Hoogenboom G. 2019. A review of coupled hydrologic and crop growth models. Agricultural Water Management 224: 105746. https://doi.org/10.1016/j.agwat.2019.105746

Swain SS, Mishra A, Chatterjee C, Sahoo B. 2021. Climate-changed versus land-use altered streamflow: A relative contribution assessment using three complementary approaches at a decadal time-spell. Journal of Hydrology 596: 126064. https://doi.org/10.1016/j.jhydrol.2021.126064

Valdez-Lazalde JR, Aguirre-Salado CA, Ángeles-Pérez G. 2011. Análisis de los cambios en el uso del suelo en la cuenca del río Metztitlán (México) usando imágenes de satélite: 1985-2007. Revista Chapingo Serie Ciencias Forestales y del Ambiente 17 (3): 313–324. https://doi.org/10.5154/r.rchscfa.2010.06.041

Xuan W, Xu YP, Fu Q, Booij MJ, Zhang X, Pan S. 2021. Hydrological responses to climate change in Yarlung Zangbo River basin, Southwest China. Journal of Hydrology 597: 125761. https://doi.org/10.1016/j.jhydrol.2020.125761

Yang W, Long D, Bai P. 2019. Impacts of future land cover and climate changes on runoff in the mostly afforested river basin in North China. Journal of Hydrology 570: 201–219. https://doi.org/10.1016/j.jhydrol.2018.12.055

VOLUME 58, NUMBER 4 | MAY 16 - JUNE 30, 2024 | MEXICO